MOLECULAR AND MECHANICAL REGULATORS OF MESENCHYMAL STEM CELL MICROENVIRONMENTS

A Dissertation
Presented to
The Academic Faculty

By

Kathleen M. McAndrews

In Partial Fulfillment
Of the Requirements for the Degree
Doctor of Philosophy in Chemical and Biomolecular Engineering

Georgia Institute of Technology

August 2015

MOLECULAR AND MECHANICAL REGULATORS OF MESENCHYMAL STEM CELL MICROENVIRONMENTS

Approved by:

Dr. Michelle R. Dawson, Advisor
School of Chemical & Biomolecular Engineering
Georgia Institute of Technology

Dr. Mark Prausnitz
School of Chemical & Biomolecular Engineering
Georgia Institute of Technology

Dr. J. Carson Meredith
School of Chemical & Biomolecular Engineering
Georgia Institute of Technology

Dr. Susan N. Thomas
School of Mechanical Engineering
Georgia Institute of Technology

Dr. John F. McDonald
School of Biology
Georgia Institute of Technology

Date Approved: July 15, 2015

ACKNOWLEDGEMENTS

A number of people have helped make my PhD possible. I'd like to thank my family for teaching me the value of hard work and encouraging me to leave my comfort zone, move across the country and pursue my PhD. Their understanding and support has been instrumental in my success.

I'd also like to thank my advisor, Dr. Michelle Dawson. Her support and guidance were critical for the completion of my project. She was very flexible about the direction of my project, which allowed me to pursue interesting studies. Thank you to my current and past committee members, Dr. Carson Meredith, Dr. John McDonald, Dr. Mark Prausnitz, Dr. Lakeshia Taite, and Dr. Susan Thomas. My committee's support and critical evaluation of my work helped shape my final project and encouraged me to think about the implications of my work. I would like to thank Dr. Andrés García and the CTEng Steering Committee for allowing me to be a part of the training grant. Serving on the training grant gave me exposure to people from different backgrounds and helped shape the way I approach research.

I'd also like to thank the Dawson group members, specifically undergraduate students who have worked with me. Nhat Quach performed many of the preliminary experiments that shaped my Physical Biology paper. In some ways he taught me more than I taught him, as his molecular biology expertise has been invaluable to the group and me. Tuyet Lam and Flora Kim put in countless hours to characterize gelatin scaffolds. I also appreciate all of Jaeyoon Yi's work running adhesion assays and the data analysis Kishan Patel performed. All of these students were extremely dedicated and helped

motivate me to finish these studies. I'd also like to thank Dr. Deepraj Ghosh who trained me when I first joined the lab. I could always count on him to be around to shut down experiments in the middle of the night, which was much appreciated.

Finally, I would like to thank Daniel McGrail who significantly contributed to my work. He was supportive through countless failures and equally excited about successes. He was always more than willing to help and be a sounding board for ideas, which was crucial for both the completion of my studies and maintaining my sanity. I'd also like to thank his family who has always treated me as if I was one of their own. It's been great having a support system while being away from my family and home.

TABLE OF CONTENTS

LIST OF TABLES

LIST OF FIGURES

LIST OF SYMBOLS AND ABBREVIATIONS

MSC	Mesenchymal Stem Cell
TGF-β	Transforming Growth Factor-β
PDGF	Platelet Derived Growth Factor
EGF	Epidermal Growth Factor
VEGF	Vascular Endothelial Growth Factor
FGF	Fibroblast Growth Factor
SDF-1	Stromal Cell Derived Factor-1
ECM	Extracellular Matrix
CAF	Carcinoma Associated Fibroblast
FAK	Focal Adhesion Kinase
VASP	Vasodilator-stimulated Protein
MLC	Myosin Light Chain
ROCK	Rho-associated Kinase
EMT	Epithelial to Mesenchymal Transition
ABP	Actin Binding Protein
AFM	Atomic Force Microscopy
MTC	Magnetic Twisting Cytometry
MPTM	Multiple Particle Tracking Microrheology
MSD	Mean Square Displacement
τ	Time Lag
D	Diffusion Coefficient

k_b	Boltzmann's constant
T	Temperature
a	Particle Radius
η	Fluid Viscosity
Γ	Creep Compliance
G^*	Complex Shear Modulus
Γ	Gamma Function
α	First Derivative of MSD Curve, Anomalous Diffusion Coefficient
β	Second Derivative of MSD Curve
G'	Elastic (Storage) Modulus
G''	Viscous (Loss) Modulus
HUVEC	Human Umbilical Vein Endothelial Cell
TCM	Tumor Conditioned Media
CM	Control Media
AM	Adipogenic Media
OM	Osteogenic Media
MDM	Mixed Differentiation Media
SEM	Standard Error of the Mean
TS	Traction Stress
MLCK	Myosin Light Chain Kinase
MYH9	Myosin Heavy Chain 9
MYL9	Myosin Light Chain 9
ESC	Embryonic Stem Cell

iPSC	Induced Pluripotent Stem Cell
qRT-PCR	Quantitative Real-Time Polymerase Chain Reaction
δ	Phase Angle
GTA	Glutaraldehyde
G	Gelatin
ALP	Alkaline Phosphatase
E	Young's Modulus
F	Force Exerted
A_0	Initial Area of Scaffold
ΔL	Change in Length
L_0	Initial Length
LoG	LaPlacian of Gaussian
W_d	Dry Weight
W_w	Wet Weight
PBS	Phosphate Buffered Saline
BCA	Bicinchoninic Acid
CCM	Control Conditioned Media
EGTA	Ethylene Glycol Tetraacetic Acid
FAP	Fibroblast Activation Protein
FSP	Fibroblast Specific Protein
MMP	Matrix Metalloproteinase
MDA	MDA-MB-231 Cell Line
CTRL	Control

RTK	Receptor Tyrosine Kinase
TGFβR	Transforming Growth Factor β Receptor
PDGFR	Platelet Derived Growth Factor Receptor
VEGFR	Vascular Endothelial Growth Factor Receptor
ρ	Pearson's coefficient
CFSE	Carboxyfluorescein Succinimidyl Ester

SUMMARY

Mesenchymal stem cells (MSCs) are multipotent cells that are recruited to sites of inflammation, where they interact with the microenvironment to induce tissue regeneration. As a result, MSCs have shown promise clinically as candidates for tissue engineering and therapeutic targets; however, implementation in the clinic has been limited by an incomplete understanding of how mechanical and chemical cues provided by the microenvironment influence MSC behavior. We first show how molecular cues change the intracellular mechanical properties of differentiating MSCs. We then developed 3D gelatin scaffolds for the expansion and differentiation of MSCs. We found that the composition of the scaffold dictated whether the mechanical or architectural properties directed MSC differentiation. In addition to aiding in tissue regeneration, MSCs are also recruited to tumors, where they interact with the tumor microenvironment to promote metastasis. We sought to elucidate if MSCs are differentially adherent, and potentially recruited more frequently, to metastatic versus nonmetastatic tumors. We found that MSCs are more adherent to metastatic cancer cells and this response can be reversed by blocking the adhesion molecule cadherin 11. Finally, we utilized a 3D coculture model to determine how interactions between metastatic cancer cells and MSCs influence cancer cell invasion. Coculture with MSCs induced directional migration in cancer cells that was dependent on transforming growth factor β (TGF-β) and downstream mechanosensitive pathways. These studies elucidate how MSCs interact with their environment and may have important implications in biomaterial design and the development of cancer therapeutics.

CHAPTER 1

INTRODUCTION

1.1 Mesenchymal Stem Cells and Sites of Inflammation

Mesenchymal stem cells (MSCs) are bone marrow-derived cells that have the ability to differentiate into connective tissue types [1]. Natively, MSCs are mobilized from the bone marrow and recruited to sites of inflammation [2], including damaged tissue and tumors. Within these environments, MSCs have several functions, including differentiating into tissue-specific cell types [1], inducing angiogenesis [3], and modulating the immune system [4]. Tissue injury leads to immune activation and secretion of a number of inflammatory molecules, including platelet-derived growth factor (PDGF), transforming growth factor-β (TGF-β), epidermal growth factor (EGF), vascular endothelial growth factor (VEGF), fibroblast growth factor (FGF), and stromal cell-derived factor-1 (SDF-1), which induce MSC migration [5,6]. MSCs differentiate into myofibroblasts in response to these factors [7,8], which produce extracellular matrix (ECM) and contractile force to promote healing [9]. Upon completion of wound healing, myofibroblasts undergo apoptosis to restore normal tissue homeostasis [9].

MSCs can directly interact with immune cells to alter the immune response and influence tissue healing. MSCs suppress inflammation by secreting TGF-β and prostaglandin E2, which alter the cytokine secretion profiles of dendritic cells, T cells, and natural killer cells [4]. Consequently, MSCs are thought to be important mediators of

wound healing as inflammation suppression is a critical step for proper wound healing [10]. In some instances MSCs promote inflammation; however, it is not understood why MSCs are immunosuppressive in some instances and inflammatory in other contexts [11]. MSCs may worsen or improve disease depending on whether MSCs display an inflammatory or immunosuppressive phenotype. It appears that the microenvironment can have profound effects on the inflammatory phenotype of MSCs [11], suggesting MSCs are influenced by cues from the extracellular environment.

1.1.1 MSCs and Tissue Regeneration

MSCs differentiate into a number of connective tissue cell types, including adipocytes, osteoblasts, chondrocytes [1], and myoblasts [12]. MSCs can be isolated from adult bone marrow, circumventing the ethical issues associated with embryonic stem cells (ESCs). In addition, MSCs are immunosuppressive [4], allowing for allogenic transplantation. As a result of these characteristics, MSCs have shown promise for tissue regeneration applications. Clinical trials utilizing MSCs for the treatment of a number of degenerative diseases, including myocardial infarction, diabetes, spinal cord injury, graft versus host disease, and orthopedic injuries, are currently underway [13].

Successful translation of MSCs for tissue regeneration in the clinic is dependent on control of MSC function and differentiation. MSCs require specific chemical factors to differentiate along each lineage [1]. Soluble factors can also influence MSC lineage [14]. EGF, but not PDGF, induces MSC differentiation along the osteogenic lineage [15]. TGF-β enhances both myogenesis [7] and chondrogenesis [1]. MSCs also secrete a number of soluble factors that allow for tissue repair through angiogenesis induction, production of ECM, and direct differentiation (**Table 1.1**).

Table 1.1 Growth factors critical for MSC-mediated tissue regeneration [11].

Soluble Factors	Role in MSC-mediated Tissue Regeneration
EGF	Wound healing, tissue regeneration
PDGF	Tissue repair
FGF	Tissue repair, cell survival and regeneration
TGF-β	Wound healing
VEGF	Angiogenesis, wound healing
IGF-1	Wound healing

In addition to biochemical signals, MSCs are also influenced by mechanical signals. Mechanical stimulation can improve differentiation along the myogenic [7] and osteogenic lineages [16]. The stiffness of the ECM can direct MSC lineage [17]. Stiffer environments are more conducive for osteogenesis, whereas MSCs differentiate along the adipogenic lineage in soft environments. The geometry of ECM can also influence MSC differentiation [18,19]. MSCs that are unable to spread differentiate along the adipogenic lineage [19]. In contrast, highly spread MSCs differentiate into osteoblasts [19]. Shear stress enhances osteogenesis [20] and endothelial differentiation [21] of MSCs. Mechanical signals also influence the angiogenic properties of MSCs. Mechanical stimulation enhances angiogenesis through FGFR1 and VEGFR signaling [22]. MSCs utilize adhesion molecules to attach to endothelial cells and promote blood vessel sprouting [23]. In addition, ECM degradation is required for MSC-mediated blood vessel growth [24].

1.1.2 MSCs and Cancer

Tumors are thought of as wounds that do not heal, as the tumor microenvironment resembles wound tissue [25]. Inflammatory factors secreted by wounds are also secreted by tumors and facilitate the recruitment of a number of cell types that support the growth

of the tumor, including endothelial cells, immune cells, fibroblasts, and MSCs [26]. Within the tumor, MSCs contribute to angiogenesis and tumor growth through the secretion of IL-6 [27], CCL5 [28], SDF-1, and VEGF [29]. In addition, CCL5 secreted by MSCs promotes breast cancer metastasis [28]. Consequently, MSCs have been proposed as therapeutic targets for cancer.

Tumor-secreted soluble factors induce MSC differentiation into carcinoma-associated fibroblasts (CAFs), which have a myofibroblast-like phenotype [30] and serve similar functions to myofibroblasts within wounds. CAFs produce and crosslink ECM, provide contractile force, promote angiogenesis [31], and induce inflammation [32]. It is hypothesized that CAFs stiffen the ECM, which promotes a malignant phenotype [33]. CAFs are thought to be a rate-limiting determinant for tumor progression [34], as the presence of a CAF gene signature is associated with poor patient prognosis [35]. Thus, MSCs serve similar functions in wounds [10] and tissues [29]. MSCs recruited to damaged tissue are involved in tissue repair allowing for tissue regeneration. In contrast, MSCs present in tumors promote disease progression.

1.2 Cell Mechanics

Cells are exposed to a variety of biochemical and mechanical signals from the extracellular environment. Cells sense and respond to mechanical signals by altering their intracellular mechanical properties in order to resist forces. These mechanical signals can be transduced into biochemical signals inside the cell which ultimately regulate gene expression and cell phenotype. Thus, intracellular and extracellular mechanical properties can have profound effects on how cells behave, influencing both normal and disease states.

1.2.1 Cell Adhesion, Force Generation, and Migration

Cells are anchored to the extracellular environment through cell adhesion proteins. ECM is a scaffold of proteins that provides structural stability and mechanical and biochemical cues critical for the formation, maintenance, and repair of tissues. These proteins contribute to the rigidity and viscoelasticity of tissues. In addition, ECM regulates the availability and activity of soluble factors. Cells dynamically remodel the composition, physical properties, and topography of ECM. Integrins on the cell surface bind to specific ligands in the ECM, such as collagen, fibronectin, and laminin. These receptors are involved in migration, invasion, ECM remodeling, proliferation, and survival [36].

The actin cytoskeleton inside the cell is linked to the ECM through focal adhesions, which consist of transmembrane integrins that bind to matrix proteins and cytoplasmic proteins that link integrins to actin filaments (**Figure 1.1**). A number of cytoplasmic proteins make up focal adhesions, including focal adhesion kinase (FAK), paxillin, talin, vinculin, zyxin, vasodilator-stimulated phosphoprotein (VASP), and α-actinin [37]. Focal adhesions transmit force between inside the cell and the extracellular environment. Interactions between myosin motors and actin generate traction forces. This force generation is activated by phosphorylation of myosin light chain (MLC) [38]. Rho-kinase (ROCK) regulates the phosphorylation of MLC and is responsible for generating traction forces at focal adhesions [39]. Force transmission plays a critical role in many cellular processes, including proliferation [40], differentiation [17], and migration [41].

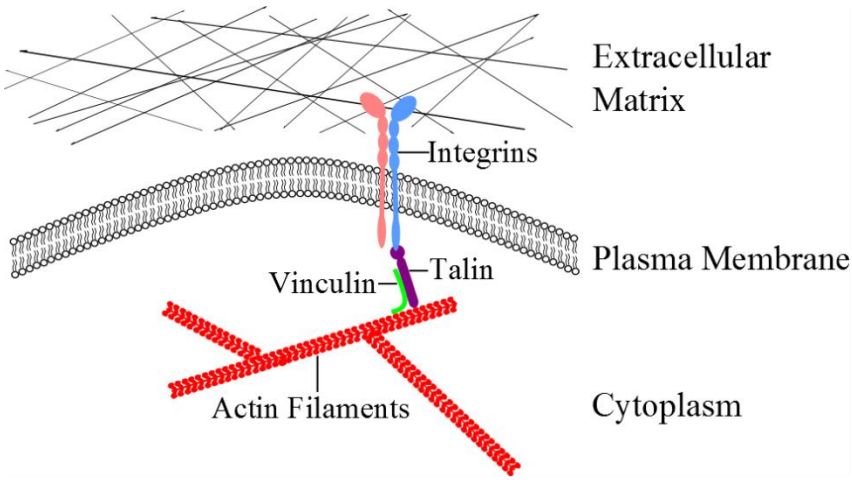

Figure 1.1 Diagram of the connection between the actin cytoskeleton and ECM. Actin filaments bind to focal adhesion proteins (vinculin and talin) which form a complex with integrins.

Traction forces exerted by cells can be measured using traction force cytometry. This technique involves seeding cells on a perfectly elastic substrate with embedded particles. Cells pull on the matrix, displacing the beads. Cells are then detached causing the beads to return to their unstressed position. The displacement of the beads can be related to the traction stress using the following equation:

$$Displacements(\vec{r}) = G(|\vec{r} - \vec{r}'|) \otimes Traction(\vec{r})$$

G is Green function and r is displacement.

Cells coordinate mechanical and biochemical signals in order to migrate. Cell motility is critical for the formation and organization of tissues. In addition, motility plays a role in a number of disease states, including wound healing, tissue regeneration, and metastasis. A number of coordinated steps must occur for a cell to migrate (**Figure 1.2**). Cells first polymerize actin to polarize their forces and form a protrusion at the leading edge. This leading edge then forms adhesions to the ECM. Proteases that degrade

ECM are then secreted to allow space for the migrating cell. Myosin provides the force to contract the cell body. Finally, adhesions are turned over which allows for the cell to move forward [42].

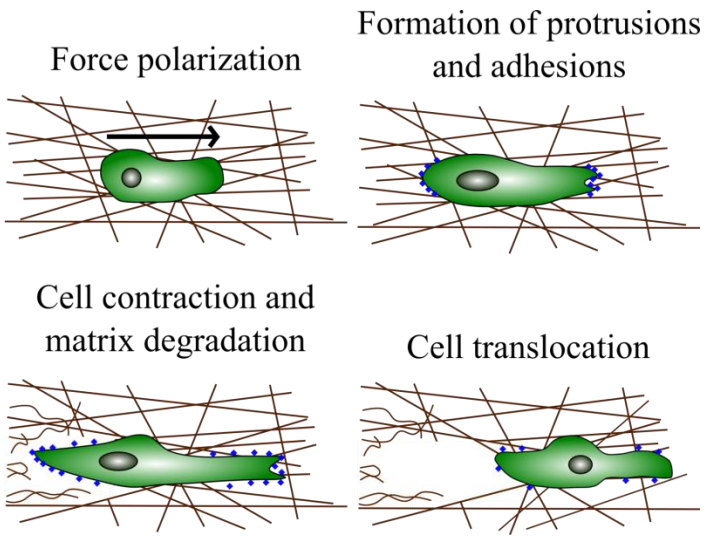

Figure 1.2 Diagram of the steps of cell migration.

Epithelial cells maintain cell-cell contacts and interactions with the basement membrane, which maintain tissue homeostasis. During development or after tissue injury, cells will undergo changes to a mesenchymal phenotype, known as epithelial to mesenchymal transition (EMT), that allow it to become more motile. Epithelial cells express high levels of E-cadherin, a cell-cell adhesion molecule, and ECM proteins laminin 1 and collagen IV [43]. During EMT, cells downregulate these proteins and gain expression of integrins including α5β1 integrin, the ECM protein fibronectin, and cell adhesion proteins N-cadherin and OB-cadherin [43]. In addition, cells reorganize their cytoskeleton and alter extracellular force generation after EMT [44]. This allows for cells

to remodel and interact with ECM in order to invade. Evidence of EMT has been observed at the invasive fronts of tumors [45] and in patients [46]. This suggests that acquisition of this phenotype allows tumor cells to acquire a more malignant phenotype [47].

CHAPTER 2

THESIS OVERVIEW

MSCs are natively recruited to sites of inflammation, including wounds and tumors. The biochemical and mechanical characteristics of the microenvironment that MSCs interact with influences their ability to promote tissue healing or worsen disease state. MSCs are strong candidates for tissue engineering and therapeutic targets for cancer because of these characteristics. The overall goal of this project was to understand how MSCs interact with their microenvironment in the context of tissue regeneration and cancer to develop novel tissue engineering and cancer therapeutic strategies.

We first provide an overview of intracellular particle tracking microrheology. We then simultaneously measured intracellular rheology and extracellular force generation to determine how MSCs alter forces during differentiation in environments that were favorable and non-conducive for differentiation. We probed intracellular and extracellular force generation in response to chemical differentiation factors and substrate rigidity. We hypothesized that MSCs would alter their intracellular rheology and extracellular force generation in order to differentiate and this may be an indicator of differentiation potential. In addition, we sought to determine if MSCs spatially regulate their intracellular and extracellular forces during differentiation.

In order to understand the effects of matrix architecture on MSC function, we developed cross-linked gelatin scaffolds with varying architectural and mechanical properties. We evaluated the proliferation and differentiation along the myogenic and

osteogenic lineages of MSCs cultured on scaffolds. We hypothesized that matrix architecture could promote the self-renewal and directed differentiation of MSCs.

We next sought to elucidate how MSCs engraft in tumors. We hypothesized that differences in cell adhesion may contribute to the differential engraftment of the CAF precursors fibroblasts and MSCs to invasive tumors. To test this, we analyzed the adhesion of fibroblasts and MSCs to invasive and non-invasive breast, ovarian, and prostate cancers. We then elucidated how stromal cells attach to invasive cancer cells to identify new targets to prevent stromal cell recruitment.

In order to determine how MSCs interact with invasive breast cancer cells to induce invasion, we utilized a 3D coculture model. We measured the migration in conjunction with force generation of metastatic breast cancer cells in coculture with MSCs. Pathways involved in MSC-induced migration were identified and inhibited, providing potential targets for blocking cancer cell invasion and subsequent metastasis.

CHAPTER 3

INTRACELLULAR RHEOLOGY[1]

3.1 Introduction

Mechanical stress can be generated from cellular processes such as cell migration [48–50], stem cell differentiation [17], protein unfolding [51], and cancerous transformation [52]. It also plays a role in various physiological and pathological events, such as embryonic development [53,54], organogenesis [55], tissue regeneration [56], and tumor growth [57]. During these events, cells respond to the mechanical stress not only with simultaneous cytoplasmic deformation but also with dynamic cytoskeleton remodeling to continually dissipate stress. Together, how the cytoplasmic region of a cell responds to external forces, i.e., the intracellular rheological property, is of interest and essential to thoroughly understand those cellular events.

The molecular mechanisms for cells to dynamically regulate the intracellular rheological properties to respond to the physical shear stress and chemical cues from external environments are conserved across all cell types and species [58]. It requires the reorganization of the cytoskeleton, a complex network which acts as a scaffold to support the cell's structure from the cell cortex to the nucleus [59]. The cytoskeleton contains three filamentous structures, actin (F-actin), microtubules and intermediate filaments. Among them, the rheological properties of actin-cytoskeleton are most well-studied. Intracellular mechanics have previously been related mainly to the organization of F-actin [60,61], which controls cell shape, structure, and force generation [62]. Chemical

[1] Adapted from: Dawson, MR, Tseng, Y, Lee, JS, & McAndrews, KM. "Intracellular Particle Tracking Rheology." In: C. P. Neu & G. M. Genin (Eds.), *Handbook of Imaging in Biological Mechanics* (pp. 377–384). CRC Press, 2014. ISBN 978-1-466-58813-4

and physical stimuli from the extracellular environment alter cell mechanics through Rho GTPases, including RhoA, Rac1 and Cdc42, which act as the molecular switches to interact with downstream effector molecules and trigger signaling pathways to manifest actin cytoskeleton re-organization [18,19,63].

The actin-cytoskeleton contains a multitude of regulatory proteins, molecular motors, and actin-binding proteins (ABPs) that together mediate the organization of actin-cytoskeleton. The actin stress fibers link the actin-cytoskeleton to the ECM via focal adhesions. Motor protein myosin binds to F-actin and utilizes ATP to generate contraction force that propagates tension along actin filaments [64]. Distinct ABPs individually possess specific actin-binding activities, such as severing and elongating to regulate the filamentous length of actin filaments, branching, crosslinking and bundling to formulate the architecture of the actin network, and sequestering and nucleation to control the amount of available globular actin (G-actin) for filament formation in the cytoplasmic pool. Together, the functions and activities of motor proteins and ABPs provide dynamics and structural diversity to support a broad range of rheological properties and architecture to the actin network.

3.2 Fluid Mechanics and Cell Rheology

Rheology is the study of deformation of soft matter, which is used to explain the mechanical behavior of complex fluids, including polymeric solutions, colloidal suspensions and biological gels. Complex fluids are viscoelastic in nature since they act as elastic solids (resisting permanent deformation) at short times and viscous fluids (deforming irreversibly) at longer times [65]. A rheometer is a tool to characterize the time- or frequency-dependent viscoelastic properties of complex fluids from the

mechanical deformations that result from the application of controlled stress or strain [66]. Bulk-fluid rheometers have previously been used to characterize the mechanical behavior of reconstituted solutions of cytoskeletal proteins [67]; however, these tools are not applicable to living cells with respect to their small size and soft cytoplasm that requires the application of extremely small forces (~ pN) and deformations (~ nm) [68]. Quantitative microscopic techniques, such as atomic force microscopy (AFM), micropipette aspiration, magnetic twisting cytometry (MTC), and multiple particle tracking microrheology (MPTM) have been developed in recent years to characterize the rheological properties of the cell cytoskeleton in microscopic domains for their rheological response during intracellular processes.

3.3 Limitations of Current Methods for Measuring Cell Mechanics

Current methods for measuring cellular rheology include AFM, micropipette aspiration, and MTC, as shown in **Figure 3.1**.

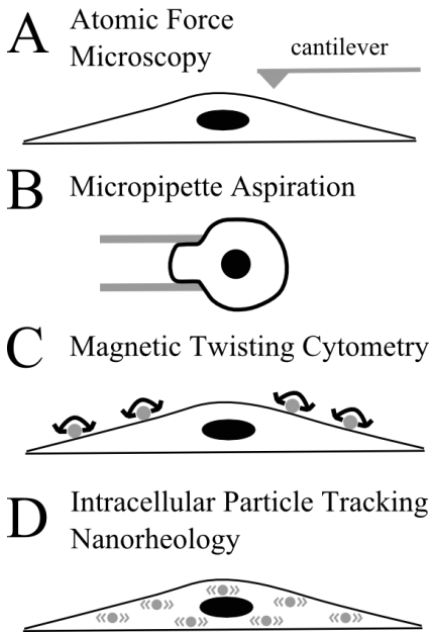

Figure 3.1 Current methods for measuring cell rheology.

Utilizing AFM, cell mechanical properties are determined from the deflections of a cantilever tip on a cell surface. AFM results depend heavily on the accuracy of the spring constant of the tip and the interaction of the tip with the cell surface, which in turn may change the mechanical properties of the cell for subsequent measurements [69]. Moreover, it is only capable of measuring surface properties that may reflect larger actin stress fibers or membrane properties. Micropipette aspiration involves deforming a cell by aspirating it into a micropipette and measuring the geometric changes of the whole cell as bulk cellular rheology. In MTC, ligand-coated magnetic beads are attached to the surface of the cell and magnetic pulses are applied which deform the cell. Rheological properties measured with MTC vary depending on the ligand chemistry and density on the probe beads [70], which given heterogeneous molecule expression across the cell could lead to results that are inconsistent or unable to be compared between experiments. All of the aforementioned methods are also unable to simultaneously measure multiple points across a cell and as such are time consuming and relatively low-throughput. In addition, as mechanical properties are probed from the extracellular surface, this limits local measurements of intracellular microrheology and analysis of cytoskeletal heterogeneity. Finally, applications of AFM and micropipette aspiration are limited to those in which the probe can directly contact the cell and thus prevents the measurement of cells in three-dimensional environments or cells subjected to flow.

3.4 Intracellular Particle Tracking Microrheology

In order to better assess intracellular cytoskeletal heterogeneity and avoid the difficulties associated with other extracellular rheological measurement methods, MPTM was developed [71]. MPTM can be used to determine the mechanical properties of

complex fluids with the accuracy of traditional bulk-fluid strain-controlled cone and plate rheometry [72]. MPTM can also be used to probe the local mechanical properties of complex fluids within microscopic domains, which is not possible with bulk-fluid rheological techniques. For the original approach, fluorescent submicron particles were microinjected into the cytoplasmic region of individual cells. This method was improved in efficiency by the development of ballistic intracellular particle tracking nanorheology to massively inject submicron particles into a million cells at once [73], thereby making it a powerful technique for quickly characterizing the rheological properties of samples that could not be achieved before.

Using MPTM, the displacements of the submicron particles, which result from the interaction between the particles and its surrounding cytoskeletal network, are used to determine the rheological properties of the cell cytoplasm (**Figure 3.1D**). It offers unique capacities compared to other methods for measuring the rheological properties of cells. Embedding particles in the cytoplasm allows for highly localized rheological measurements without the use of external probes [74]. Cytoplasmic viscoelasticity can be analyzed with this method in a variety of different conditions, including 3D culture [52,75], shear [73], and *in vivo* [76]. Moreover, the contributions of the plasma membrane and nucleus to the mechanical properties of the cell can be distinguished from cytoskeletal contributions [77]. Rheological measurements for a single cell can be acquired under a minute so that the short-term response of cells to specific factors can be analyzed [48,78]. The technique has also been used to determine the viscoelasticity of concentrated solutions of DNA [79], cystic fibrotic sputum [80], and actin filament solutions [81–84] in addition to the cell cytoplasm [48,49,73–75,77,78].

The displacements of fluorescent particles embedded in the filamentous network (**Figure 3.2**) are captured using a fluorescence microscope with high magnification and a fast speed camera for good spatial and temporal resolution.

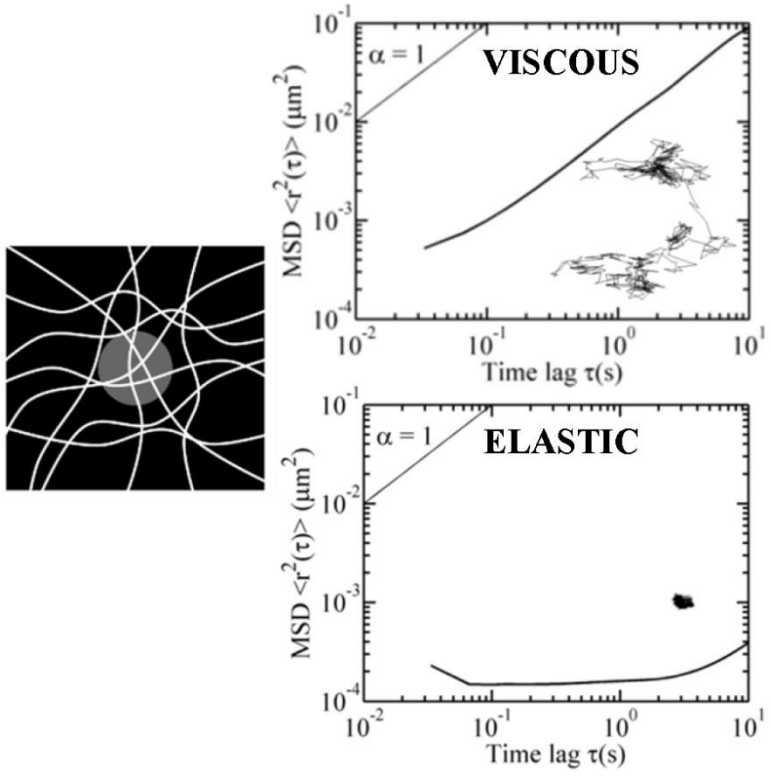

Figure 3.2 Brownian motion and mean square displacements of nanoparticles embedded in the cytoplasm. Schematic of particle embedded in the cytoplasm (left). Example traces and mean square displacement (MSDs) plots of cytoplasm with viscous (top right) and elastic (bottom right) character.

High resolution of particle displacements is obtained by tracking the intensity weighted centroids of the particles in the plane of focus of the objective. Particle trajectories in the focal plane are 2D projections of 3D displacements, thus, 2D tracking assumes that the fluid is locally isotropic. In 2D, the MSD of the particle is obtained by the following equation:

$$MSD = < r^2(\tau) > = < \left[x(t+\tau) - x(t) \right]^2 + \left[y(t+\tau) - y(t) \right]^2$$

The MSD of the particle is related to the local diffusivity of the network, which is determined:

$$D = \frac{\left\langle \Delta r^2(\tau) \right\rangle}{4\tau}$$

In a purely viscous fluid, such as water or glycerol, the thermal fluctuation-driven particle motion is only hindered by viscous drag with the Stokes-Einstein equation:

$$D = \frac{k_B T}{6\pi a \eta}$$

,

where D is the diffusion coefficient, k_B is Boltzmann's constant, T is temperature, a is particle radius, and η is viscosity of the fluid. Therefore, the particle tracking data can be used to extract the viscosity of the fluid surrounding the particle.

However, in the complex filamentous network space when the particle size is greater than the pore size of the meshwork, which is the distance between filaments aligned in any direction, particle motion is not only affected by the viscosity of the fluid but also the elasticity of the filamentous network. The creep compliance (Γ), which measures the deformability of the cytoplasm, can be directly calculated from the MSD:

$$\Gamma(\tau) = \left(\frac{3\pi a}{2k_B T} \right) MSD(\tau)$$

In order to facilitate analysis of additional viscoelastic properties of the cytoplasm, the MSD is transferred to the frequency domain. The frequency-dependent form of the Stokes Einstein equation is used to determine the viscoelastic properties of the fluid:

$$G^*(\omega) = \frac{2k_B T}{3\pi a \left\langle \Delta r^2 \left(\frac{1}{\omega} \right) \right\rangle \Gamma\left[\left(1+\alpha(\omega)\right)\left(1+\beta(\omega)/2\right) \right]}$$

where G^* is the frequency-dependent complex shear modulus, Γ is the gamma function (different from the creep compliance, Γ), α is the first derivative and β is the second derivative of the MSD curve. The complex shear modulus can be further divided into the in phase component, or elastic (storage) modulus (G'), and the out of phase component, or viscous (loss) modulus (G''):

$$G'(\omega) = \left|G^*(\omega)\right| \cos\left(\frac{\pi\alpha(\omega)}{2} \right)$$

$$G''(\omega) = \left|G^*(\omega)\right| \sin\left(\frac{\pi\alpha(\omega)}{2} \right)$$

Cells behave more like an elastic solid at high frequencies, or low time scales, with G' being greater than G''. Typical values of G' at 1 Hz are shown in Table 1. The shear viscosity can be estimated as the product of the plateau modulus and the relaxation time. The plateau modulus is the value of the elastic modulus at intermediate frequencies where it reaches a quasi-plateau value. Relaxation time is the inverse of frequency at which elastic and viscous moduli are equal.

3.5 Intracellular Particle Tracking Microrheology Applications

With MPTM, the mechanical properties of the cytoplasm are determined from the transport patterns of hundreds of individual nanoparticle probes. Each particle probes the rheology of the surrounding cytoplasm, which is heavily affected by differences in the degree of actin crosslinking and the local microstructure. Micromechanical mapping of Swiss 3T3 fibroblasts revealed the cytoplasm is significantly more heterogenous than reconstituted actin filament networks [74]. In addition, the perinuclear region is typically

more compliant than the lamella [74]. Crosslinking actin with α-actinin increases the stiffness and heterogeneity of the cytoplasm [74], in agreement with actin solution studies [85]. Statistical analysis of the distributions of particles' MSDs at specific time scales is used for heterogeneity analysis of the cytoplasmic region for different cell types or the same cell type under different treatments. Local mechanical properties from particle tracking analysis can also be traced back to specific regions of the cell, which can be used to determine how differences in cytoskeletal mechanics affect cell function.

Intracellular particle tracking microrheology has also been used to elucidate how fibroblasts spatially coordinate movement [49]. Rac1 and Cdc42 activation coordinate stiffening in the leading lamella and perinuclear region during migration [49]. Although depolymerizing microtubules has no effect on overall cell rheology, it prevents mechanical polarization and cell migration [49]. In addition, cancerous transformation potential has been associated with cytoplasmic stiffening in response to matrix stiffening[86], which is correlated with increased migration [87]. In contrast, treatment of human umbilical vein endothelial cells (HUVEC) embedded in a 3D peptide-based hydrogel with VEGF, which increases endothelial cell migration, decreases the elasticity of the cytoplasm [75]. This increase in elasticity can be reversed by inhibition of ROCK [75]. ROCK also plays an important role in stiffening of fibroblasts in response to flow [73]. Tumor conditioned media (TCM), which is a cocktail of pro-migratory factors that mimics factors secreted by tumors, induces stiffening and migration in both human and murine MSCs [48,78]. AFM, micropipette aspiration, and MPTM have been used to characterize the viscosity of human MSCs [78,88,89]. While AFM and micropipette aspiration viscosity measurements are similar, the viscosity measured with ballistic

intracellular particle tracking nanorheology is significantly different, presumably because it measures the local viscoelastisity of the cytoplasm, while the other methods mainly probe large stress fibers and include contributions of the nucleus and plasma membrane.

Cytoplasmic stiffness has been associated with metastatic potential in both breast cancer [90] and ovarian cancer [91]. The cytoplasm of OVCAR3 human ovarian cancer cells is viscoelastic, whereas OSE10 normal human ovarian epithelial cells are primarily viscous [92]. SKOV3 human metastatic ovarian cancer cells have a higher α value, or slope of the MSD curve, than both OSE10 and OVCAR3 cells (**Figure 3.3B**), suggesting less restricted particle movement in the cytoplasm. A distribution of MSDs exists in particles embedded in the cytoplasm of SKOV3 cells (**Figure 3.3C**), similar to previous reports with other cell lines [49,73,74,76–78,93]. The slope of the time-dependent creep compliance curve is higher than OSE10 and OVCAR3 cells (**Figure 3.4A**), indicating that SKOV3 have a more compliant cytoplasm in agreement with previous AFM measurements [91]. The viscous modulus (G'') dominates over the elastic modulus (G') at all frequencies. These results suggest the cytoskeletal network of SKOV3 is highly deformable, which may be important for squeezing through blood vessels in order to metastasize [50].

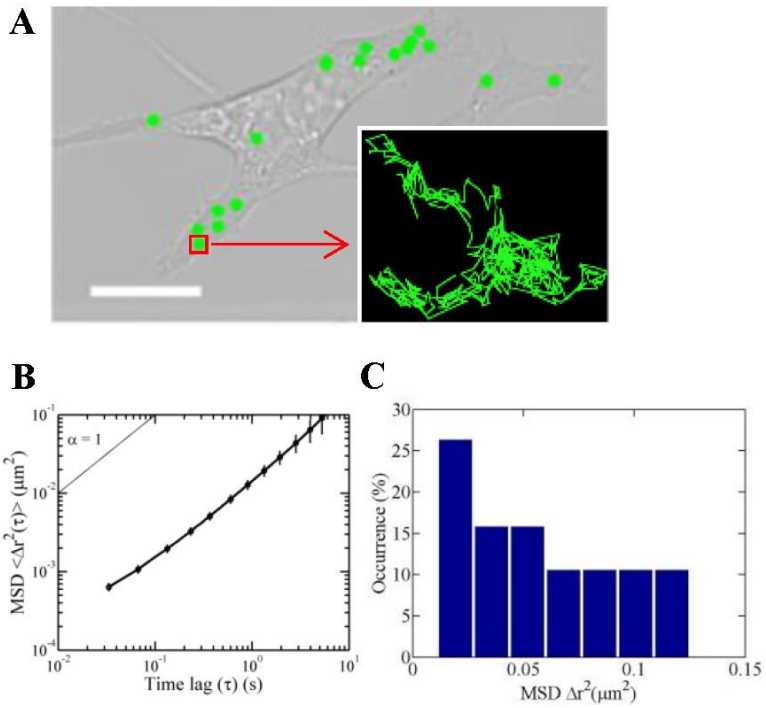

Figure 3.3 Brownian motion of nanoparticles embedded in the cytoplasm of SKOV3 cells. Phase-contrast micrograph of SKOV3 cell ballistically-injected with 100 nm green particles and trace of a single particle's motion (inset, A). Time-dependent ensemble average MSD of particles embedded in the cytoplasm of SKOV3 cells (B). Histogram showing the distribution of particle MSDs within a single SKOV3 cell for time scale τ = 1 s (C).

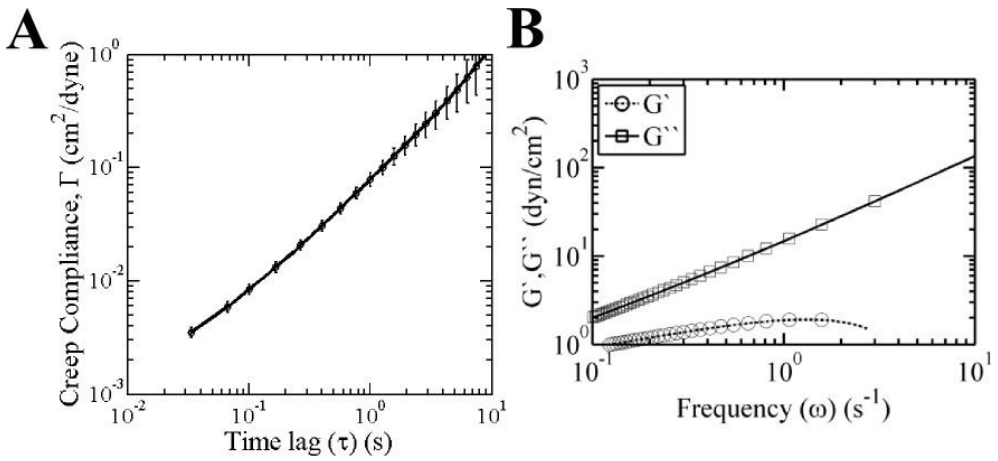

Figure 3.4 Creep compliance and viscous and elastic moduli for SKOV3 cells. Average creep compliance (Γ) of SKOV3 cells (A). Frequency-dependent viscous (G', dashed line) and elastic (G'', solid line) moduli of SKOV3 cells (B). Properties determined from ensemble-averaged MSD in Figure 1.5B.

3.6 Conclusions

Intracellular particle tracking microrheology is a powerful tool for measuring the mechanical properties of cells in physiologically relevant conditions. This method allows for the measurement of local rheological properties which cannot be measured with any other current method. In addition, intracellular particle tracking microrheology can be high-throughput and can measure changes in the intracellular rheological properties at multiple time scales. The corresponding changes in intracellular viscoelasity can elucidate a wide variety of critical cellular processes including differentiation, migration, cancerous transformation, and response to extracellular stimuli. Future applications for this technique include in vivo three-dimensional microrheology and screening of drugs for mechanical-related mechanisms.

CHAPTER 4

SPATIALLY COORDINATED CHANGES IN INTRACELLULAR RHEOLOGY AND EXTRACELLULAR FORCE EXERTION DURING MESENCHYMAL STEM CELL DIFFERENTIATION[2]

4.1 Summary

The mechanical properties within the cell are regulated by the organization of the actin cytoskeleton, which is linked to the extracellular environment through focal adhesion proteins that transmit force. Chemical and mechanical stimuli alter the organization of cytoskeletal actin, which results in changes in cell shape, adhesion, and differentiation. By combining particle-tracking microrheology and traction force cytometry, we can monitor the mechanical properties of the actin meshwork and determine how changes in the intracellular network contribute to force generation. In this study, we investigated the effects of chemical (differentiation factors) and mechanical (substrate rigidity) stimuli important in MSC differentiation on the intracellular mechanics and traction stress generation. We found the presence of adipogenic factors resulted in stiffening of the actin meshwork regardless of substrate rigidity. In contrast, these factors increased traction stresses on hard substrates, which was associated with increased expression of contractility genes. Furthermore, MSCs cultured on hard substrates expressed both adipogenic and osteogenic markers indicative of mixed differentiation. On hard substrates, heterogeneity in the local elastic modulus-traction stress correlation was also increased in response to adipogenic factors, indicating that

[2] Adapted from: McAndrews, KM, McGrail, DJ, Quach, ND, & Dawson, MR. (2014). Spatially coordinated changes in intracellular rheology and extracellular force exertion during mesenchymal stem cell differentiation. *Physical Biology*, 11(5), 056004.

these mechanical properties may be reflective of differences in level of MSC differentiation. These results suggest intracellular rheology and traction stress generation are spatially regulated and contribute insight into how single cell mechanical forces contribute to MSC differentiation.

4.2 Introduction

MSCs are adult bone marrow-derived stem cells with the ability to differentiate into connective tissues, including adipocytes and osteoblasts [1]. MSCs are ideal for tissue engineering applications due to their multipotency and immunosuppressive characteristics [4]; however, an incomplete understanding of how microenvironmental factors collectively direct stem cell fate hinders their therapeutic potential. Current techniques, such as histological staining and transcriptional analysis, measure the overall rate of MSC differentiation, not local differences in differentiating cells. A holistic understanding of how the microenvironment, including soluble factors and mechanical cues, directs stem cell differentiation on a cellular level is critical for clinical translation of MSC-based therapeutics.

Early MSC differentiation studies utilized a cocktail of soluble factors to induce differentiation on tissue culture plastic [1]; however, further studies demonstrated that biophysical factors such as matrix rigidity [17], cell shape [19], and geometric cues [18] also influence differentiation. In addition, mechanical cues, including intracellular and extracellular mechanics, can influence the effects of soluble factor cues from growth factors and cytokines [14]. This led to probing of intracellular mechanical properties [88,94,95] and traction force generation [96–98] and forecasting of stem cell fate based on actin cytoskeleton organization [63].

During the differentiation process, MSCs rearrange their cytoskeleton [63,99] which leads to changes in intracellular mechanical properties [95] and traction force generation [98]. Traditional intracellular mechanical characterization techniques, such as AFM, typically do not allow for simultaneous measurement of traction forces; consequently, the connection between intracellular and extracellular forces is not completely understood. MPTM, which involves tracking the motion of hundreds of individual particles embedded in the cell cytoplasm, can be used to rapidly probe the local and bulk rheological properties of the cell cytoplasm to determine mechanical properties in a high-content and spatial manner [92]. Cells ballistically injected with nanoparticles can be cultured on elastic substrates for simultaneous measurement of intracellular rheology and cell traction stress.

In this study, we combined MPTM and traction force microscopy to gain further insight into the mechanical properties and force generation of MSCs undergoing differentiation. Human MSCs were cultured on soft (~2 kPa) and hard (~8 kPa) substrates in the presence of control, adipogenic, osteogenic, and mixed differentiation media. We monitored local intracellular rheological properties and traction stress simultaneously and found MSCs increase the elastic character of their cytoplasm in response to adipogenic factors. On soft substrates, which were conducive for adipogenesis, cells did not alter traction stresses in response to differentiation factors; however, on hard substrates traction stresses increased in cells cultured with adipogenic factors. This increase in traction stresses was associated with an increase in heterogeneity in the correlation between local intracellular rheology and local traction stress as well as decreased adipogenesis. The percentage of areas in the cell with highly elastic cytoplasm and high

local traction stress also increased, suggesting cells spatially regulate cytoplasmic elastic modulus and traction stress in response to these factors. Gene expression analysis revealed MLCK and MYH9 were both upregulated, which is potential mechanism by which these cells increase traction stresses. This study establishes that MSCs spatially alter cytoplasmic rheology and traction stresses during differentiation.

4.3 Results

4.3.1 Differentiation Capacity of MSCs in Response to Mechanical and Chemical Factors

In order to analyze the ability of MSCs to differentiate along the adipogenic and osteogenic lineage, qRT-PCR and histological staining were performed after 3 and 5 weeks of culture, respectively. As previously observed [98], cells cultured in mixed differentiation media (MDM) displayed higher expression of adipsin on soft substrates (**Figure 4.1A**) and higher expression of osteocalcin on hard substrates (**Figure 4.1B**) though adipsin and osteocalcin expression in MDM were approximately equal to the negative control on glass and soft substrates, respectively. Though osteocalcin expression was higher for MSCs cultured in MDM on the hard substrate (8 kPa), this intermediate rigidity resulted in mixed differentiation into osteoblasts and adipocytes. These results were confirmed by histology with enhanced Oil Red O coverage on soft substrates (**Figure 4.1C**) and increased Alizarin Red on hard substrates (**Figure 4.1D**). These results suggest that in the presence of mixed chemical cues, the rigidity of the environment directs differentiation.

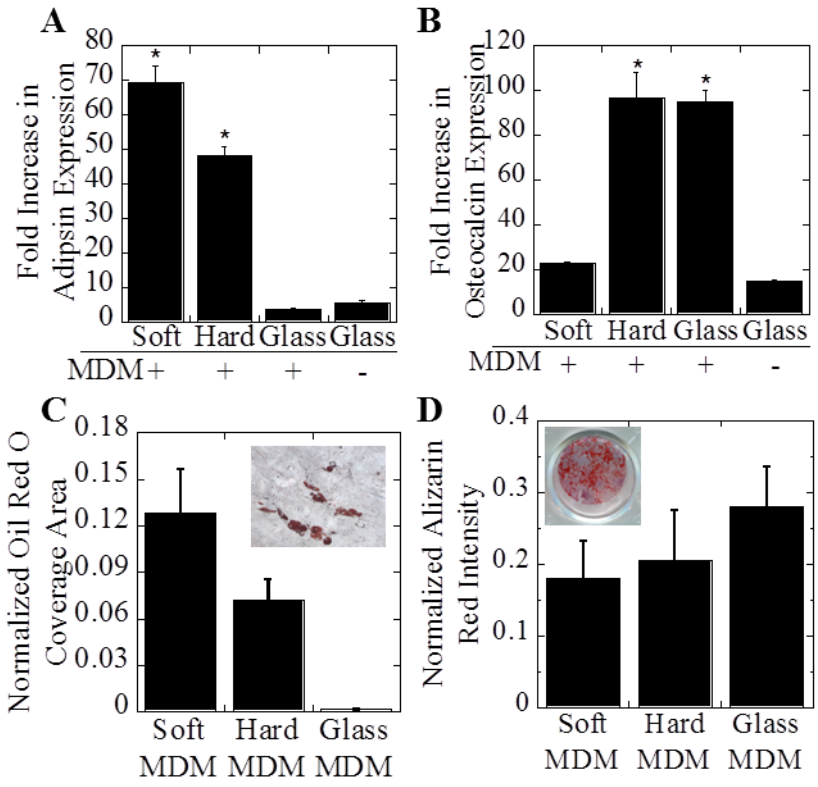

Figure 4.1 Differentiation capacity of MSCs cultured in different rigidity environments. mRNA expression analysis of adipogenic (A) and osteogenic (B) markers. GAPDH was used as an endogenous control and all data was normalized to the glass CM condition. Quantification of Oil Red O coverage (C) and Alizarin Red intensity (D). * denotes $p<0.05$.

4.3.2 Adipogenic Factors Increase Elastic Character of MSCs

MPTM was used to determine the local and bulk rheological properties of the cytoplasm for cells cultured in control or differentiation media on substrates early in the differentiation process (1 week). The use of MPTM allowed for the simultaneous measurement of intracellular rheological properties and traction stresses (**Figure 4.2A**). Substrate rigidity had no effect on the bulk rheological properties determined from the ensemble average particle MSDs (**Figure 4.2B**).

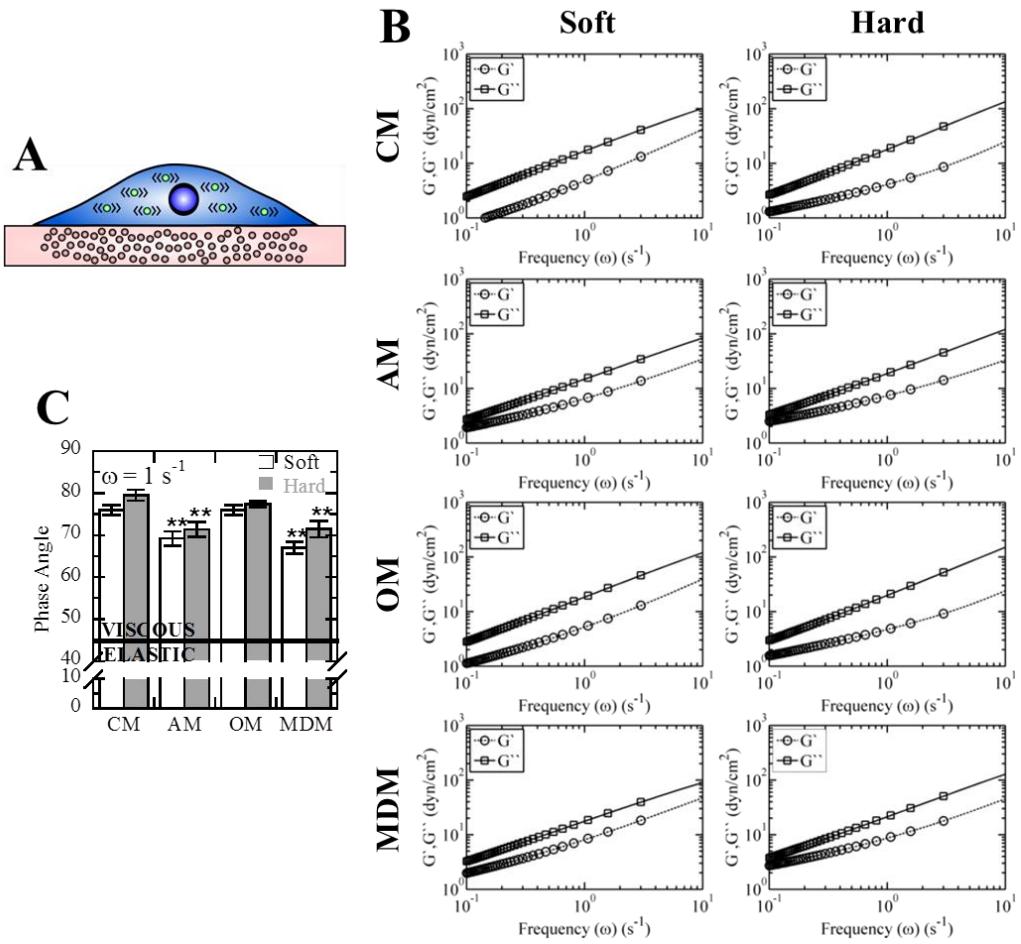

Figure 4.2 Microrheological characterization of MSCs undergoing differentiation on soft and hard substrates. Rheological properties and traction stresses of MSCs on substrates were simultaneously measured (A). Frequency-dependent elastic (G', open circles) and viscous (G'', open squares) moduli of differentiating MSCs (B). Viscoelastic character was determined by calculating the phase angle at 1 s^{-1} (C). ** denotes $p<0.01$.

The presence of adipogenic factors in either adipogenic media (AM) or MDM increased the elastic modulus (G') on both soft and hard substrates (**Figure 4.3A**). Differentiation and mechanical factors had less of an effect on the viscous modulus (G'', **Figure 4.3B**). To further characterize the viscous and elastic properties of the cytoplasm, the phase angle δ was calculated with δ = 90° for a liquid and δ = 0° for a solid. The MSC cytoplasm was primarily viscous for all conditions, as indicated by phase angles much larger than 45°. The phase angle was not altered by OM, indicating that osteogenic factors had no effect on the bulk mechanical properties within the range of substrate rigidities used in this study. AM and MDM significantly ($p<0.01$) decreased the phase angle in both soft and hard environments, suggesting that adipogenic factors were responsible for the intracellular stiffening response in MDM (**Figure 4.2**).

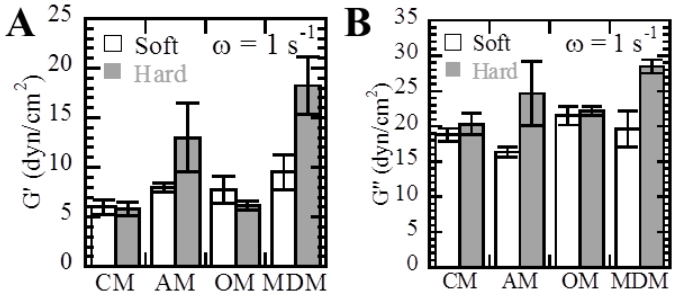

Figure 4.3 Rheological properties of MSCs differentiating on soft and hard substrates. Elastic (G', A) and viscous (G'', B) moduli of the cytoplasm of MSCs cultured on substrates with differentiation factors.

4.3.3 Stiffer Environments Lead to Altered Force Profiles in Response to Adipogenic Factors

Traction force cytometry was used to determine the traction stress profiles of differentiating MSCs. Traction stresses are affected by two main factors: substrate

elasticity, and matrix displacement. Traction stresses were independent of media composition on soft substrates where the mean traction stress was ~500 Pa for all conditions (**Figure 4.4A**). In agreement with previous studies [100], the traction stress on hard substrates was increased approximately 2-fold in control conditions and up to 5-fold when adipogenic factors were present. Analysis of the displacements on each substrate revealed that cells in AM and MDM maintained the same matrix displacements on soft and hard substrates, whereas displacements decreased for CM and OM (**Figure 4.4B**). Cells in CM and OM had similar traction stress profiles and displacements, suggesting increases in forces in MDM are due to adipogenic factors, not osteogenic factors.

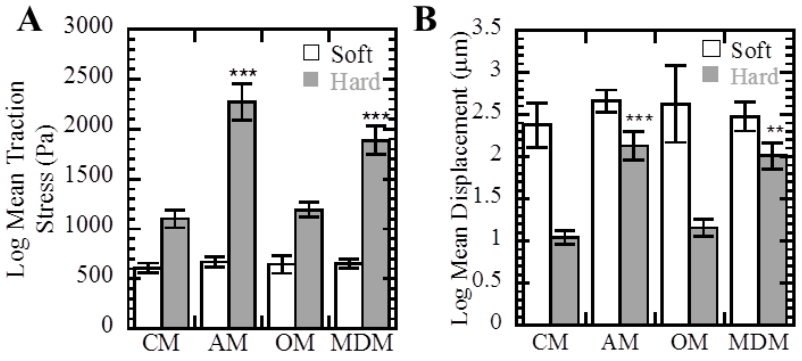

Figure 4.4 Traction stresses exerted by differentiating MSCs on soft and hard substrates. Quantification of log mean traction stress (A) and bead displacement (B) of cells cultured on different rigidity substrates in the presence of CM, AM, OM, or MDM. ** and *** denote $p<0.01$ and $p<0.001$, respectively.

4.3.4 Adipogenic and Mixed Differentiation Media Lead to Shifts in Rheology-Traction Stress Spatial Regulation in Hard Environments

In order to determine how local rheological properties are related to local traction stresses, the spatial relationship between these two properties was evaluated. For these calculations, the rheological properties of the cytosol surrounding a single particle were

calculated and related to the traction stress exerted on the substrate below that point (**Figure 4.5**).

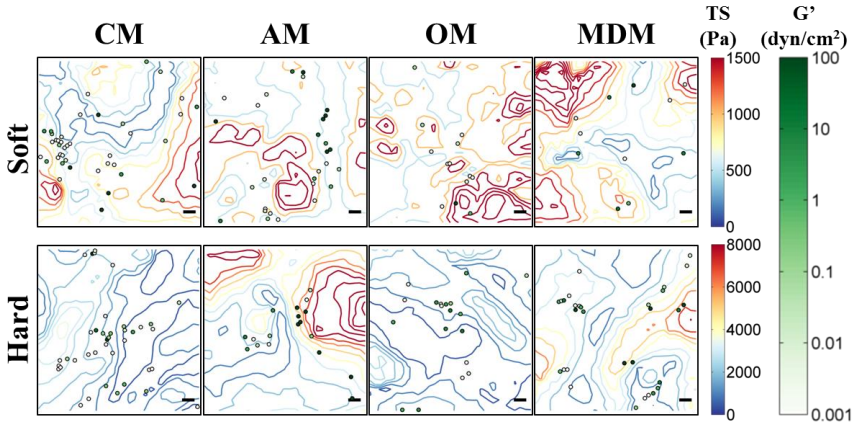

Figure 4.5 Spatial analysis of elastic modulus of the cytoplasm and traction stress. Contour maps of traction stress (TS) overlaid with local elastic modulus (G') surrounding particles embedded in the cytoplasm (scale bar=10 μm). Particles have been enlarged for visualization purposes.

Cells in AM and MDM on both rigidity substrates displayed an increased number of particles with high elastic modulus (G'). In addition, this number appeared to be further increased on hard substrates with AM and MDM. Particles associated with high G' also appeared to be colocalized with areas of high traction stress; therefore, spatial analysis of these two properties was performed to quantify this observation. On soft substrates, spatial regulation of traction stress and elastic modulus was relatively unaffected by differentiation media. The local elastic and viscous (G'') moduli and local traction stress of cells in CM or OM on hard substrates clustered around a low normalized traction force value and similar elastic modulus; however, the presence of adipogenic factors in AM and MDM introduced a large degree of heterogeneity in this relationship (**Figure 4.6**).

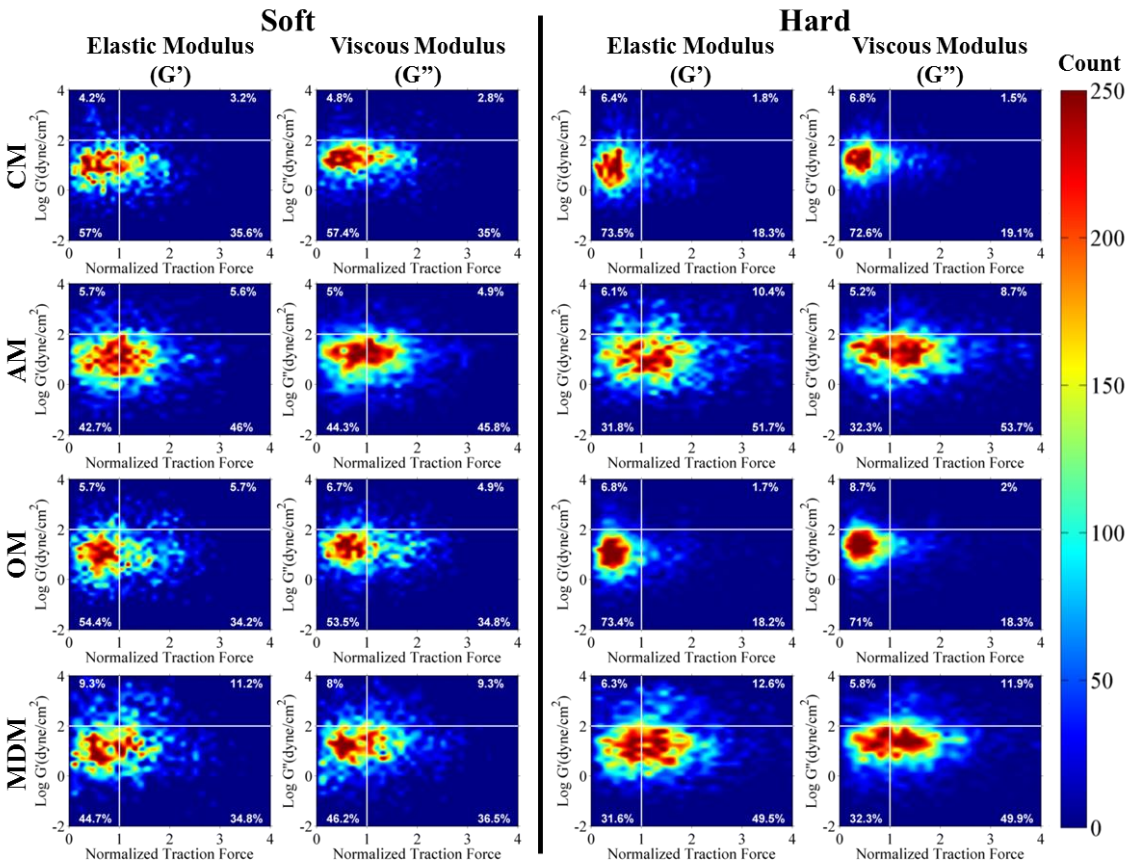

Figure 4.6 Correlation of traction stress with microrheological properties. Correlation of local elastic (G') and viscous (G'') modulus with local normalized traction force (B, n is number of particles analyzed. Soft CM: n=2389, Soft AM: n=3537, Soft OM: n=2031, Soft MDM: n=1889, Hard CM: n=3923, Hard AM: n=3830, Hard OM: n=4125, Hard MDM: n=4466). Heat bar is number of counts (intracellular particles analyzed).

In addition, the percentage of particles with a corresponding high traction stress increased for cells in AM and MDM on hard, with approximately a 5-fold increase of particles with high G' and high traction stress and a 2.5-fold increase in particles with low G' and high traction stress. A similar trend was found between traction stress and G''.

4.3.5 Increased Forces in Response to Adipogenic Factors are Associated with Increased Contractility Gene but not Adhesion Protein Expression

Cells exert forces through sites of adhesion; consequently, increased adhesion protein expression may lead to increased traction stresses. In order to determine if enhanced traction stresses exerted by cells was a result of increased adhesion protein expression, cells were stained for F-actin and vinculin and imaged using confocal microscopy. F-actin and vinculin distribution were similar across substrate rigidity and media conditions (**Figure 4.7A**). Quantification of the ratio of vinculin to F-actin [48] revealed vinculin expression was not upregulated in AM and MDM on stiff substrates (**Figure 4.7B**), suggesting the increase in traction force is not a result of increased adhesion.

Focal adhesion proteins connect the extracellular environment to the actin cytoskeleton, which mediates force generation through actin myosin contraction. Changes in contractility genes may lead to increased traction stress; therefore, we evaluated gene expression of MLCK, MYH9, and MYL9. On soft substrates, contractility genes were either downregulated or unchanged in MDM compared to CM; however, on hard substrates both MLCK and MYH9 were significantly upregulated (**Figure 4.7C**).

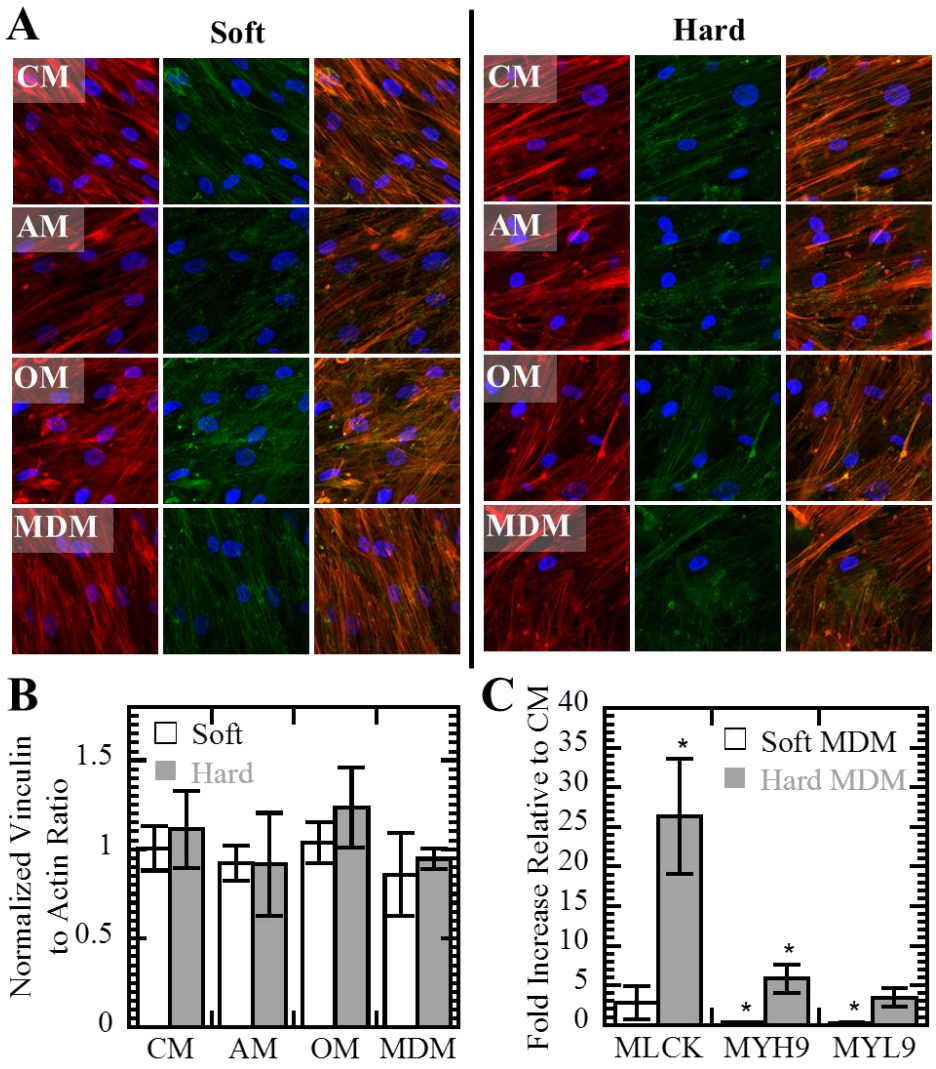

Figure 4.7 Analysis of mechanisms for traction stress generation. Maximum intensity projection immunofluorescent images of hMSCs stained for F-actin (red), vinculin (green), and nuclei (blue) (A). Images were used to calculate the vinculin to actin ratio and normalized to Soft CM condition (B). Gene expression compared to CM of MLCK, MYH9 and MYL9 (C). * denotes $p<0.05$.

4.4 Discussion

In this study, we simultaneously characterized changes in intracellular rheology and traction force generation during MSC differentiation on soft (~2 kPa) and hard substrates (~8 kPa). High rigidity environments are typically more conducive for osteogenesis, whereas low rigidity environments favor adipogenesis; however, high rigidity environments inhibit adipogenesis to a greater degree than low rigidity environments inhibit osteogenesis [98]. As a result, lower rigidity substrates were selected to allow for differentiation along both lineages. Initially, the cytoplasm was primarily viscous; however, the elastic character increased with exposure to adipogenic factors. MPTM has previously been utilized to show that undifferentiated ESCs, induced pluripotent stem cells (iPSCs) [93], and MSCs [48,78] have cytoplasms that are primarily viscous. In ESCs and iPSCs intracellular stiffening was also associated with the degree of stem cell differentiation [93,101]. A similar trend is present when comparing the cytoplasm of *C. elegans* embryos to that of more differentiated cells [48,78,93]. The cytoplasm of MSCs in AM and MDM had increased elastic character, suggesting this intracellular stiffening response during stem cell differentiation may be conserved in adipogenesis and may be critical for adipogenesis to occur. In addition, unspread cells are more likely to become adipocytes, whereas more spread cells are more likely to differentiate along the osteogenic lineage [19]. The actin cytoskeleton is a regulator of cell shape; thus, its ability to rearrange and alter its rheological properties may be critical for cell shape changes necessary for differentiation. The elastic character could also be a potential marker for MSC differentiation. Compared to traditional methods, MPTM can be performed without fixing or lysing cells which would allow for screening of

differentiation in live cells. In addition, changes in the cytoplasm were detected at 1 week, whereas traditional differentiation analysis techniques such as PCR and staining cannot detect differences until much later in the differentiation process (approximately 3-5 weeks).

We recognize that this intracellular stiffening response seems to contradict previous findings with AFM, which showed that adipocytes have lower elasticities than MSCs and osteoblasts [88]. However, this discrepancy may be a result of inherent differences in mechanical characterization techniques because AFM typically probes large stress fibers [69], whereas MPTM probes much smaller actin filaments on the order of nanometers [102] that are not accessible via AFM. Thus, particles embedded in cells for MPTM interact with smaller actin meshworks in the cell body, whereas AFM tips interact with significantly stiffer stress fibers in the cell cortex [77]. Since fully differentiated adipocytes lose their larger stress fibers [103], mechanical properties probed by MPTM may be more relevant for these more differentiated cells. In addition, decreased stress fiber formation has been associated with increased elastic moduli in cancer cells [52] and in MSCs treated with tumor-conditioned media [48]. Thus, the adipogenic process may lead to loss of stress fibers in favor of a more confined actin meshwork that has previously not been detected using other mechanical characterization techniques.

The rheological properties of cells were relatively unaffected by the presence of OM (**Figure 4.2, 4.3**). MSCs and osteoblasts have previously been shown in one study to have similar mechanical properties as measured by AFM [88]; however, there is not a clear consensus as to whether MSCs differentiating along the osteogenic lineage are

stiffer or softer than their undifferentiated counterparts [88,94,104]. Osteogenic differentiation is typically characterized by loss of thin parallel filaments and gain of a few actin filament bundles at the periphery of the cell [99]. MPTM cannot probe thick actin filaments [77] so these changes in cytoplasmic rheology may not be detected, but our results do demonstrate that the actin microstructure is unchanged during osteogenesis. Contrary to previous studies performed on microposts conducive for osteogenesis [98], OM also did not alter the traction stresses exerted by MSCs (**Figure 4.4**). Osteogenesis is typically favored in stiff environments [17,97]; consequently, MSCs may alter their rheological and traction profiles outside of the rigidity range studied here.

A relatively modest increase in substrate rigidity (~2 kPa to 8 kPa) led to dramatic traction stress exertion differences. Though traction stresses were increased in cells cultured in AM and MDM on hard substrates, on soft substrates, which were more conducive for adipogenesis (**Figure 4.1**), traction stress was independent of media composition (**Figure 4.4A**). Previous studies have demonstrated that MSCs undergoing differentiation on micropatterned substrates conducive for adipogenesis do not significantly alter their traction stresses [98]. Inhibition of cell contractility, which can regulate traction stresses, in MSCs cultured with mixed differentiation factors in significantly stiffer glass environments induces adipogenesis [19]. Moreover, in stiffer environments, which are more conducive for osteogenesis, traction stresses are increased. Consequently, inhibiting the high traction stresses generated in less favorable (stiffer) environments in the presence of adipogenic factors may enhance differentiation along the adipogenic lineage by reducing the energy barrier. Previous studies have demonstrated that enhanced mitochondrial respiration is required for adipogenesis [105]; therefore,

ATP required for cell contractility purposes would not be available for mitochondrial respiration. Taken together, these results could imply that alteration of traction forces in non-conducive mechanical environments may prevent MSC differentiation along the adipogenic lineage, offering further insight into how matrix stiffness directs cell lineage.

Deformation of the substrate decreased with increasing substrate rigidity for cells in CM, in agreement with studies with fibroblasts [106]. The presence of adipogenic factors on hard substrates was associated with increased levels of substrate deformation similar to substrate deformations caused by cells on soft substrates (**Figure 4.4B**). In addition, these factors were associated with an increase in actomyosin contractility gene expression on hard substrates (**Figure 4.7**). Previous studies have shown cell stiffness measured by magnetic twisting cytometry increases in order to balance tensile stress [107]; however, how local cytoplasmic stiffness changes with local traction stresses has not been elucidated. In agreement with average rheological properties measured (**Figure 4.2**), cells cultured in AM and MDM displayed increased numbers of areas with high cytoplasmic elastic modulus (G', **Figure 4.5**). This response was amplified on hard substrates and was associated with high traction stresses (**Figure 4.5**), suggesting high local G' may be associated with high traction stress. Spatial analysis revealed adipogenic factors increase the percentage of areas with high G' with corresponding high local traction stresses (**Figure 4.6**). Moreover, AM and MDM induced approximately a 5-fold increase the percentage of particles with surrounding high elasticity and viscosity cytoplasm and high local traction stress. This suggests that the cell increases the number of areas with spatially regulated cytoplasmic rheological properties and traction stress in response to adipogenic factors. The elastic and viscous character of the cytoplasm is

simultaneously spatially altered with traction force in response to AM and MDM. The elasticity and viscosity of the cytoplasm concurrently changing has been documented previously in MSCs treated with TCM [48,78], endothelial cells treated with VEGF [75], and in model actin solutions [81,108]. Greater increases in average G' than G'' occurred in response to AM and MDM compared to CM and OM (**Figure 4.3**), phase angle was calculated (**Figure 4.2C**) and decreased in these conditions, suggesting changes in the elastic modulus are dominating this response. In addition, the percentage of particles with low elastic and viscous moduli and low traction stress decreased in AM and MDM compared to CM and OM for both substrate rigidities. This may reflect a mechanical signature of MSCs undergoing adipogenesis and could potentially be used as a subcellular marker for differentiation. Increases in cell stiffness in response to increasing tensile stress has been attributed to myosin-based contractile machinery activation [107]. Expression of MLCK and MYH9 were upregulated in cells cultured on hard substrates in MDM, suggesting that myosin may also play a critical role in mechanotransduction in MSCs differentiating on hard substrates.

4.5 Conclusions

In conclusion, we simultaneously measured the local intracellular rheological properties and traction stress generation of MSCs undergoing differentiation on soft and hard substrates. The cytoplasm of MSCs cultured with adipogenic factors was more elastic independent of substrate rigidity. However, these factors only induced increases in traction stresses on hard substrates, which was associated with increased expression of contractility-related genes and decreased differentiation, suggesting force generation is critical for directing differentiation. Increased heterogeneity was present in the

correlation between rheological properties and traction stress for MSCs cultured on hard substrates with adipogenic factors. In addition, there was an increase in percentage of areas in the cell with highly elastic cytoplasm and high local traction stress, suggesting local cytoplasmic rheology and traction stress are spatially regulated during differentiation. These results may have important implications for detecting single cell differentiation important in regenerative medicine applications.

4.6 Materials and Methods

4.6.1 Cell Culture

Human MSCs isolated from a 22 year old healthy male donor (Donor 7071L) were obtained from Texas A&M Institute for Regenerative Medicine and cultured in αMEM (Corning) with 20% FBS (Atlanta Biologicals), 1% penicillin-streptomycin (Corning), and 1% L-glutamine (Corning). For differentiation assays, control media (CM) consisted of αMEM with 10% FBS, 1% penicillin-streptomycin, and 1% L-glutamine. Cells were seeded at a density of 25,000 cells/cm^2 in order to allow for differentiation along the adipogenic lineage [19]. Adipogenic media (AM) was CM supplemented with 10 μg/mL human insulin, 0.5 μM dexamethasone, 0.5 μM isobutylmethylxanthine, and 50 μM indomethacin [109]. Osteogenic media (OM) was CM with 10 nM dexamethasone, 50 μM ascorbate-2-phosphate, and 20 mM β-glycerolphosphate (Sigma Aldrich) added [109]. Mixed differentiation media (MDM) was created by mixing AM and OM at a 1:1 ratio. Media was replaced every 3 days for all differentiation assays.

4.6.2 Substrate Synthesis

Polyacrylamide substrates were synthesized for cell analysis as previously described[110]. Two different rigidity substrates were fabricated: soft with 8% acrylamide (Sigma Aldrich) and 0.02% bis-acrylamide (~2 kPa, GE Healthcare Life Sciences) and hard (8% acrylamide and 0.06% bis-acrylamide, ~8 kPa). Briefly, glass coverslips were activated by incubation in 1% 3-aminopropyltriethoxysilane followed by 0.5% glutaraldehyde. Acrylamide solutions were made with 200 nm red particles (Invitrogen) and ammonium persulfate and tetramethylethylenediamine were added to initiate gel polymerization. This solution was then added to glass slides and an activated coverslip added on top. In order to allow for cell adherence, the surface was activated with 0.2 mg/mL sulfosuccinimidyl-6-(4'-azido-2'-nitrophenylamino)-hexanoate (G-Biosciences) and coated with 0.2 mg/mL rat tail collagen I (Corning), which has previously been shown to play a critical role in MSC differentiation [111], overnight at 4˚C with agitation. Substrates were sterilized under UV light and incubated in media for at least an hour before use. Mechanical properties of the substrates were assessed via compression testing using a Bose Endura TEC ELF 3200 Uniaxial Testing System (data not shown). The Young's modulus was calculated from the slope of the linear region of the stress vs. strain curve at less than 10% strain.

4.6.3 Gene Expression Analysis

mRNA was isolated from hMSCs using Ribozol reagent (Amresco) and its quality confirmed using spectrophotometry. cDNA was reverse transcribed from mRNA using iScript cDNA synthesis kit (BioRad). PrimerBLAST was used to design primers for osteogenic and adipogenic differentiation (**Table 4.1**). In order to quantify gene

expression, SsoAdvanced SYBR Green Supermix (BioRad) was used along with primers to amplify target sequences in a Step One Plus thermocycler (Applied Biosystems). Gene expression was determined using a comparative C_T method [112] with GAPDH as an endogeneous control for all experiments. Data is relative to the glass CM condition for analysis of differentiation genes. For contractility gene analysis, data is reported as gene expression relative to CM for the corresponding substrate rigidity.

Table 4.1 Primers used for quantitative real-time PCR (qRT-PCR) for cells differentiating on substrates.

Gene		Primer Sequence	Accession Number
GAPDH	Forward 5’	GAAGGTGAAGGTCGGAGTC	NM 002046
	Reverse 5’	GAAGATGGTGATGGGATTTC	
Osteocalcin	Forward 5’	GGCAGCGAGGTAGTGAAGAG	NM 001199662
	Reverse 5’	CTGGAGAGGAGCAGAACTGG	
Adipsin	Forward 5’	GGTCACCCAAGCAACAAAGT	NM 001928
	Reverse 5’	CTACAAGCACCCACCTCCAT	
MLCK	Forward 5’	CGGAGGGAGTGGAGTACATC	NM 053025
	Reverse 5’	CACAAATTCTGGGGTGCCAA	
MYH9	Forward 5’	AGGACCAGAACTGCAAGCTG	NM 002473
	Reverse 5’	GCGCTCTTCCAAGTCAGTGA	
MYL9	Forward 5’	AAAGGCGTTGCGAATCACAT	NM 006097
	Reverse 5’	ACCCCACAGACGAATACCTG	

4.6.4 Differentiation Staining

After 5 weeks in differentiation media, cells were fixed in formalin and stained for either lipid droplets using 1.5% Oil Red O (Sigma Aldrich) or calcium deposits using 1% Alizarin Red (Sigma Aldrich) [78]. Images of fat droplets were taken using a Nikon Eclipse TS100 Inverted Microscope. A segmentation algorithm in MATLAB (Mathworks) was used to determine the area covered by Oil Red O. Alizarin Red was extracted using established protocols [113] and the absorbance measured at 450 nm.

4.6.5 Microrheological Characterization

MPTM was used to determine the cytoplasmic rheological properties of hMSCs undergoing differentiation as described [78]. Previous studies have demonstrated that traction force [98] and intracellular mechanical properties [94] are altered after 1 week in differentiation media; hence, cells were analyzed after 1 week in differentiation media in order to evaluate cytoskeletal changes before traditional techniques (i.e. qRT-PCR and staining) can detect differentiation. Human MSCs were ballistically injected with 200 nm green fluorescent particles (Invitrogen), allowed to recover, and then seeded on polyacrylamide substrates. After one week in differentiation media, videos of particle motion were taken using a Nikon Eclipse Ti inverted microscope equipped with a Photometrics QuantEM CCD camera. Imaging was performed with a 40x oil immersion lens with 1.5x zoom. The x-y coordinates where each video was taken were saved for traction force analysis. An average of 15 cells with 10-20 particles per cell was analyzed per experiment. Particle traces were created by applying a bandpass filter, determining the centroid of the particle as described [114], and the trajectories linked using a Hungarian linker algorithm. MSDs of particles were determined using a previously described custom MATLAB algorithm [78] and the following equation: $\langle \Delta r^2(\tau) \rangle = \langle [x(t+\tau)-x(t)]^2+[y(t+\tau)-y(t)]^2 \rangle$. Cytoplasmic fluid is locally isotropic [115]; therefore, it is sufficient to track displacements in the x and y directions to estimate the 3D projection. The MSDs were then related to the frequency-dependent complex shear modulus (G^*) using the following equation [92]:

$$G^*(\omega) = \frac{2k_B T}{3\pi a \left\langle \Delta r^2 \left(\frac{1}{\omega} \right) \right\rangle \Gamma\left[\left(1+\alpha(\omega)\right)\left(1+\beta(\omega)/2\right) \right]}$$

k_B is Boltzmann's constant, T is temperature (37˚C), a is the particle size, Γ is the gamma function, α is the first derivative and β is the second derivative of the MSD curve. The elastic (G') and viscous (G'') moduli are the imaginary and real components of G*, respectively. Phase angle was calculated using the following equation: δ=arctan(G''/G'), where δ=0˚ is an elastic solid and δ=90˚ is a viscous liquid.

4.6.6 Traction Force Microscopy

After particle tracking videos were collected, images of the cells and stressed gels were taken. Cells were then lysed with 0.5% SDS (BioRad) and an image of the unstressed gel was obtained. In addition, an image of the stationary bottom of the gel was taken before and after detachment to correct for drift. An average of 15 cells was analyzed per experiment. A custom-written MATLAB algorithm was then used to determine the cell-generated displacement field and calculate traction forces [116].

4.6.7 Rheology-Traction Force Correlation Analysis

Local rheological properties were correlated with local traction stresses using a custom-written MATLAB algorithm. After MPTM and traction stress analysis, the mean traction stress for a 3-pixel dilation around each particle location was calculated. This calculated mean local traction stress was normalized to the mean traction stress of all conditions of the same substrate rigidity and correlated with the elastic (G') and viscous (G'') modulus of the cytosol surrounding the particle in the cell.

4.6.8 Immunofluorescence Staining and Analysis

MSCs cultured in differentiation media for 1 week were fixed in formalin, permeabilized with Triton X-100 (BioRad), blocked with serum, and stained for F-actin and vinculin using rhodamine phalloidin (Invitrogen) and rabbit anti-vinculin (Invitrogen) followed by goat anti-rabbit Alexa Fluor 488 (Invitrogen). Imaging was performed with a Zeiss LSM 700 confocal microscope at 40x magnification.

4.6.9 Statistical Analysis

Gene expression and staining experiments were performed in triplicate. For MPTM and traction force analysis, 4-6 experiments were performed. A student's t-test was used for all statistical analysis with $p<0.05$ being statistically significant (* $p<0.05$, ** $p<0.01$, *** $p<0.001$). Data were reported as the mean ± standard error of the mean (SEM) unless otherwise noted.

CHAPTER 5

ARCHITECTURAL AND MECHANICAL CUES DIRECT MESENCHYMAL STEM CELL INTERACTIONS WITH CROSS-LINKED GELATIN SCAFFOLDS[3]

5.1 Summary

Naturally-derived biomaterials have emerged as modulators of cell function and tissue substitutes. Here, we developed cross-linked glutaraldehyde scaffolds for the expansion and differentiation of MSCs. The mechanical and architectural properties of the scaffolds were altered by varying the concentration of gelatin and glutaraldehyde. Higher glutaraldehyde concentrations were associated with an increase in more confined pores and osteogenic differentiation. In addition, myogenic potential varied with crosslinking degree, although bulk mechanical properties were unaltered. Correlational analysis revealed alkaline phosphatase (ALP) activity of differentiated MSCs on higher gelatin concentration scaffolds was dependent on traditional effectors, including environment elasticity and spread area. In contrast, the differentiation capacity of cells cultured on lower gelatin concentration scaffolds did not correlate with these factors, instead were dependent on the hydrated pore structure. These results suggest scaffold composition can determine what factors direct differentiation and may have critical implications for biomaterial design.

[3] Adapted from: McAndrews, KM, Kim, MJ, Lam, TY, McGrail, DJ, & Dawson, MR. (2014). Architectural and Mechanical Cues Direct Mesenchymal Stem Cell Interactions with Crosslinked Gelatin Scaffolds. *Tissue Engineering Part A*, 20(23), 3252–3260.

5.2 Introduction

The ability to transplant organs and tissues has saved many lives and revolutionized the field of medicine; however, limitations in available donor organs and tissues, high costs associated with transport surgeries, and poor compliance with life-time regimens of immunosuppressive drugs reduce the number of patients that can benefit from this therapy. Tissue engineering provides an alternative source to obtain tissues and organs that can be used to replace or regenerate tissues damaged by disease, congenital abnormalities, or traumatic injury. Naturally derived polymers, including collagen and gelatin, have been proposed as potential tissue substitutes because they are non-immunogenic, biocompatible and biodegradable. Gelatin, which is denatured collagen, is a relatively inexpensive FDA approved biomaterial that has been utilized in a variety of applications [117–119]; however, its applicability in the clinic is limited by its poor mechanical strength. Glutaraldehyde (GTA) has been used as a cross-linker to enhance the mechanical properties of collagen-based scaffolds [120] because of its low cost and ease of availability. In addition, glutaraldehyde has been used clinically in prosthetic implants. Although glutaraldehyde can be toxic to cells, it can be neutralized by lysine [121].

The addition of cells to a regenerative biomaterial can further enhance the healing process. MSCs are multipotent adult bone marrow-derived stem cells that can differentiate into various connective tissues, including bone, fat, and cartilage [1]. MSCs have shown promise for tissue regeneration applications because they are easily accessible, are immunosuppressive [4] and do not undergo tumorigenesis *in vivo* [122] and have been used for a variety of applications clinically, including liver disease [123],

subcutaneous wounds [124], and osteogenesis imperfect [125]. The implementation of MSCs in the clinic has been limited by low implanted cell survival rates [126] and an incomplete understanding of how MSC differentiation is affected by the microenvironment [127]. Biomaterials can affect cell proliferation, differentiation, ECM secretion and remodeling, and formation of functional tissues; thus, they have shown promise for directing cell function [128] and MSC differentiation [96,97,129]. Numerous studies have highlighted the effects of physical and chemical cues from the tissue microenvironment on MSC differentiation [17–19,97], though the role of the 3D architecture has not been fully elucidated. We hypothesized that it was not just the bulk mechanical properties of tissue engineered scaffolds but the microscopic architecture of these environments that direct MSC fate.

In these studies, we fabricated gelatin-glutaraldehyde scaffolds and altered the mechanical properties (bulk elastic moduli of ~10-40 kPa) and architectural properties (pore size and fiber structure) by varying the concentration of gelatin and glutaraldehyde. Osteogenic differentiation was induced on scaffolds with relatively low amounts of glutaraldehyde (0.1-1.0% w/v). In addition, myogenic potential varied on scaffolds with similar bulk mechanical properties. We found that mechanical properties of the scaffold and the extent of cell spreading directly correlated with osteogenic differentiation on 10% (w/v) gelatin scaffolds; whereas on 5% gelatin scaffolds, the hydrated microscale pore structure played a stronger role in directing differentiation. These results suggest that in addition to matrix stiffness, cells also sense architectural properties of their local environment and integrate these cues when undergoing lineage commitment. By

elucidating the interplay of these two factors, this work seeks to improve matrix-directed MSC differentiation.

5.3 Results

5.3.1 Characterization of Gelatin-Glutaraldehyde Scaffolds

The Young's moduli of 5% (w/v) gelatin (G) scaffolds were relatively constant (~15 kPa) across GTA concentration (**Figure 5.1A**). The bulk mechanical properties of 10% G 0.1% (w/v) GTA scaffolds were similar to 5% scaffolds. Higher concentrations of GTA were associated with approximately 3-fold increase in bulk stiffness for 10% scaffolds (~50 kPa). In order to determine the stability of the scaffolds, we measured protein release over time. Scaffolds with 0.1% GTA released more gelatin than those containing 0.5 and 1% GTA ($p<0.05$); however, low amounts of protein were released from all scaffolds, suggesting they remain intact (**Figure 5.1B**). All scaffolds swelled approximately 7- to 15-fold within one day and then remained relatively constant over a seven day period (**Figure 5.1C**). Swelling in 5% gels was relatively independent of GTA concentration, while in 10% gels, swelling was significantly reduced in 0.5% and 1% GTA concentrations compared to 0.1% GTA ($p<0.01$). Together these data suggest the scaffolds are relatively stable for tissue engineering applications.

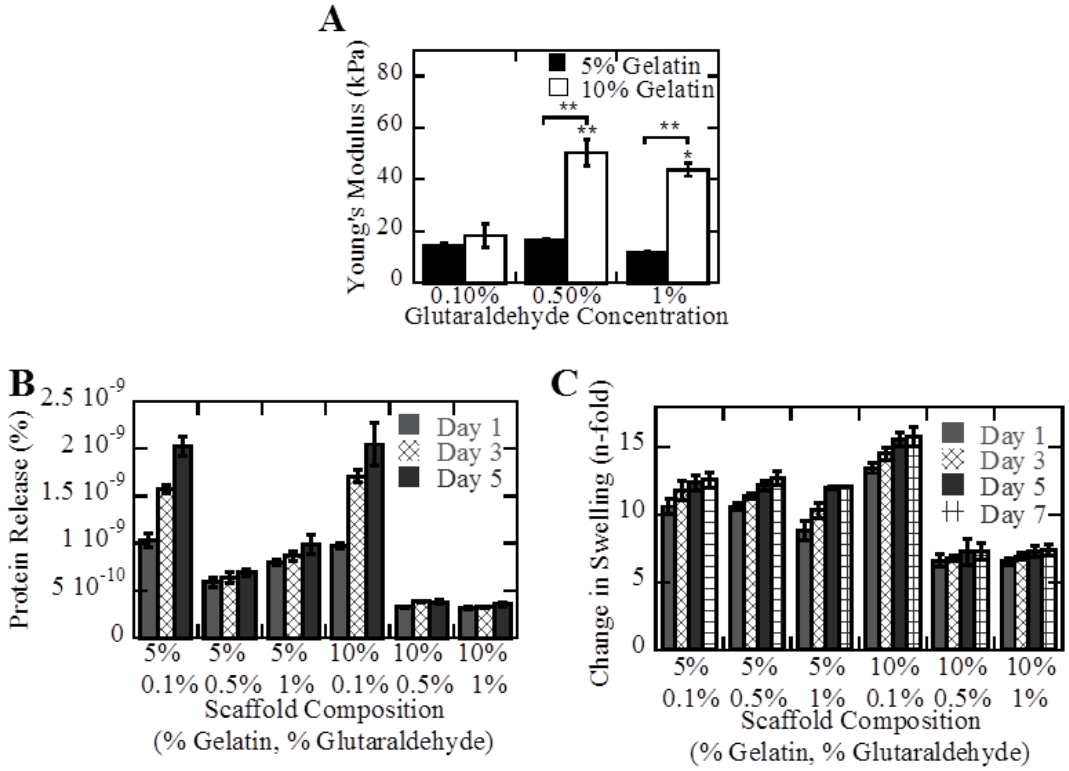

Figure 5.1 Characterization of gelatin-glutaraldehyde scaffolds. The effect of scaffold composition on the mechanical properties (A) and degradation (B) and swelling (C) characteristics were determined.

5.3.2 Scaffold Composition Alters Pore Architecture

In order to analyze the architecture of the scaffolds, we imaged the scaffolds using scanning electron microscopy and quantified pore size. Average pore size was similar for 5% G 0.1% GTA and 5% G 0.5% GTA scaffolds (30-40 μm^2). The 10% G 0.1% GTA scaffold had the largest average pore size (100 μm^2). In addition, 10% G scaffolds had larger fibers than 5% G scaffolds. The highest GTA concentration was associated with a smaller pore size. For 1% GTA concentrations, average pore size was independent of gelatin concentration; however, the variation was higher in 10% scaffolds, suggesting a more heterogeneous distribution of pore sizes (**Figure 5.2A,B**).

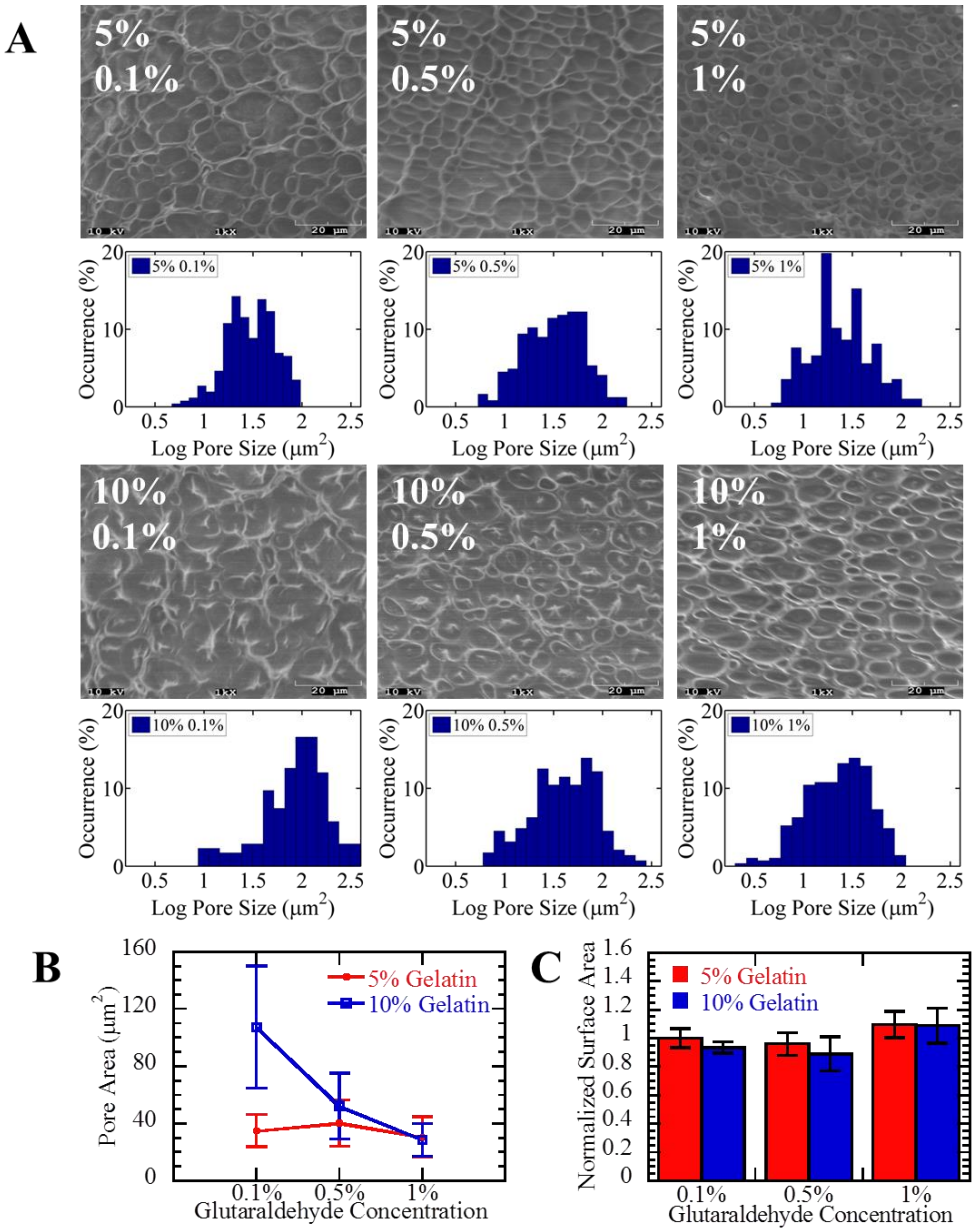

Figure 5.2 Effect of scaffold composition on pore architecture. Pore sizes were quantified from scanning electron microscopy images (A). Pore size was relatively constant cross glutaraldehyde concentration for 5% gelatin scaffolds and decreased for 10% gelatin scaffolds (B). Surface area available for cell attachment was approximately constant across scaffold compositions (C).

Although the pore size distribution varied with scaffold composition, the surface area available for cell attachment was relatively constant (**Figure 5.2C**).

5.3.3 Increasing Glutaraldehyde Concentration Leads to More Confined Pores

We utilized MPTM to probe the pore structure of hydrated scaffolds in cell culture relevant conditions. The embedded particles underwent thermal Brownian motion which was evaluated by tracking the x-y coordinates of the particles. Unlike scanning electron microscopy which has a characteristic length scale of several microns, MPTM has a characteristic length scale of approximately 100 nm. The extent of motion can be determined by calculating the MSD. MSD is time dependent for viscous fluids and time independent for elastic solids. MSD plots revealed all scaffolds behaved as elastic solids at short time scales and viscous fluids at long time scales (**Figure 5.3A**). Particle MSDs in scaffolds containing 0.1% GTA compared to higher amounts of GTA had decreased magnitude and increased heterogeneity in particle MSDs at τ=1s (**Figure 5.3B**). This suggests that a distribution of particle motions exists, with a portion of particles that displayed increased motion, whereas others did not, indicating that these particles were likely confined by the microstructure of the hydrated scaffold. In addition, particles in scaffolds with higher concentrations of GTA displayed a decreased average slope (anomalous diffusion coefficient, α) at long time scales than those with 0.1% GTA. Because α can be used to describe the relative viscoelastic character of the fluid surrounding particle, with α=0 characteristic of a Hookean elastic solid, α=1 characteristic of a Newtonian viscous fluid and $0<\alpha<1$ characteristic of a viscoelastic fluid, we further analyzed individual particles to determine if the particles are more confined ($\alpha<0.5$) or less confined ($\alpha>0.5$) by the pore structure.

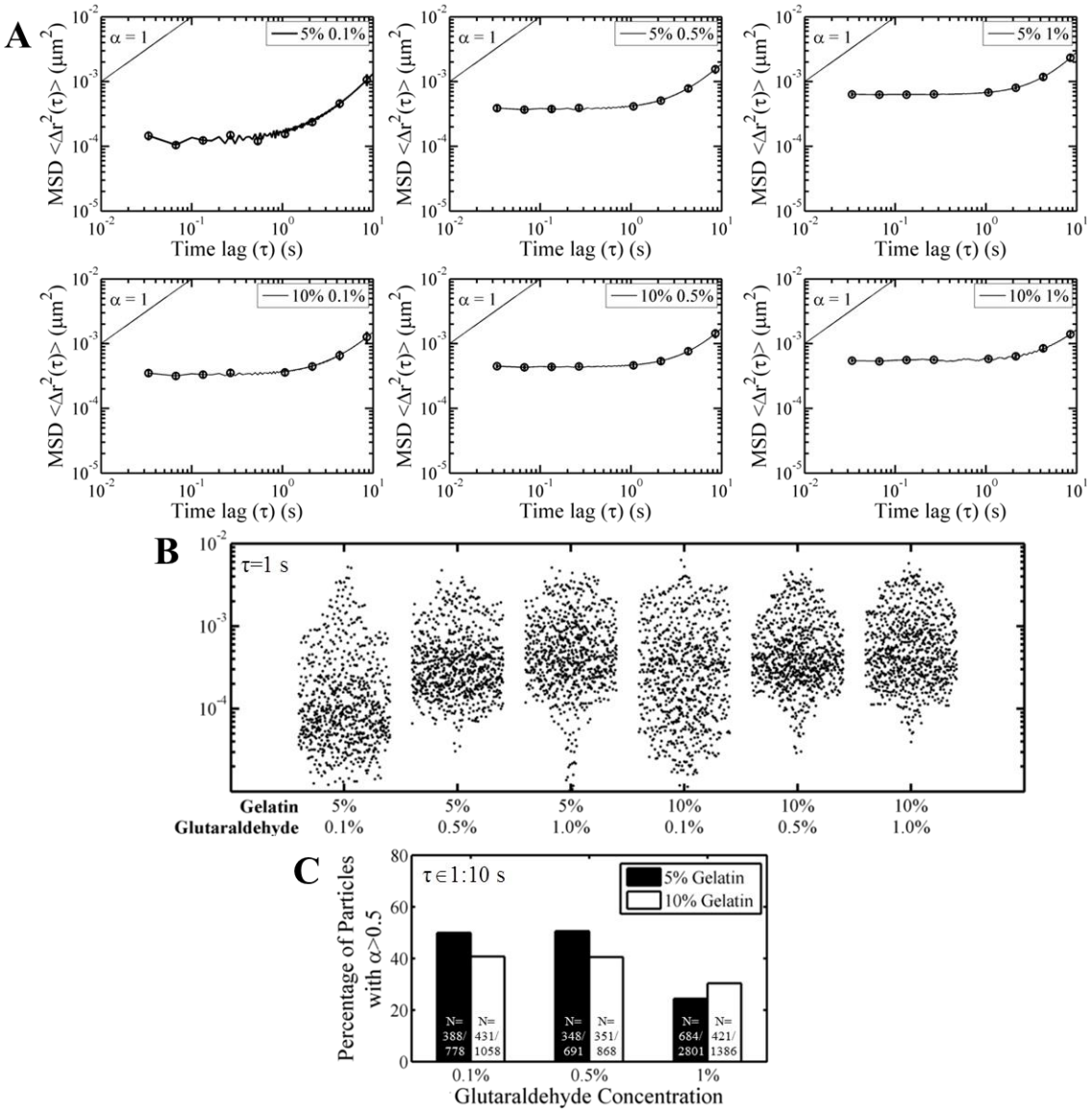

Figure 5.3 Variation in MSD and confinement of particles with changes in scaffold composition. Average particle MSDs (A), dot plot of individual particle MSDs at τ=1 s (B) and the percentage of less confined particles with α>0.5 between τ=1 s and τ=10 s (C) were determined under cell culture conditions.

All scaffolds had a characteristic relaxation time at approximately τ=1 s; therefore we analyzed α from τ=1 s to τ=10 s. The percentage of less confined particles was similar for 0.1% and 0.5% GTA concentrations independent of gelatin concentration. Cross-linking with 1% GTA was associated with a significant decrease in particles that were less confined, suggesting there is a higher percentage of smaller pores in this condition (**Figure 5.3C**).

5.3.4 Scaffold Composition Affects Proliferation and Differentiation Potential

In order to determine the effect of scaffold composition on cellular function, we performed spreading, proliferation and differentiation assays. After 24 hours on the scaffolds, images of the cells were taken (**Figure 5.4A**). Although cell spreading increased with GTA concentration, the amount of gelatin did not significantly affect cell spreading (**Figure 5.4B**). At day 3 on the 5% G, there were significantly more MSCs on the 0.5% GTA and 1% GTA scaffolds than on the 0.1% GTA scaffold. (**Figure 5.4C**). A similar trend was found by measuring MTT absorbance, with similar viability for cells on 5% G scaffolds (**Figure 5.4D**).

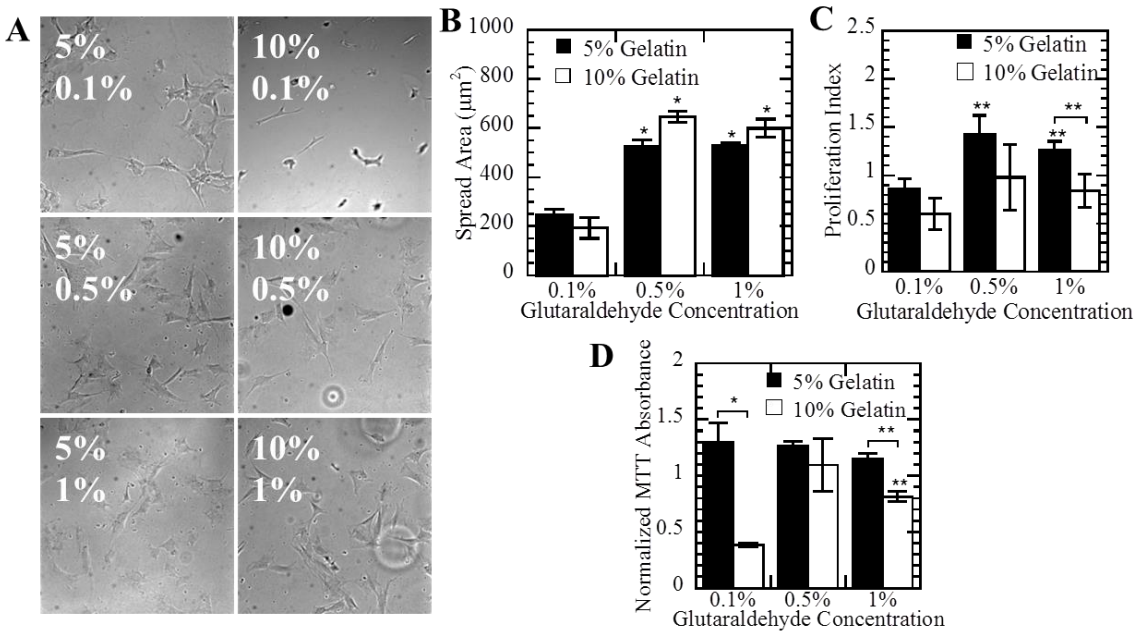

Figure 5.4 Changes in MSC spreading and proliferation on scaffolds. The spreading of MSCs on the scaffold was quantified (B) based on phase contrast images (A). Scaffold composition altered the proliferation and viability of MSCs cultured on the scaffolds for 3 days, as measured by cell count (C) and MTT absorbance (D).

Viability was significantly decreased on the 10% G 0.1% GTA scaffold. In addition, cells cultured on 5% G 1% GTA scaffolds were significantly more viable than cells on 10% G 1% GTA scaffolds.

We next sought to determine how the mechanical and architectural properties of the scaffolds affected differentiation potential. Because MSCs have increased differentiation potential along the myogenic and osteogenic lineage on 2D substrates with elasticities similar to the scaffolds we developed [17], we performed both osteogenic and myogenic induction on gelatin scaffolds. Cells were differentiated along the osteogenic lineage on scaffolds for 3 weeks and stained for ALP activity (**Figure 5.5A**). Osteogenic differentiation was inhibited on the 10% G 0.1% GTA scaffold. Although 5% G scaffolds displayed similar mechanical properties, osteogenic potential varied with GTA

concentration (**Figure 5.5B**). Gross imaging of the scaffolds after 3 weeks of differentiation revealed enhanced mineralization in the 5% G (**Figure 5.6**), in agreement with ALP activity results. Gene expression of osteopontin and osteocalcin was increased in cells cultured on 5% G scaffolds with increasing GTA concentrations (**Figure 5.5C**). In addition, cells differentiated on the 10% G 1% GTA scaffold had significantly less ALP activity and lower expression of osteocalcin, and consequently less differentiation, than the 5% G 1% GTA scaffold. In order to evaluate if gelatin scaffolds enhance differentiation along other lineages, cells were differentiated in myogenic media. Myogenin and MyoD were both upregulated in cells cultured on 5% G 1% GTA scaffolds compared to 10% G 1% GTA scaffolds (**Figure 5.5D**). Similar to osteogenic differentiation results, myogenic potential varied with GTA concentration for 5% G scaffolds.

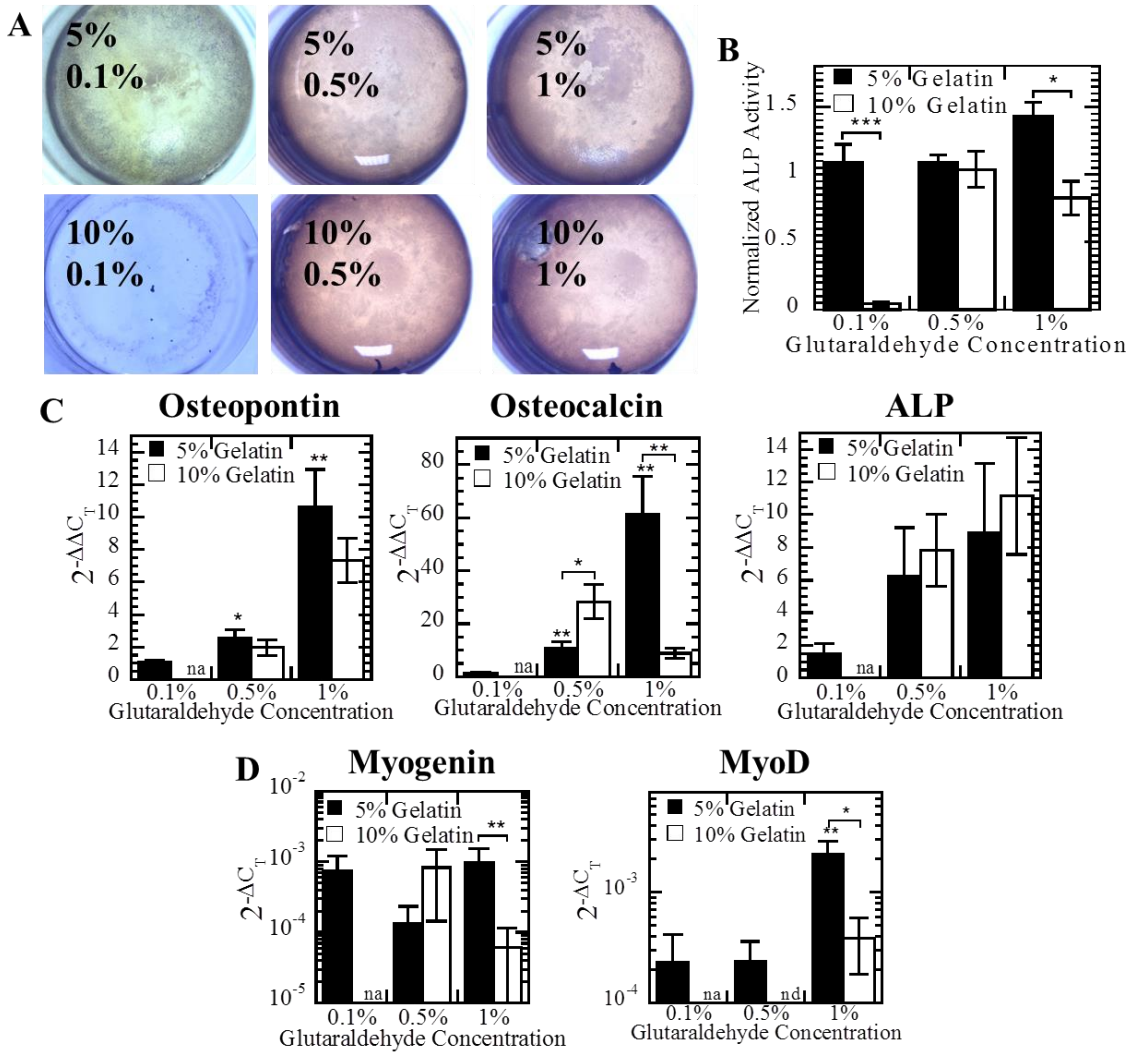

Figure 5.5 Differentiation capacity of MSCs cultured on scaffolds. Osteogenic differentiation capacity of MSCs was determined by staining for ALP activity (A) and quantified by absorbance at 595 nm (B). Expression of genes associated with osteogenic (C) and myogenic differentiation (D). na: gene expression analysis not performed due to low cell numbers, nd: no detection of gene of interest.

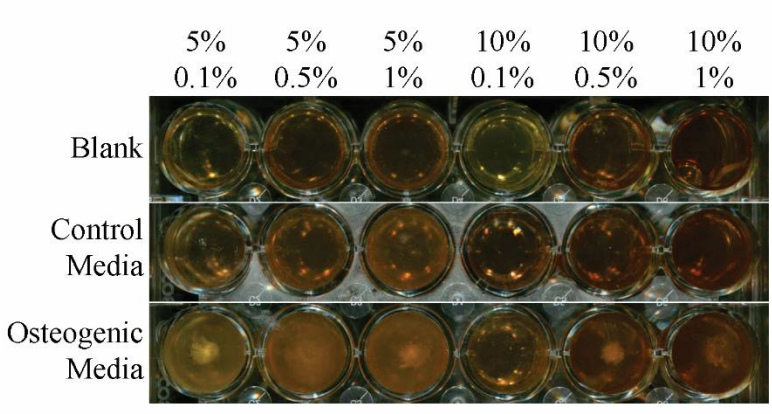

Figure 5.6 Mineralization of scaffolds by differentiating MSCs. Scanned images of blank (no cells), control media, and osteogenic media scaffolds after 3 weeks of culture reveals mineralization in osteogenic conditions but not in blank or control conditions.

5.4 Discussion

In this study, we developed gelatin scaffolds with differing mechanical properties and pore sizes by altering the concentrations of gelatin and glutaraldehyde. Lysine was used in these studies to neutralize glutaraldehyde and circumvent glutaraldehyde toxicity issues. Typically hydrated gelatin scaffolds have extremely low mechanical strength [119] and high swelling and degradability [130], limiting their use as biomaterials; however, gelatin scaffolds cross-linked with glutaraldehyde displayed enhanced mechanical properties and stability (**Figure 5.1**). Notably, increasing GTA from 0.1% to 0.5% resulted in a two-fold decrease in degradation (**Figure 5.1B**). Scanning electron microscopy images of 10% G 0.1% GTA scaffolds showed the gelatin was not completely cross-linked (**Figure 5.2**), which may be why this scaffold had a lower elasticity and higher swelling (**Figure 5.1**).

Although bulk mechanical properties were not dependent on GTA concentration for 5% G scaffolds (**Figure 5.1A**), pore architecture changed with additional GTA

(**Figure 5.2**). At the two higher GTA concentrations, the average pore sizes were similar for 5% G and 10% G gels; however, the standard deviations of the pore size distributions were different (**Figure 5.2**). These data suggest that measuring bulk or average properties alone may not accurately capture the properties of the material. In addition, samples were lyophilized for analysis which may not be representative of culture conditions. In order to analyze the pore structure while the scaffold is in cell culture conditions, we utilized MPTM. While scanning electron microscopy can probe pore structure on the order of several microns, MPTM probes a much smaller length scale, approximately 100 nm. All scaffolds behaved like elastic solids at short time scales and viscoelastic fluids at longer time scales (**Figure 5.3A**). In addition, particles encountered a heterogeneous microenvironment, consistent with MPTM results in other polymers [131]. The magnitude of the average MSD was similar for all 10% G scaffolds, but 5% G show an increasing magnitude with increasing GTA (**Figure 5.3A**). This may be a result of polymerization kinetics as increased cross-linker concentration [132] and polymer concentration [133] have been associated with increased polymerization rates. High amounts of polymer may lead to rapid polymerization, causing the formation of a network of heterogeneous fiber sizes. For lower amounts of polymer, more cross-linker is available, leading to the formation of small fibers. Small fibers may be destroyed during lyophilization and thus will not contribute to pore size measured by scanning electron microscopy, but will be intact for microrheological methods. We hypothesize that polymerization reaction of the lowest amount of gelatin (5%) and glutaraldehyde (0.1%) may be diffusion-limited and thus has more small pores, causing a decrease in the magnitude of the average MSD. While 0.1% and 0.5% GTA cross-linked scaffolds had a

similar percentage of particles that were less confined a larger percentage of particles in 1% GTA scaffolds were more confined (**Figure 5.3B**). This trend was not present in freeze-dried samples for scanning electron microscopy, suggesting the pores may be changing shape with lyophilization.

Though previous studies have shown MSCs proliferate more in stiffer environments [134], our results suggest that stiffness alone is not predicative of MSC proliferation on gelatin-glutaraldehyde scaffolds (**Figure 5.4C,D**). In addition, matrix elasticity can direct MSC lineage towards cell types with similar elasticity *in vivo* [17]. MSC myogenic potential has been enhanced on 2D substrates with elasticities around 10 kPa [17,135], similar to the elasticity of 5% G scaffolds. While myogenin expression was relatively constant across GTA concentrations for 5% G scaffolds, MyoD was significantly upregulated on 5% G 1% GTA scaffolds (**Figure 5.5D**), suggesting the bulk mechanical properties alone do not direct MSC myogenic differentiation on gelatin scaffolds.

Numerous studies have also shown that MSCs have increased propensity to differentiate into osteoblasts in stiffer environments [17,136]. MSCs differentiated on 5% G 1% GTA scaffolds had enhanced expression of osteopontin and osteocalcin (**Figure 5.5C**), which are late stage osteogenesis markers, suggesting this scaffold composition not only enhanced differentiation, but also generated a more terminally differentiated cell. Interestingly, on the scaffolds MSCs did not display enhanced differentiation on 10% G scaffolds, which had higher elastic moduli. Young's modulus correlated with ALP activity for 10% G scaffolds (R^2=0.99, **Figure 5.7A**). Pore size and osteogenic differentiation potential were weakly inversely correlated for both 5% G (R^2=0.70) and

10% G scaffolds (R^2=0.77) (**Figure 5.7B**). Increased MSC spread area has also been shown to promote differentiation along the osteogenic lineage [19]; however, there was only a correlation between spread area and ALP activity for 10% G scaffolds (R^2=0.98, **Figure 5.7C**) suggesting enhanced cell spreading does not promote differentiation on 5% G scaffolds. The differentiation potential for 5% G scaffolds directly correlates with the percentage of unconfined particles (R^2=0.99, **Figure 5.7D**), implying the effective pore size plays a more important role in directing differentiation than the bulk mechanical properties of our scaffolds and the ability of cells to spread on 5% G scaffolds. In addition, on the 10% G 0.1% GTA scaffold where pores were not completely formed (**Figure 5.2**), MSCs were unable to differentiate into osteoblasts (**Figure 5.5B**). Previous work has demonstrated that pore size is critical for bone reformation, which was attributed to enhanced MSC mineralization [137]. Other researchers have postulated that pore size and distribution and surface structure may play an important role in osteogenic differentiation [137]. Our studies demonstrate that the composition of the scaffold can affect whether architectural cues or mechanical cues dominate MSC differentiation.

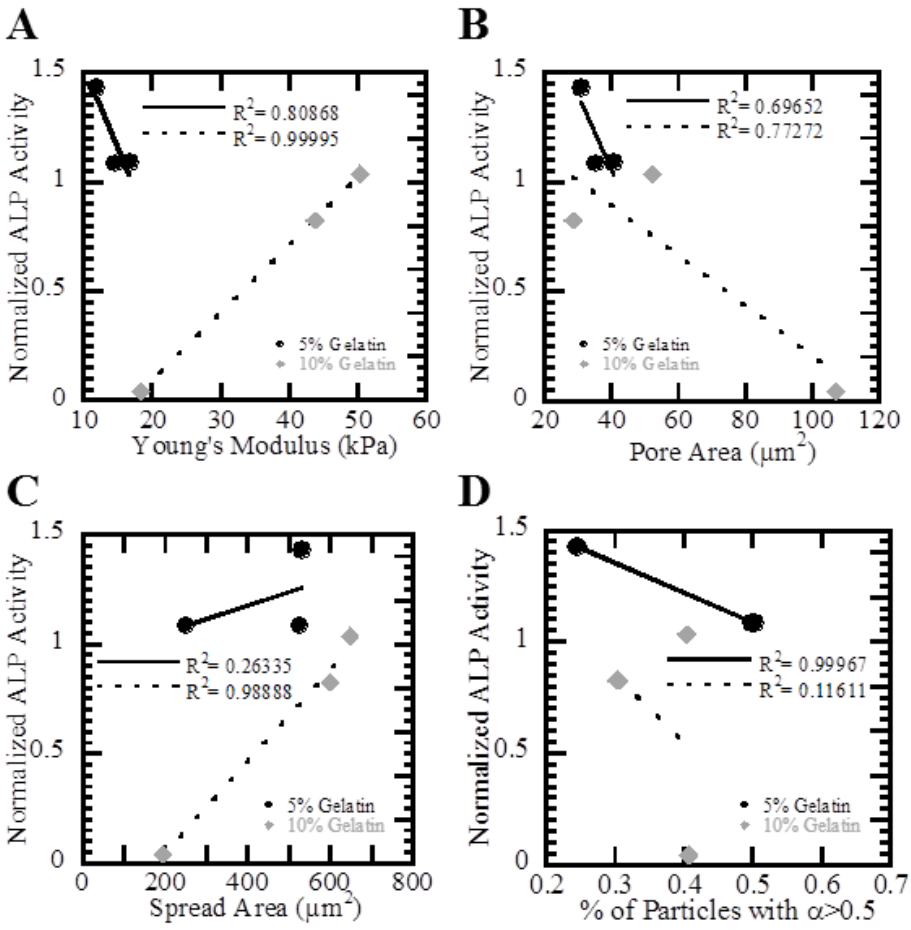

Figure 5.7 Correlation of scaffold properties with differentiation potential. Mechanical properties (A), average pore size (B), spread area (C), and the percentage of less confined particles with α>0.5 (D) correlated differently with ALP activity for 5% (black circles) and 10% gelatin (grey diamonds) scaffolds. Linear fits to each data set were performed for 5% (solid line) and 10% (dashed line) scaffolds.

5.5 Conclusions

In conclusion, we developed gelatin-glutaraldehyde scaffolds for the expansion and differentiation of MSCs. The concentration of gelatin and glutaraldehyde in the scaffold regulated the mechanical and architectural properties, which ultimately determined the differentiation potential of MSCs cultured on the scaffold. These findings may have important implications for scaffold design for tissue engineering applications.

5.6 Materials and Methods

5.6.1 Materials

Gelatin was purchased from Sigma Aldrich. IMDM, L-glutamine, and penicillin-streptomycin were purchased from Corning. Premium select FBS was purchased from Atlanta Biologicals (Lot L12163). Fluorosphere carboxylate-modified 200 nm red particles were purchased from Invitrogen. All other materials were purchased from VWR.

5.6.2 Preparation of Scaffolds

Gelatin was dissolved in distilled water for 15 min at 70℃ under magnetic stirring to make 5 wt% and 10 wt% solutions. A 5% GTA solution was then added to mixtures to form 0.1, 0.5, and 1.0 wt% solutions. The mixture was vortexed and then cast. The scaffolds were refrigerated at 4°C before use. Scaffolds were lyophilized for scanning electron microscopy imaging and water absorption studies.

5.6.3 Mechanical Testing

Gelatin scaffolds were prepared in a petri dish. After 24 hours, scaffolds were cut into 3 sections and rehydrated in PBS. The Young's modulus was measured by compression testing using a Bose Endura TEC ELF 3200 Uniaxial Testing System. The Young's modulus was calculated from the slope of the stress vs. strain curve in the linear region at less than 10% strain using the following equation:

$$E = \frac{FL_0}{A_0 \Delta L}$$

F is force exerted, A_0 is initial area of the scaffold, ΔL is change in length, and L_0 is initial length.

5.6.4 Scanning Electron Microscopy Imaging

Lyophilized scaffolds were coated with gold for 30 seconds using gold sputter coater. Scaffolds were imaged using a Hitachi S800 field emission gun scanning electron microscope. The pore area was calculated by manually tracing the pores in ImageJ software (NIH). To calculate surface area, gelatin fibers were segmented in a custom-written MATLAB algorithm after convolution with a LaPlacian of Gaussian (LoG) mask.

5.6.5 Multiple-Particle Tracking Microrheology

Twenty second videos of the thermal displacements of 200 nm carboxylated particles embedded in the scaffold were captured using a Photometrics QuantEM CCD camera at 30 frames per second and a Nikon epifluorescent microscope with a TIRF 100x lens (Nikon) at 37˚C. The coordinates of the particles were determined and analyzed using a custom written MATLAB algorithm. Briefly, a bandpass filter was applied to the images and the centroid of the particle determined with sub-pixel accuracy as described [138]. Particle trajectories were determined using a Hungarian linker algorithm. The MSD were calculated using a previously described custom MATLAB algorithm [48,139] and the following equation: $\langle MSD(\tau) \rangle = \langle [x(t+\tau)-x(t)]^2+[y(t+\tau)-y(t)]^2 \rangle$. MSD can be described by a power law: $\langle MSD(\tau) \rangle = 4D\tau^{\alpha}$, where D is the diffusion coefficient and α is the anomalous diffusion coefficient. The anomalous diffusion coefficient can be used to describe the motion of the particle, with $\alpha=0$ characteristic of a Hookean solid, $\alpha=1$ characteristic of a Newtonian fluid and $0<\alpha<1$ characteristic of a viscoelastic fluid. The slope of the logarithmic MSD curve (α) was calculated by using finite difference between $\tau=1$ s and $\tau=10$ s. Any slope greater than one (indicative of convective transport) or less

than zero was automatically excluded from analysis to eliminate the effects of motion artifact from sample drift.

5.6.6 Water Absorption Test

Lyophilized scaffolds were weighed to obtain dry weight (W_d). Cell culture growth media was added to the scaffold to reach saturation. Samples were incubated at 37℃ to mimic culture conditions. The wet weight (W_w) of each scaffold was obtained after 24, 48, 72, and 96 hrs. The water absorption ability of the scaffolds was calculated with the following equation:

$$Media\ absorption(n-fold) = \frac{W_w - W_d}{W_d}$$

5.6.7 Degradation

Phosphate buffered saline (PBS) solution was added into polymerized scaffolds and incubated at 37℃. The supernatant was collected at 24, 48, and 72 hrs. BCA assay was used to determine the amount of gelatin released using a standard curve.

5.6.8 Cell Culture

MSCs were isolated from 4 week old Balb/C mice (Jackson Laboratory) as described previously[48]. Cells were cultured in IMDM supplemented with 20% FBS, 2 mM L-glutamine, and 100 U/mL penicillin-streptomycin. Flow cytometry was performed to confirm cells were Sca-1^+, $CD29^+$, $CD105^+$, $CD11b^-$ and $CD45^-$ and osteogenic and adipogenic assays on tissue culture plastic were performed to confirm the MSC phenotype (data not shown). For all experiments, gelatin was autoclaved prior to scaffold formation. Uncross-linked glutaraldehyde was neutralized by multiple changes of 1% glycine and 10 μg/mL human fibronectin was added to promote cell adhesion.

5.6.9 Cell Proliferation

MSCs were seeded on scaffolds at a density of 5,000 cells per scaffold (10,000 cells/cm^2) in order to allow space for proliferation and cultured for 3 days. The cells were then removed by trypsinization, resuspended in Isoton II solution, and counted using a Beckman Coulter Multisizer 3 Coulter Counter. Proliferation index was calculated as the number of cells for each condition divided by the overall average number of cells for each experiment.

5.6.10 MSC Differentiation

For osteogenesis experiments, MSCs were cultured on scaffolds in either control media (IMDM, 20% FBS, 1% penicillin-streptomycin and 1% L-glutamine) or osteogenic media (IMDM, 20% FBS, 1% penicillin-streptomycin, 1% L-glutamine, 10 nM dexamethasone, 20 nM β-glycerolphosphate, 50 μM ascorbate-2-phosphate, and 50 ng/mL L-thyroxine sodium pentahydrate) as described previously [109] for 3 weeks. Cells were then fixed with formalin and stained for ALP expression using NBT/BCIP reagent. Images were taken using a Nikon SMZ745T stereoscope. ALP activity was determined from the absorbance at 595 nm of cells cultured in osteogenic media normalized by absorbance of cells cultured in control media. For myogenic differentiation, MSCs were cultured on scaffolds in control media supplemented with 10 ng/mL human recombinant TGF-β1 (Biolegend) for 1 week.

5.6.11 Gene Expression Analysis

RNA was isolated from MSCs cultured on scaffolds in osteogenic media for 3 weeks or myogenic media for 1 week using Ribozol reagent (Amresco) and reverse transcribed to cDNA using iScript cDNA synthesis kit (BioRad). Gene expression

analysis was not performed on cells cultured on 10% gelatin 0.1% GTA scaffolds due to low cell numbers. Primers were designed using Primer3 software [140]. qRT-PCR was performed on the target sequences listed in **Table 5.1** using SsoAdvanced SYBR Green Mastermix (BioRad) in a StepOne Plus Thermocycler (Applied Biosystems) for 40 cycles. For osteogenesis experiments, data was reported after normalization to endogenous GAPDH and expression of cells cultured on 5% gelatin 0.1% glutaraldehyde scaffold. Data for myogenesis was normalized to GAPDH and Wilcoxon-Mann-Whitney rank sum test was used for statistical analysis.

Table 5.1 Primers used for qRT-PCR for cells differentiating on gelatin scaffolds.

Gene		Primer Sequence	Accession Number
GAPDH	Forward 5'	AGGTCGGTGTGAACGGATTTG	NM 008084
	Reverse 5'	TGTAGACCATGTAGTTGAGGTCA	
ALP	Forward 5'	TCAGGATGAGACTCCCAGGA	NM 007431
	Reverse 5'	GTGTGTGTGTGTCCTGTC	
Osteocalcin	Forward 5'	CAGTATGGCTTGAAGACCGC	NM 007541
	Reverse 5'	AGAGAGAGAGGACAGGGAGG	
Osteopontin	Forward 5'	GAGAGCGAGGATTCTGTGGA	NM 001204201
	Reverse 5'	CGACTGTAGGGACGATTGGA	
Myogenin	Forward 5'	ACCTTCCTGTCCACCTTCAG	NM 031189
	Reverse 5'	CACCGACACAGACTTCCTCT	
MyoD	Forward 5'	TGGTTCTTCACGCCCAAAAG	NM 010866
	Reverse 5'	ACTTCTGCTCTTCCCTTCCC	

5.6.12 Statistical Analysis

All experiments were performed in triplicate. Unless otherwise noted, a student's t-test was used for statistical analysis with $p<0.05$ being statistically significant (* $p<0.05$, ** $p<0.01$, *** $p<0.001$) and data were reported as the mean ± SEM.

CHAPTER 6

ENHANCED ADHESION OF STROMAL CELLS TO INVASIVE CANCER CELLS REGULATED BY CADHERIN 11[4]

6.1 Summary

Cancer-associated fibroblasts (CAFs) are known to promote tumor growth and metastasis; however their differential accumulation in invasive and non-invasive tumors is not fully understood. We hypothesized that differences in cell adhesion may contribute to this phenomenon. To test this, we analyzed the adhesion of CAF-precursors fibroblasts and MSCs to invasive and non-invasive cancers originating from the breast, ovaries, and prostate. In all cases stromal cells preferentially adhered to more invasive cancer cells. Modulating integrin and cadherin binding affinities with calcium chelation revealed that adhesion was independent of integrin activity but required cadherin function. Invasive cancer cells had increased expression of mesenchymal markers cadherin 2 and 11 that localized with stromal cell cadherin 11, suggesting that these molecules are involved in stromal cell engraftment. Blockade of cadherin 11 on stromal cells inhibited adhesion and may serve as a target for metastatic disease.

6.2 Introduction

The progression of cancer from a benign mass of abnormal cells to a malignant tumor requires the development of a tumor-promoting microenvironment, which includes a scaffold of ECM proteins and a network of supporting cells and growth factors [26]. A multitude of cell types are recruited to the tumor under the influence of tumor-secreted

[4] Adapted from: McAndrews, KM, Yi, J, McGrail, DJ, & Dawson, MR. (2015). Enhanced Adhesion of Stromal Cells to Invasive Cancer Cells Regulated by Cadherin 11. *ACS Chemical Biology*. doi:10.1021/acschembio.5b00353

growth factors and chemokines; this includes immune cells, endothelial cells, and fibroblasts that play an important role in tumor growth by modulating the immune response, promoting angiogenesis, and forming the stroma [141]. In part to the critical role of the tumor microenvironment in cancer progression, drugs targeting these stromal cells have been increasing in demand. Several drugs that target the inflammatory signal COX-2 have been investigated for the treatment of cancer including rofecoxib and celecoxib [142]. In addition, bevacizumab, sorafenib, sunitinib, pazopanib, and everolimus are FDA-approved drugs that alter angiogenic activity in tumors [143]. Stromal fibroblasts have been specifically targeted with imatinib, sunitinib, and sibrotuzumab [26]. Fibroblasts and MSCs are recruited to the tumor microenvironment from nearby tissue and the bone marrow [144], possibly through increased migration in response to tumor-secreted soluble factors [48,78,145]. Within the tumor, these cells promote tumor growth, invasion, and angiogenesis [28,146]. Both MSCs and fibroblasts can differentiate into CAFs, or myofibroblasts, within the tumor. CAFs promote inflammation [32], tumor growth, matrix remodeling, and angiogenesis [141], further supporting tumor progression. Clinically, the presence of a CAF gene signature is associated with therapy resistance and poor prognosis [35]. Thus, MSCs and fibroblasts are potential therapeutic targets for metastatic cancer.

Though the recruitment of stromal cells in response to soluble factors has been well-documented [147,148], the involvement of cell adhesion is not fully understood. Cell adhesion molecules, including cadherins and integrins, play a critical role in cancer progression. Alterations in cell adhesion molecules are associated with EMT, a mechanism by which cancer cells become invasive [43]. EMT is characterized by

disruption of cell-cell junctions, including loss of endothelial cadherin 1 (E-cadherin), and gain of cadherin 2 (N-cadherin), cadherin 11 (OB-cadherin), as well as cell-ECM adhesions, including α5β1 integrin [43]. Gain of cadherin 2 expression is linked to increased invasiveness and survival of tumor cells [149] and increased expression of α5β1 integrin is linked with poor prognosis and metastasis [36]. In addition, cadherin 11 has been implicated in breast [150] and prostate cancer [151] metastasis. Evidence of EMT has been observed at the invasive front of colorectal cancer [45], in metastatic ovarian cancer [46], and circulating breast cancer cells [152], suggesting this transition is critical for metastasis.

In this study, we sought to understand if these changes in cell adhesion molecules during cancer progression affected the engraftment of stromal cells such as fibroblasts and MSCs. We show that stromal cells are more adherent to invasive cancer cells than non-invasive cells. Integrins are not required for these cell-cell interactions, but cadherins are critical for stromal cell attachment to invasive cancer cells. Cadherin 11 and 2 were colocalized at sites of adhesion and blockade of cadherin 11 on stromal cells reversed this adhesive response, providing insight into stromal cell engraftment in invasive tumors.

6.3 Results

6.3.1 Stromal cells are more adherent to invasive cancer cells

In order to probe the adhesion of stromal cells (fibroblasts and MSCs) to non-invasive and invasive cancer cells, a fluorescence-based plate reader assay was utilized. Both stromal cell types were more adherent to invasive than non-invasive breast and prostate cancer cells (**Figure 6.1A,B**).

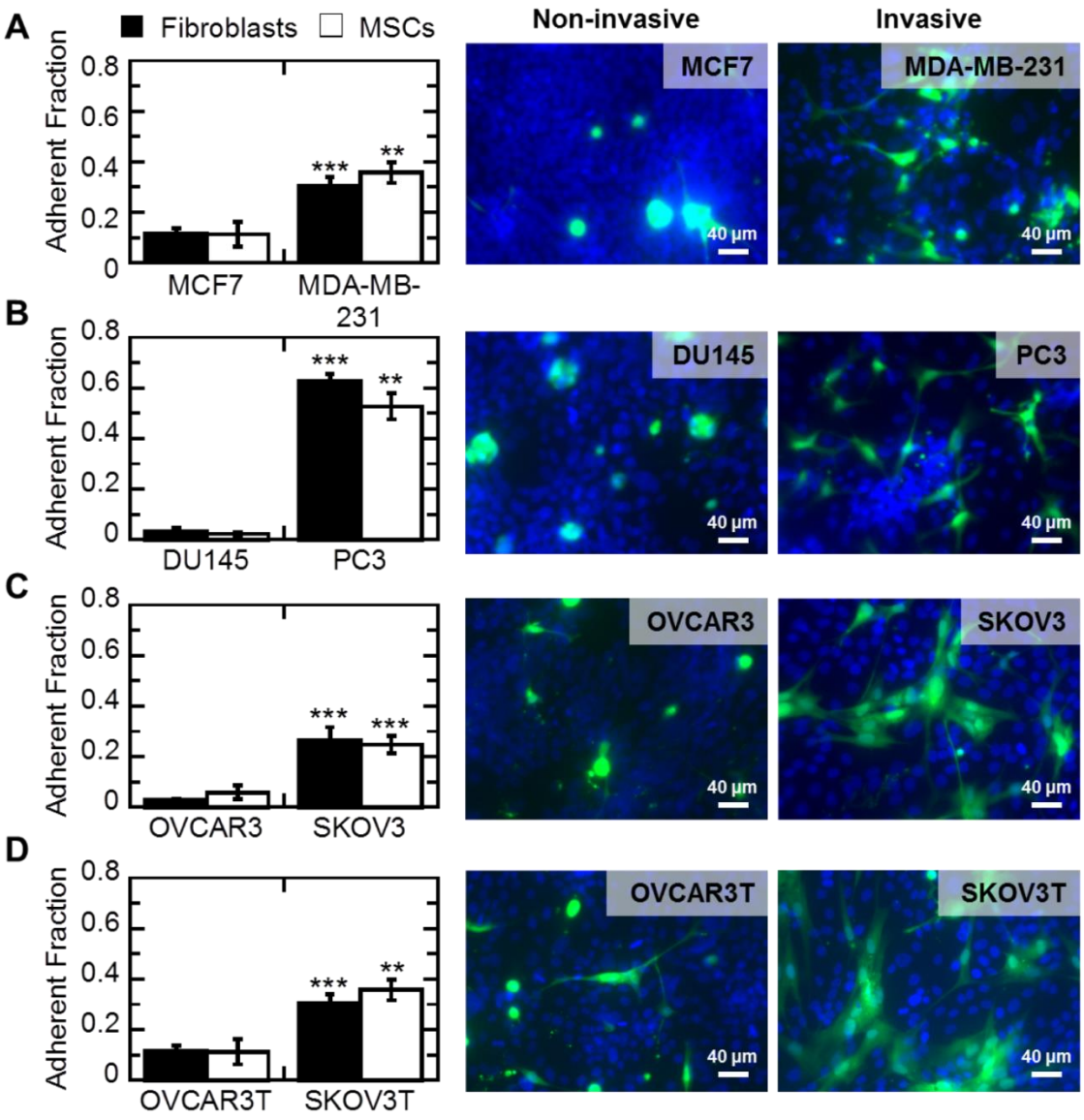

Figure 6.1 Stromal cells attach and spread more on invasive cancer cells. Fibroblasts and MSCs were more adherent on invasive breast (A), prostate (B), ovarian (C), and chemoresistant ovarian cancer cells (D). Fibroblasts were labeled with CFSE and allowed to spread on cancer cells for 24 hours followed by counterstaining with DAPI (right images). Scale bar=40 µm.

A similar trend was found comparing adhesion to ovarian cancer cell lines SKOV3 and OVCAR3 (**Figure 6.1C**) and their chemoresistant counterparts SKOV3T and OVCAR3T (**Figure 6.1D**). Stromal cells adhesion was significantly increased on chemoresistant compared to chemoresponsive ovarian cancer cells (OVCAR3 vs. OVCAR3T, SKOV3 vs. SKOV3T, $p<0.001$). In addition, fibroblasts and MSCs were able to spread more on invasive cells than non-invasive cells (**Figure 6.1, Figure 6.2**).

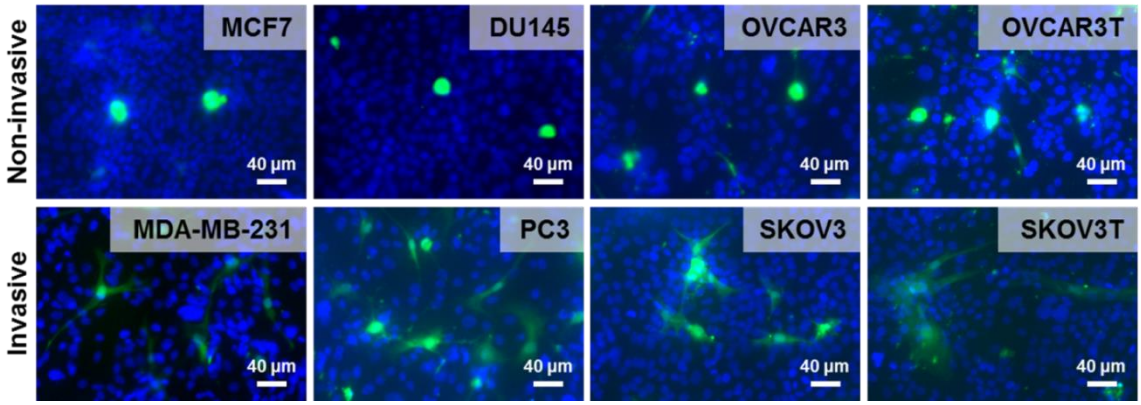

Figure 6.2 MSCs spread more on invasive cancer cells. MSCs were labeled with CFSE and seeded on cancer cell monolayers for 24 hours followed by labeling nuclei (blue). Scale bar= 40 µm.

6.3.2 Stromal cell adhesion to cancer cells is not mediated through soluble factors or integrins

Previous studies have demonstrated that conditioned media (CCM) derived from non-invasive cancer cells differs from CM from invasive cancer cells [153,154]; consequently, we tested whether the increase in adhesion to invasive cancer cells was due to differences in soluble factor secretion. The accumulation of soluble factors (24 hr CCM) did not alter adhesion to non-invasive or invasive breast cancer cells (**Figure 6.3A**).

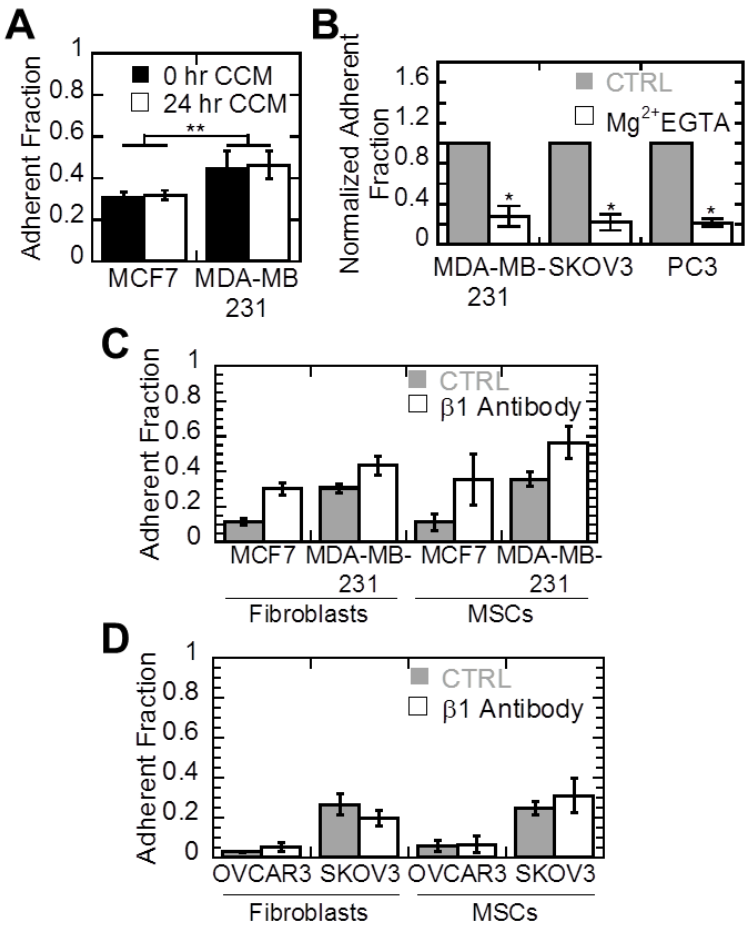

Figure 6.3 Stromal cell adhesion to cancer cells is mediated by cadherins. The accumulation of soluble factors (24 hr CCM) did not have a significant effect on MSC adhesion to MCF7 or MDA-MB-231 (A). Chelation of Ca2+ with EGTA decreased fibroblast adhesion to MDA-MB-231, SKOV3, and PC3 (B). β1 inhibition with 10 μg/mL antibody did not significantly decrease the adhesion of stromal cells to breast (C) or ovarian cancer cells (D).

To determine if stromal cell adhesion to invasive cancer cells is mediated through integrins or cadherins, integrins were activated with Mg^{2+} and ethylene glycol tetraacetic acid (EGTA) [155]. Cadherins are Ca^{2+} dependent; thus, chelation of Ca^{2+} with EGTA will also deactivate cadherins. Stromal cell adhesion was not increased with the addition of EGTA (**Figure 6.3B**), suggesting that it is not integrin mediated. To confirm stromal cells were not adhering to invasive cancer cells through integrins, β1 integrin, which has been shown to be highly expressed in invasive breast [156] and ovarian cancer [157], was blocked. Blockade of β1 integrin did not reverse adhesion to breast or ovarian cancer cells (**Figure 6.3C,D**). These results suggested stromal cell adhesion is mediated by cadherins.

6.3.3 Cadherin 11 and 2 are highly expressed in stromal cells and invasive cancer cells

Integrin activation and inhibition experiments suggested that stromal cell adhesion to invasive cancer cells is mediated through cadherins (**Figure 6.3**). Non-invasive cancer cells can utilize EMT, a process by which cancer cells alter cell-cell and cell-ECM adhesion, to acquire a migratory or invasive phenotype [43]. This transition is characterized by increased expression of cadherin 2 (N-cadherin) and cadherin 11 (OB-cadherin) [43]; thus, immunostaining was performed for these two proteins. Fibroblasts and MSCs expressed high levels of cadherin 11 and 2 (**Figure 6.4A**). Invasive breast and prostate cancer cells express high levels of cadherin 11 whereas non-invasive cells do not (**Figure 6.4B,C**). Although invasive prostate cancer cells (PC3) express cadherin 2 (**Figure 6.4C**), the invasive breast cancer cell line MDA-MB-231 does not (**Figure 6.4B**).

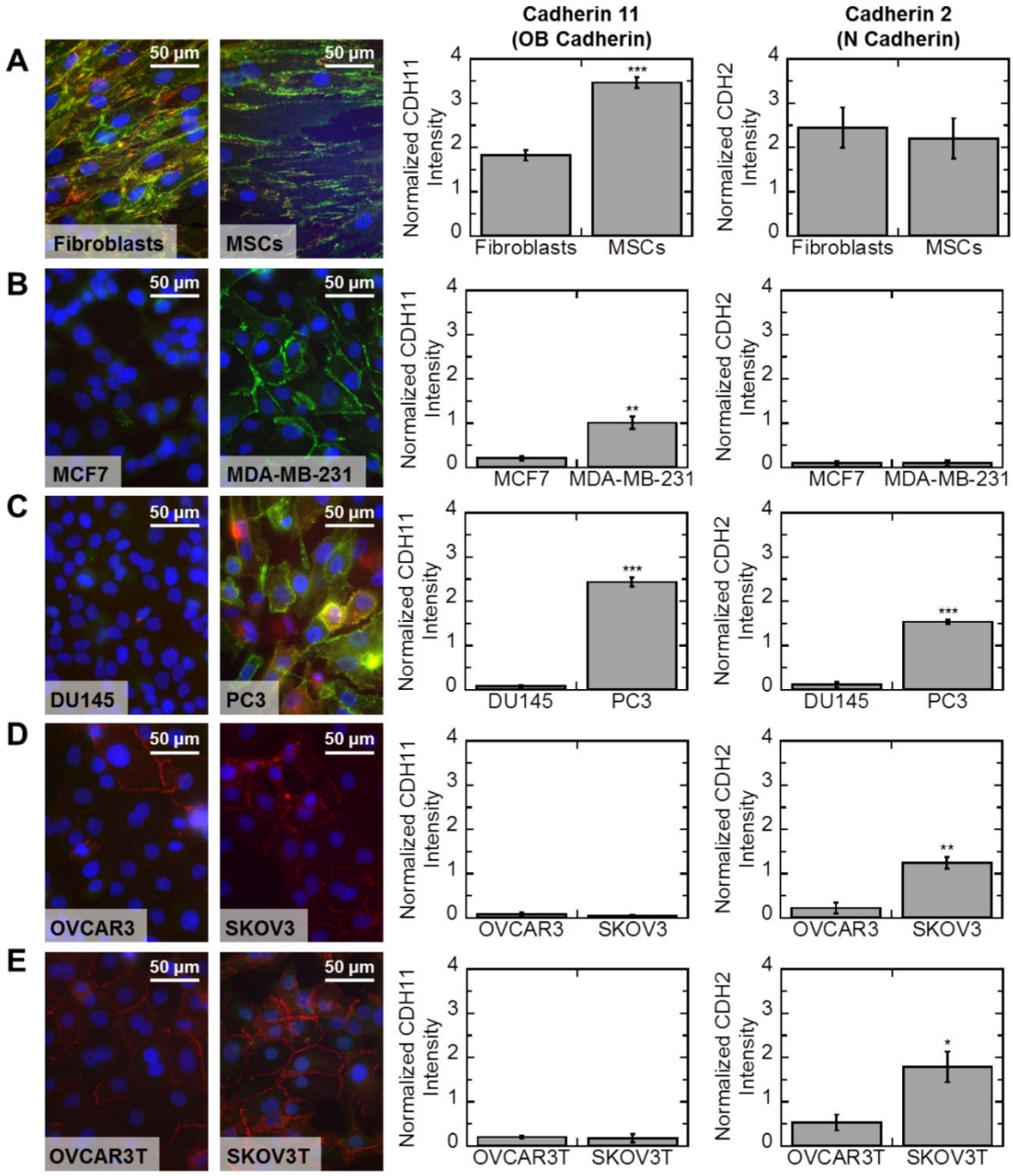

Figure 6.4 Cadherin 11 and 2 are highly expressed in stromal cells and invasive cancer cells. Immunofluorescent images of fibroblasts and MSCs (A), and breast (B), prostate (C), ovarian (D), and chemoresistant ovarian cancer cells (E) labeled for cadherin 2 (red), cadherin 11 (green), and nuclei (blue). Scale bar=50 µm. Cadherin intensity was calculated as the integrated intensity of the segmented cadherin divided by the total number of cells (nuclei) per image. To account for batch differences in light intensity, each experiment was normalized to its respective average.

Ovarian cancer cells did not express cadherin 11; however, invasive ovarian cancer cells express high levels of cadherin 2. Expression of cadherin 2 was further increased in chemoresistant compared to chemoresponsive ovarian cancer cells (**Figure 6.4D,E**).

6.3.4 Stromal cell adhesion to invasive cancer cells is mediated through cadherin 11 interactions

High expression of cadherin 11 in stromal cells coupled with increased expression of cadherin 11 in invasive cancer cells suggested stromal cells may utilize this protein to attach to invasive cancer cells. Blocking cadherin 11 on fibroblasts significantly reduced their adhesion to invasive breast and ovarian cancer cells (**Figure 6.5A**), although invasive ovarian cancer cells do not express cadherin 11 (**Figure 6.4**). A similar trend was observed with MSCs (**Figure 6.5B**). A higher concentration of antibody was required to block adhesion, in agreement with increased cadherin 11 expression (**Figure 6.4A**). Immunostaining for cadherin 11 and 2 revealed cadherin 11 colocalizes with cadherin 2 at sites of cell-cell adhesion in both fibroblasts and MSCs (**Figure 6.5C**). Cadherin 11 and 2 were also colocalized at sites of adhesion of fibroblasts to MDA-MB-231 and SKOV3, but not MCF7 or OVCAR3 (**Figure 6.5D**). A similar trend was found with MSCs (**Figure 6.6**).

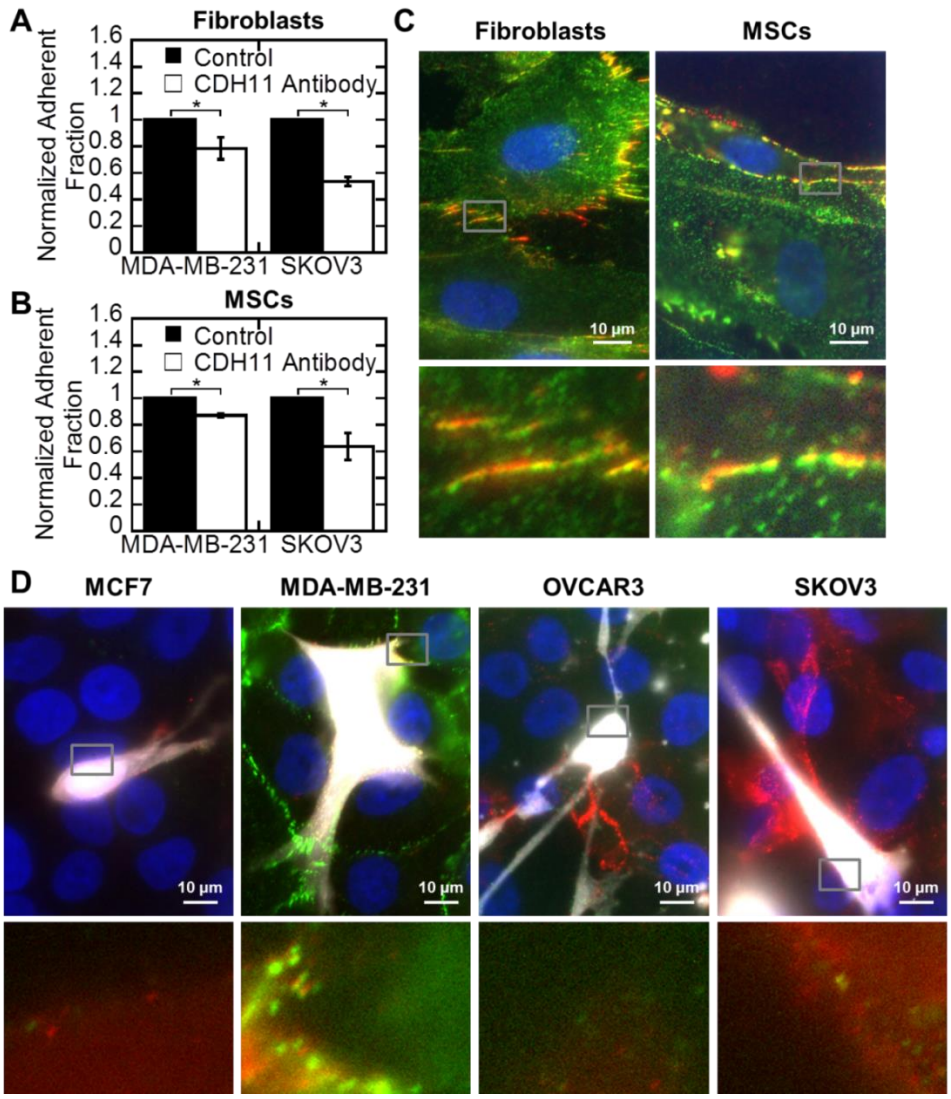

Figure 6.5 Stromal cell adhesion to invasive cancer cells is mediated through cadherin 11 interactions. Fibroblast (A) and MSC (B) adhesion to MDA-MB-231 and SKOV3 is decreased with cadherin 11 blocking antibody. Immunofluorescent images of cells labeled for cadherin 2 (red), cadherin 11 (green), and nuclei (blue) with zoomed images of highlighted regions revealed cadherin 2 and 11 colocalize at sites of cell-cell adhesion (C). Fibroblasts were labeled with CFSE (white). Cadherin 2 and 11 colocalize at sites of fibroblast adhesion to MDA-MB-231 and SKOV3 but not MCF7 and OVCAR3 (D). Scale bar=10 μm.

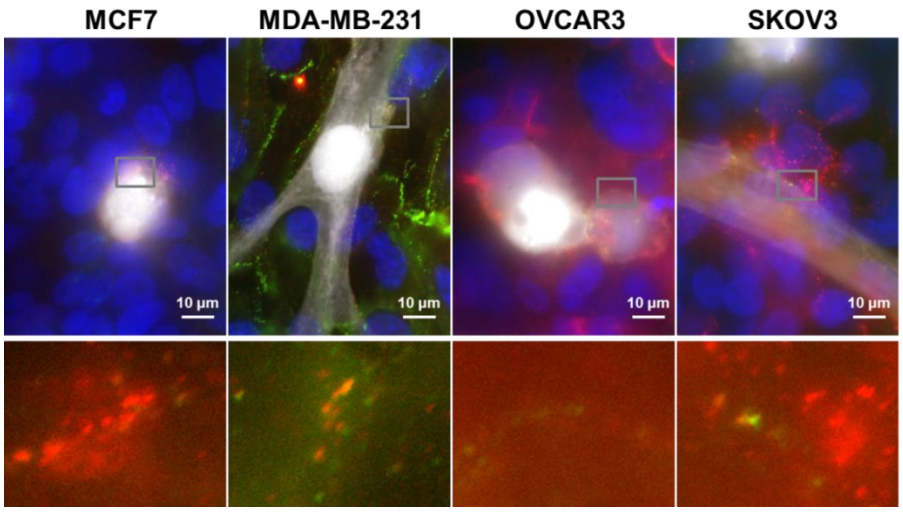

Figure 6.6 MSC adhesion to invasive cancer cells is mediated through cadherin 11 interactions. Immunofluorescent images of cells labeled for cadherin 2 (red), cadherin 11 (green), and nuclei (blue) with zoomed images of highlighted regions. MSCs were labeled with CFSE (white). Cadherin 2 and 11 colocalize at sites of MSC adhesion to MDA-MB-231 and SKOV3 but not MCF7 and OVCAR3 (D). Scale bar=10 µm.

6.4 Discussion

Soluble factors from fibroblasts are known to promote cell transformation and tumor growth [158]. Likewise, MSCs secrete soluble factors such as CCL5, IL6, TGFβ, VEGF and SDF-1 that promote tumor progression by increasing cancer cell proliferation, migration, and invasion [29]. Previous studies have demonstrated that MSCs must be in close proximity to cancer cells to induce CCL5 secretion required for increased cancer cell migration and invasion [28]. Both cell types induce angiogenesis within the tumor, allowing for influx of nutrients for growth as well as additional avenues for escape [141]. In addition, fibroblasts are primed by interstitial flow to remodel the ECM to promote invasion [159]. Fibroblast remodeling of the matrix generates tracks for cancer cells to follow promoting collective invasion [160]. High expression of EMT markers has been observed at this invasive front of tumors [141], which may subsequently recruit more

stromal cells, further promoting cell invasion. Consequently, increased engraftment of stromal cells on invasive cancer cells observed in this study may further promote the proliferative and invasive properties of cancer cells.

Non-invasive cells display an epithelial phenotype characterized by high levels of cadherin 1 and low levels of cadherin 2 [43]. Homotypic cadherin 1 bonds are significantly stronger than homotypic cadherin 2 and 11 bonds; however, heterotypic cadherin 1 and 2 bonds infrequently form [161,162]. Previous studies have demonstrated that MSCs form adherens junctions with MCF7 cells consisting of MCF7 cadherin 1 and MSC cadherin 2, and blocking either of these proteins, but not cadherin 11, abolishes cell adhesion [163]. Cadherin 2 was present at sites of stromal cell adhesion to non-invasive cells (**Figure 6.5, 6.6**), suggesting that this is the mechanism of adhesion to non-invasive cells. Few stromal cells were able to attach and spread on non-invasive cells; thus, this type of adhesion may not be conducive for long-term stromal cell engraftment. Homotypic cadherin 11 bonds are stronger than cadherin 2 junctions [164]; consequently, enhanced adhesion to invasive cancer cells may be a result of differences in bond strength. Stromal cell adhesion was enhanced on PC3 compared to MDA-MB-231 and SKOV3 (**Figure 6.1**), and this is associated with enhanced cadherin 11 expression of PC3 (**Figure 6.4**), further supporting this mechanism.

Stromal cells were largely unable to spread on non-invasive cancer cells, but were able to do so on invasive cancer cells. The inability of cells to spread has been associated with apoptosis [165]; thus, the inability of stromal cells to spread on non-invasive cancer cells may reduce their long term survival. Cell spreading [19] and cadherin 11 expression [8,166] are also critical in MSC differentiation and fibroblast differentiation into tumor-

promoting myofibroblasts [8,166], which are thought to have similar characteristics to cancer-associated fibroblasts (CAFs) [34]. In addition, cadherin 11 is upregulated in myofibroblasts and is important for contractile activity [33]. Enhanced contractility of stromal cells leads to matrix remodeling that promotes cancer cell growth, survival, and invasion [33]. This suggests that stromal cells recruited to invasive tumors may be more likely to differentiate into myofibroblasts or CAFs and further promote invasion and metastasis.

Surprisingly, blocking cadherin 11 on stromal cells reversed their adhesion to invasive SKOV3 cancer cells that do not express cadherin 11. Cadherins typically form homotypic junctions; however, cadherin 11 has been shown to bind to cadherin 2 [167]. Immunofluorescent images of adhesion sites of stromal cells to SKOV3 displayed colocalization of cadherin 11 with cadherin 2 (**Figure 6.5D**), suggesting stromal cells utilize cadherin 11 to bind to both cadherin 2 and 11, which are frequently expressed on invasive cancer cells that have undergone EMT [150,151]. In addition, EMT has been linked to chemoresistance [168]. Consequently, this mechanism of adhesion may be conserved across many types of cancer and is a potential therapeutic target for metastatic cancer. Blocking cadherin 11 with the FDA-approved rheumatoid arthritis drug celecoxib has inhibited the growth of glioblastoma, breast, and prostate cancer cells [169]. This suggests that in vivo cadherin 11 inhibition may have effects on both tumor cell growth and stromal cell recruitment.

6.5 Conclusions

Our studies showed that stromal cells preferentially adhere to invasive breast, ovarian, and prostate cancer and chemoresistant ovarian cancer cells. Sites of stromal cell

adhesion to invasive cancer cells were characterized by colocalization of cadherin 11 and 2. Blocking cadherin 11 on stromal cells reversed adhesion to invasive cancer cells. These studies elucidate how stromal cells attach to cancer cells by cadherin-mediated interactions and provide a new approach for treating invasive cancers by targeting cell adhesion molecules on stromal cells.

6.6 Materials and Methods

6.6.1 Cell Culture

Human MSCs (Donor 7071L) were obtained from Texas A&M Institute for Regenerative Medicine and cultured in αMEM (Corning) with 20% FBS (Atlanta Biologicals), 1% penicillin-streptomycin (Corning), and 1% L-glutamine (Corning). Cell lines Hs27 (foreskin fibroblasts), MCF7 (non-invasive breast cancer), OVCAR3 (non-invasive ovarian cancer), SKOV3 (invasive ovarian cancer), DU145 (non-invasive prostate cancer), and PC3 (invasive prostate cancer) were obtained from ATCC and cultured in RPMI (Corning) with 10% FBS and 1% penicillin-streptomycin. MDA-MB-231 (invasive breast cancer) were obtained from ATCC and cultured in low glucose DMEM (Corning) 10% FBS and 1% penicillin-streptomycin. Chemoresistant OVCAR3 (OVCAR3T) and SKOV3 (SKOV3T), which are characterized by a 10-fold higher IC50 value than chemoresponsive OVCAR3 and SKOV3, were isolated by repeated exposure to 10 nM Taxol and allowed to recover as described [157].

6.6.2 Adhesion Assays

MSCs or fibroblasts were labeled with calcein AM (Enzo) and allowed to adhere on cancer cell monolayers in HBSS (Corning) with 100 mM $CaCl_2$ and 100 mM $MgSO_4$ for 1 hour before taking an initial fluorescence reading. Plates were rinsed with HBSS to

remove non-adherent cells and a final reading was taken. Adherent fraction was calculated as the final reading divided by initial reading after subtraction of background fluorescence. To determine the effect of soluble factors on adhesion, serum-free DMEM was added to cancer cell monolayers for 24 hours (24 hr CCM condition). For 0 hr CCM, serum-free DMEM was replaced immediately before seeding MSCs to remove accumulated soluble factors. MSCs were labeled with carboxyfluorescein succinimidyl ester (CFSE, Biolegend) and allowed to adhere on cancer cell monolayers in serum-free DMEM for 1 hour before taking an initial fluorescence reading, then rinsing with serum free DMEM, and taking a final fluorescence reading. In order to activate integrins, fibroblasts were labeled with CFSE and incubated with 100 mM $MgSO_4$ and 1 mM EGTA (Corning) [155]. For integrin blocking experiments, fibroblasts were incubated with 10 μg/mL β1 integrin antibody (DSHB) for 30 minutes prior to seeding on cancer cell monolayers. In order to block cadherin 11, 10 μg/mL cadherin 11 antibody (R&D Systems) was used for fibroblasts and 15 μg/mL cadherin 11 antibody for MSCs. Titration experiments were performed for MSCs, as they displayed increased expression of cadherin 11 compared to fibroblasts, to determine the antibody concentration (**Figure 6.7**).

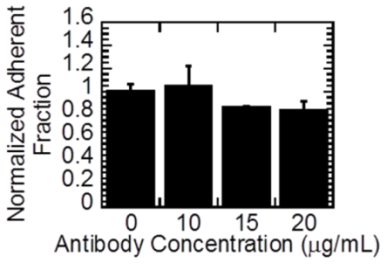

Figure 6.7 Cadherin 11 antibody titration for MSCs. MSCs were treated with increasing concentrations of cadherin 11 antibody until adhesion was inhibited at 15 μg/mL.

6.6.3 Immunofluorescence Assays

For imaging of cadherin 2 and 11, cells seeded on glass coverslips were fixed with 4% formaldehyde, blocked with 5% horse serum (Sigma Aldrich), followed by incubation with human cadherin 11 antibody, Dylight 650 conjugated rabbit anti-goat antibody (Thermo Scientific), human cadherin 2 antibody (Biolegend), and Alexa Fluor 547 conjugated goat anti-mouse antibody (Invitrogen) for 1 hour each. Cells were counterstained with DAPI (Anaspec) and coverslips sealed with Vectashield (Vector Labs). Cells were imaged using a Nikon Eclipse Ti microscope at 40x magnification. For imaging of fibroblast adhesion to cancer cells, fibroblasts were labeled with CFSE and allowed to adhere for 24 hours prior to staining as described above. Cells were imaged using a Nikon Eclipse Ti microscope at 100x magnification.

6.6.4 Image Quantification

Nuclei were segmented using a 3 standard deviation threshold above the mean following band pass filtering. Nuclei centers were determined as local maximums of band passed images and used to separate any touching nuclei by a seeded watershed method [170]. Cadherin images were segmented using Otsu's method following median filtration and background subtraction. Cadherin density was defined as the integrated intensity of the segmented region divided by the total number of cells per image as determined from the nuclei segmentation. To account for batch differences in light intensity, each experiment was normalized to its respective average.

6.6.5 Statistical Analysis

All experiments were performed in triplicate or more. A student's t-test was used for all statistical analysis with $p<0.05$ being statistically significant (* $p<0.05$, ** $p<0.01$,

*** $p<0.001$). ANOVA with a Tukey post-hoc test was utilized for comparison of OVCAR3 and SKOV3 to OVCAR3T and SKOV3T. Data were reported as the mean ± SEM unless otherwise noted.

CHAPTER 7

MESENCHYMAL STEM CELLS INDUCE THE DIRECTIONAL MIGRATION OF INVASIVE BREAST CANCER CELLS THROUGH THE TGF-β PATHWAY

7.1 Summary

MSCs are recruited to the tumor microenvironment and influence tumor progression; however, how MSCs induce the invasion of cancer cells is not completely understood. Here, we used a 3D coculture model to determine how MSCs affect the migration of invasive breast cancer cells. Coculture with MSCs increases the elongation, directional migration, and traction generation of breast cancer cells. While PDGFR is important for breast cancer cell directional migration when cultured alone, this pathway is dispensable in coculture. MSC-induced directional migration directly correlates with force generation and is mediated by TGFβR and the migratory proteins ROCK, FAK, and MMPs. Treatment with recombinant TGF-β1 elicits a similar migration response to coculture. Taken together, this work suggests TGF-β is secreted when breast cancer cells are cocultured with MSCs, leading to force-dependent directional migration of invasive cancer cells. These pathways may be potential targets for blocking cancer cell invasion and subsequent metastasis.

7.2 Introduction

The tumor microenvironment consists of malignant cells, a network of ECM proteins, and a variety of recruited cells. All of these components dynamically interact to influence cancer progression. These interactions are mediated by chemical signals, including cytokines, chemokines, growth factors, and matrix remodeling proteins. In

addition, mechanical signals provided by the tumor microenvironment can have profound effects on tumor progression [33]. Drugs that minimize the crosstalk between cells in the tumor microenvironment have been proposed as potential targets for cancer prevention [171] and treatment [26,172]. A number of drugs targeting different components of the microenvironment, including blood vessels, ECM, fibroblasts, and immune cells, have been developed [26]. Sibrotuzumab was developed to target fibroblast activation protein (FAP), which is involved in matrix degradation and is expressed by fibroblasts in the tumor microenvironment[31]. In addition, imatinib targets receptor tyrosine kinases (RTKs) critical for fibroblast function [26].

MSCs are recruited from the bone marrow and local adipose tissue [144] in response to tumor-secreted soluble factors [48,78]. Gene expression of stromal cells is indicative of patient prognosis [35], suggesting these recruited cells play a critical role in regulating tumor progression. MSCs promote the growth of tumors through differentiation into CAFs, angiogenesis induction, and secretion of growth factors [27]. While local adipose-derived MSCs express markers characteristic of vascular stroma (NG2, CD31, αSMA), stromal cells derived from bone marrow MSCs express high levels of CAF-associated markers FAP and fibroblast specific protein (FSP), both of which are thought to be critical for invasion and metastasis [144]. MSCs can also induce the metastasis of breast tumors through secretion of soluble factors such as of CCL5 [28] and enhancing cancer stem cell properties [173]. Thus, a better understanding of how MSCs induce the invasive properties of cancer cells could provide potential therapeutic targets for metastatic cancer.

The ECM also plays a critical role in cancer progression. During breast cancer progression, stromal cells deposit fibrillar collagen [174], which increases cancer cell proliferation and invasion [175]. In addition, the mechanical properties of the ECM can induce a malignant phenotype [40], promote tumor progression [176], and are critical for the generation and maintenance of the CAF phenotype [177]. In order to migrate in 3D environments, cancer cells must navigate and remodel dense ECM [178–181]. Two major types of migration are utilized by individual cancer cells to migrate in 3D: amoeboid and mesenchymal. Amoeboid migration is characterized by rounded cells that circumnavigate ECM without the use of adhesion proteins or matrix degradation; whereas for mesenchymal migration, cells elongate, establish integrin-mediated adhesion to the ECM, degrade ECM with matrix metalloproteinases (MMPs), and contract the cell body via MLCK, Rho, and ROCK [182]. Previous studies have demonstrated that fibroblasts utilize Rho-mediated matrix remodeling to generate tracks to enable the invasion of cancer cells [160]. In addition, interstitial flow causes fibroblasts to reorganize collagen fibers through Rho, which promotes cancer cell invasion [159]. Fibroblasts have similar gene expression profiles [183] and immunomodulatory properties [184] to MSCs; thus, we hypothesized that MSCs may induce the invasion of cancer cells through similar mechanisms.

In this study, we show that coculture with MSCs causes MDA-MB-231 invasive breast cancer cells to elongate and directionally migrate. Small molecule inhibitor studies revealed MSC-induced directional migration is mediated by TGF-β, ROCK, FAK, and MMPs, but not PDGF or VEGF. Force generation appeared to be critical for cancer cell migration, as directional migration directly correlated with traction generation. Treatment

of cancer cells with recombinant TGF-β1 elicited a strikingly similar response to MSC coculture, suggesting that TGF-β secreted in coculture activates ROCK, FAK, and MMPs to facilitate the directional migration of cancer cells. These results elucidate how MSCs induce breast cancer cell invasion and may provide therapeutic targets to prevent invasion and metastasis.

7.3 Results

7.3.1 Coculture with MSCs induces the elongation and directional migration of breast cancer cells

Alterations in cell shape are critical for cell migration in 3D [42]; thus, we characterized morphological changes after coculture. MDA-MB-231 breast cancer cells (MDA) cultured alone in collagen gels remained largely unspread (**Figure 7.1A**). Upon coculture with MSCs, MDA appeared more elongated (**Figure 7.1B**). Quantification of the aspect ratio of cells revealed MDA were significantly more elongated in coculture (**Figure 7.1C**).

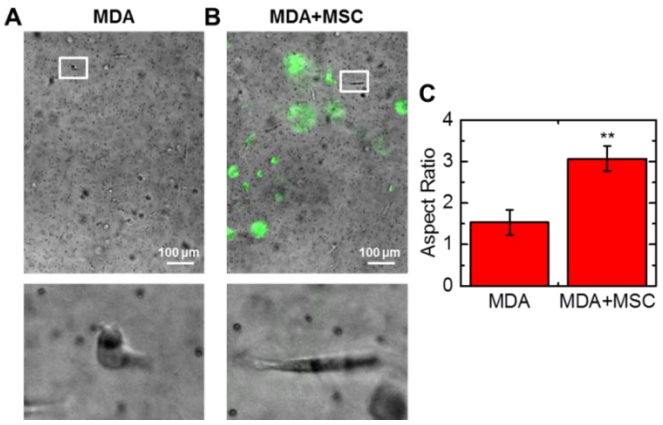

Figure 7.1 Breast cancer cells display an elongated phenotype in coculture. Images of invasive breast cancer cells (MDA-MB-231, MDA) cultured alone (A) and in coculture with MSCs (green, B). (C) MDA were significantly ($P<0.01$) more elongated in coculture. * $P<0.05$, ** $P<0.01$, *** $P<0.001$.

Cell elongation has been associated with enhanced tumor cell invasion and metastasis [182]; consequently, we next evaluated cell migration of MSCs and MDA-MB-231 in collagen gels (**Figure 7.2A**). MSCs moved in a directional manner, but the presence of MDA did not increase their directional migration (**Figure 7.2B**). The migration of MDA was more random, which corresponded to a lower directional velocity than MSCs (**Figure 7.2B,C**). Coculture with MSCs led to an increase in MDA directional velocity which is critical for cancer invasion [185] (**Figure 7.2C**) as well as random migration (**Figure 7.3**).

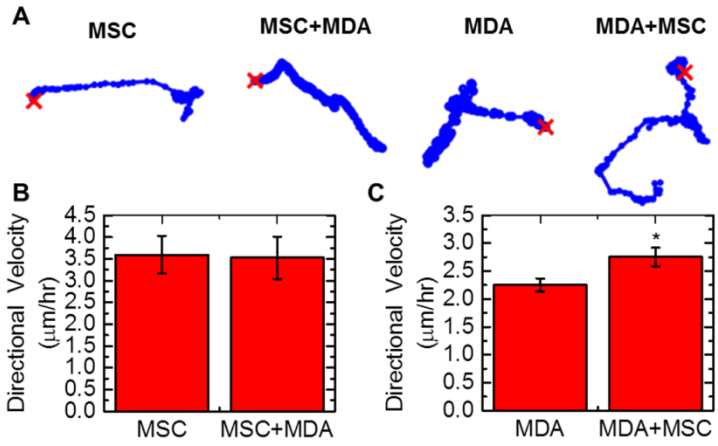

Figure 7.2 Coculture induces the migration of breast cancer cells but not MSCs. (A) Traces of MSC and MDA migration alone and in coculture. The directional migration of MSCs (B) and MDA (C). * P<0.05, ** P<0.01, *** P<0.001.

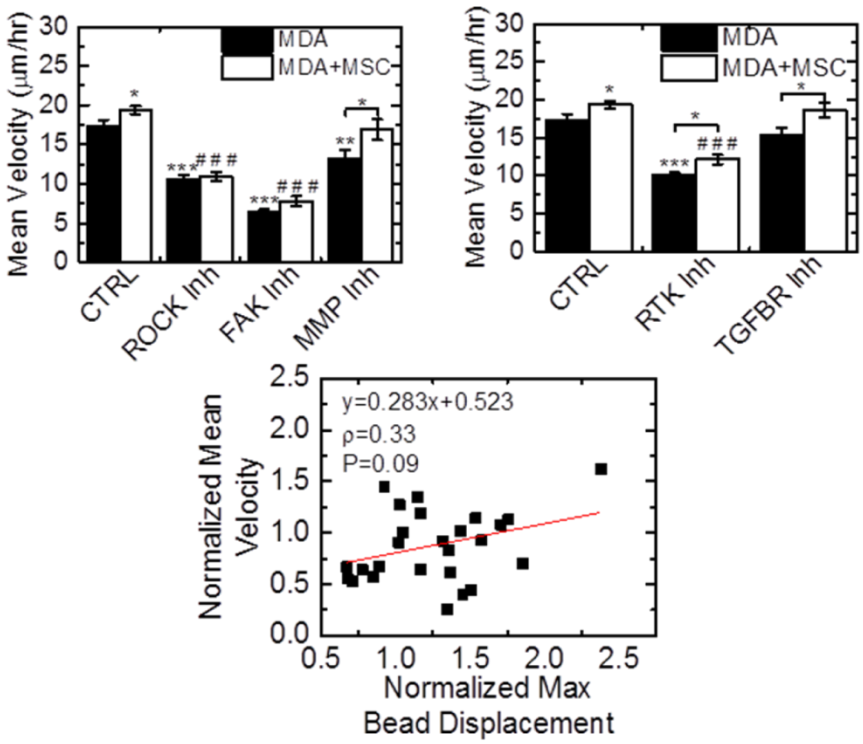

Figure 7.3 TGFβR is involved in directional migration but not overall motility. MDA were treated with control media (CTRL, SF DMEM), ROCK inhibitor (1 μM H-1152), FAK inhibitor (20 μM PF-573228), MMP inhibitor (20 μM GM-6001), RTK inhibitor (1 μM Sunitinib) or TGFβR inhibitor (1 μM SB-505124). Mean velocity does not significantly correlate with max bead displacement (ρ=0.33, P=0.09). Significance is indicated relative to MDA control cells with *'s and relative to MDA+MSC with #'s. * P<0.05, ** P<0.01, *** P<0.001.

In order to determine if MSC-induced directional migration is specific to invasive breast cancer cells, we cocultured MSCs with the non-invasive breast cancer cell line MCF7. MSCs did not induce a significant increase in random or directional migration of MCF7 (**Figure 7.4**), indicating the MSC-induced migration observed is specific to invasive breast cancer cells.

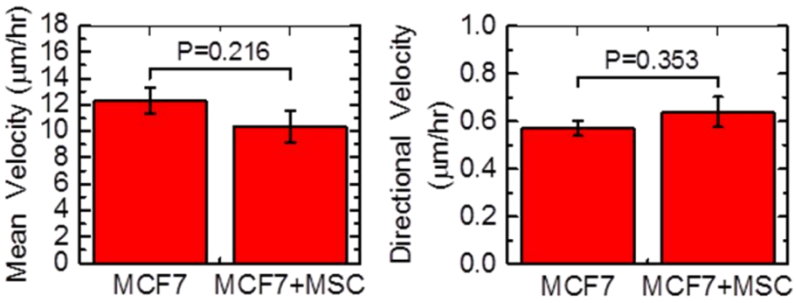

Figure 7.4 MSCs do not induce the migration of non-invasive breast cancer cells. The random (mean velocity) and directional migration (directional velocity) of MCF7 alone and in coculture with MSCs. Mean velocity and directional velocity were not significantly changed in coculture (P=0.216, P=0.353, respectively).

7.3.2 MSC-induced directional migration is mediated through TGFβR and mechanotransduction pathways

Cell elongation has been associated with the mesenchymal mode of migration, where cells utilize cell contractility, focal contacts, and MMPs to migrate [182]; thus, we hypothesized these pathways may be involved in MSC-induced directional migration of MDA. We targeted cell contractility with a ROCK inhibitor (H-1152), adhesion turnover with a FAK inhibitor (PF-573228), and MMP activity with a MMP inhibitor (GM-6001). Inhibition of these proteins decreased the directional velocity of MDA cultured alone (**Figure 7.5A**). In addition, differences in directional migration between MDA alone and MDA in coculture with MSCs were abrogated with inhibition of ROCK, FAK, and MMPs (**Figure 7.5A**), suggesting these pathways are critical for MSC-induced migration. In order to determine the signal upstream of these pathways, we targeted growth factor receptors known to be associated with breast cancer prognosis and metastasis, VEGFR, PDGFR and TGFβR [186–188].

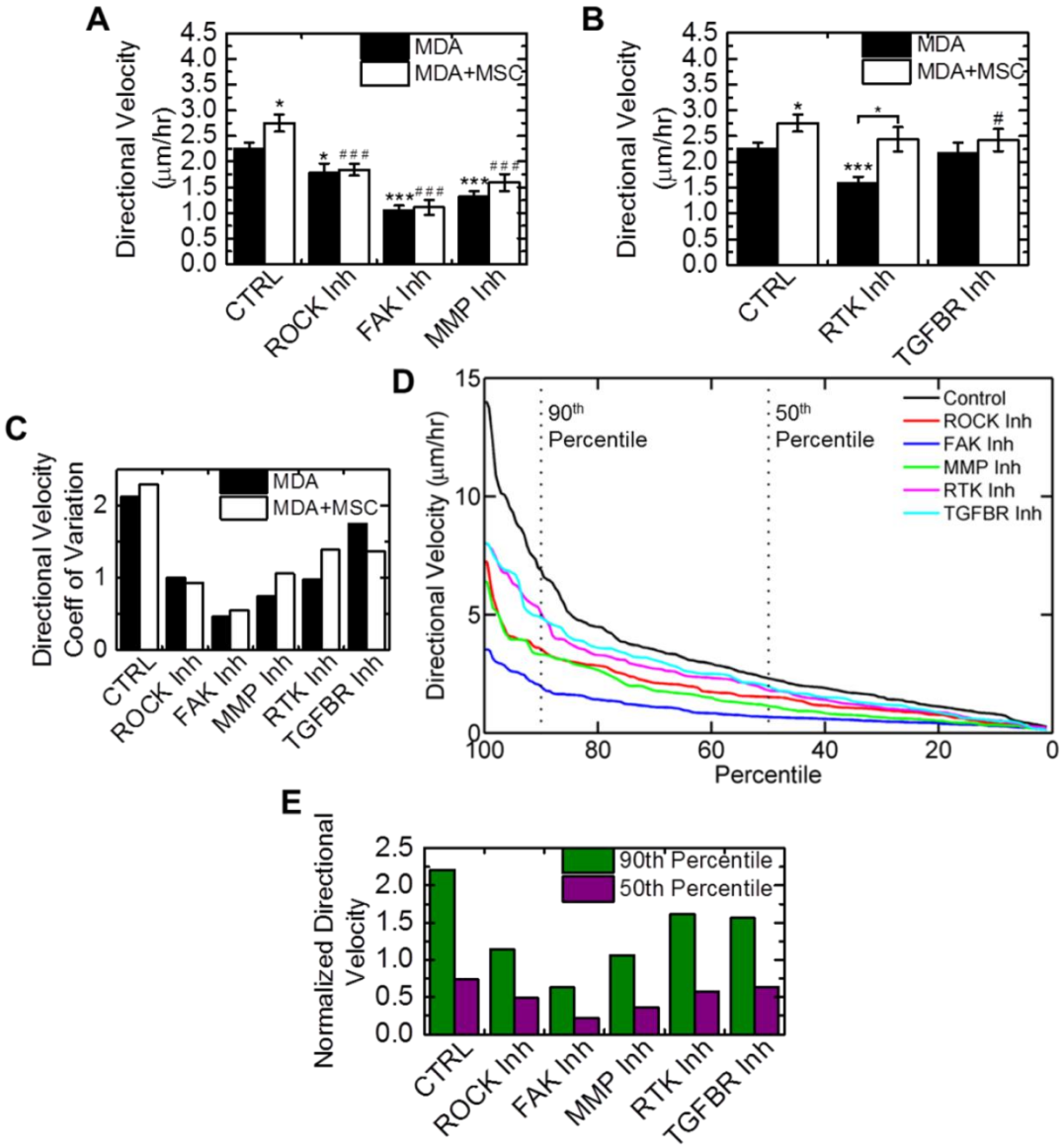

Figure 7.5 MSCs induce the directional migration of invasive breast cancer cells through TGFβR and downstream mechanotransduction pathways. (A,B) The directional velocity of MDA treated with inhibitors. (C) Directional velocity coefficient of variation was calculated. (D) Percentile curves of the directional velocities of MDA in coculture with MSCs. (E) Directional velocity was normalized to the mean directional velocity control cells to determine relative changes in the most motile cells versus average cells. Significance is indicated relative to MDA control cells with *'s and relative to MDA+MSC with #'s. * P<0.05, ** P<0.01, *** P<0.001.

Inhibition of VEGFR and PDGFR with a RTK inhibitor (Sunitinib) decreased the directional velocity of MDA alone; however, it failed to reduce the MSC-induced directional migration response. In contrast, TGFβR did not alter MDA directional migration when cultured alone, but inhibition of this pathway abolished the MSC-induced directional migration response (**Figure 7.5B**). These results suggest that while VEGFR and PDGFR are important for cancer cell migration, they do not mediate this MSC-induced directional migration, which is controlled by TGFβR.

7.3.3 Inhibitors primarily target most motile cells

Heterogeneity in tumor cells has been well documented in breast cancer [189]; thus, we looked at heterogeneity in the directional velocity of breast cancer cells. Both MDA alone and in coculture with MSCs had a high coefficient of variation, indicating that their migration varied widely, similar to the heterogeneous gene expression observed in breast tumors [189]. We also used the coefficient of variation in directional velocity to determine if MDA were responding heterogeneously to inhibition of pathways critical for MSC-induced migration. Treatment with inhibitors generated a more homogenous distribution of velocities (**Figure 7.5C**). ROCK, FAK, and MMP inhibition were associated with the lowest coefficients of variation. In coculture, MDA treated with both MMP and RTK inhibitors had a higher degree of heterogeneity in directional velocity compared to MDA cultured alone. The opposite trend was observed with TGFβR inhibitor treated cells, suggesting this inhibitor elicits a more homogenous response in coculture where TGFβR is more critical for migration. To further determine what was leading to this observed heterogeneous response, we sorted the directional velocities my magnitude and plotted their values as percentile curves of directional velocities for MDA

in coculture with MSCs. The percentile curve was steep for MDA control cells indicating a more heterogeneous distribution of velocities, but after molecular inhibition, the curves were more shallow indicating reduced variation in directional velocity (**Figure 7.5D**). Next, we compared the directional velocity of the 90^{th} and 50^{th} percentiles normalized to the control values for these percentiles; this is a measure of the inhibitor response in the fastest and the average moving cells (**Figure 7.5E**). ROCK, RTK and TGFβR inhibition elicited similar responses, with the top 10% most motile cells displaying the larger differences from non-treated cells compared to average moving cells (**Figure 7.5E**). This suggests that these inhibitors primarily target the most motile cells, with much smaller effects on less motile cells, whereas other inhibitors target all cells to a similar extent. FAK and MMP inhibitors had large effects on both the most motile cells and average moving cells; however, the decrease in directional velocity compared to control cells was similar for each of these percentiles. This indicates that in contrast to ROCK, RTK and TGFβR inhibition, FAK and MMP inhibition more equally targets all cells.

7.3.4 MSCs induce cancer cell force generation which is critical for directional migration

Force generation has been implicated in tumor progression [40] and cell motility [190] and is critical for the mesenchymal mode of migration [182]; thus, we measured the displacement of beads embedded in the collagen gel while cells were migrating. Coculture with MSCs increased the displacement of beads, and inhibition of ROCK, FAK, or MMPs abrogated this increase (**Figure 7.6A**). ROCK inhibition, but not FAK or MMP inhibition, was associated with decreased traction generation compared to non-treated MDA cultured alone. In addition, RTK inhibition did not significantly alter

traction generation (**Figure 7.6B**) or MSC-induced migration (**Figure 7.5B**). Inhibition of TGFβR did not significantly alter traction for MDA cultured alone; however, it did lead to similar traction generation alone and in coculture.

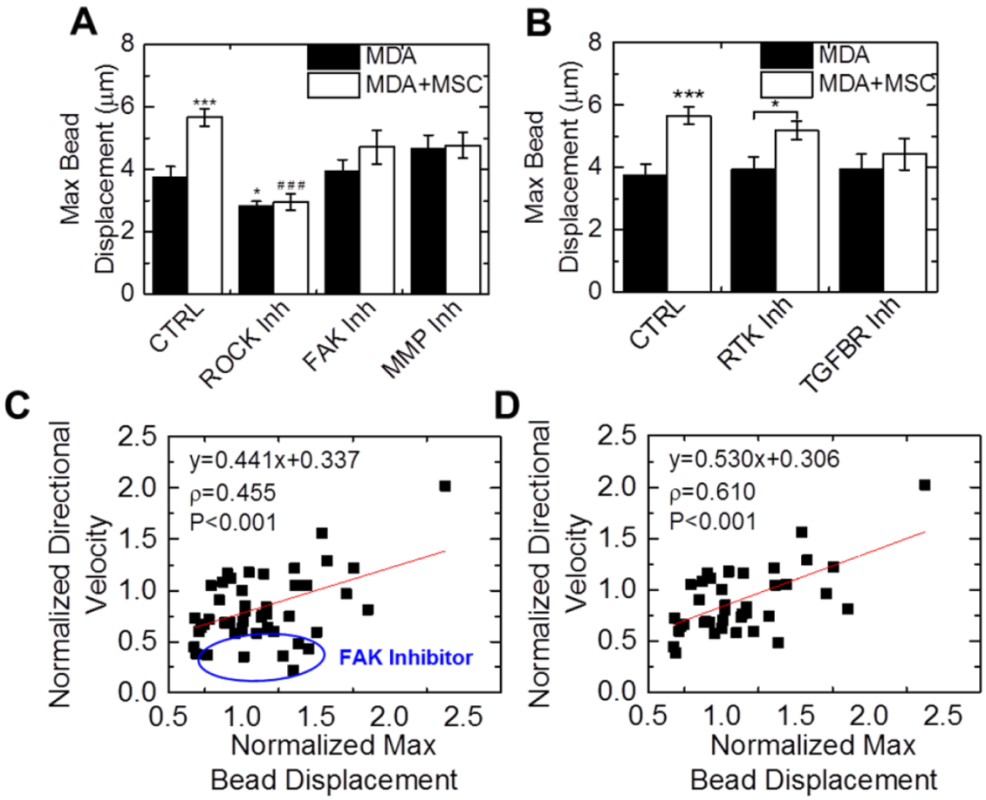

Figure 7.6 MSCs induce cancer cell force generation which is critical for directional migration. (A, B) Max bead displacement exerted by MDA. (C) Directional velocity correlates with max bead displacement (ρ=0.455, P<0.001). (D) Cells treated with FAK inhibitor (identified with blue circle) were identified as outliers (P<0.05) and excluded from analysis, which generated a stronger correlation between directional velocity and max bead displacement (ρ=0.610, P<0.001). Significance is indicated relative to MDA control cells with *'s and relative to MDA+MSC with #'s. * P<0.05, ** P<0.01, *** P<0.001.

These results appeared to follow trends seen with directional velocity (**Fig 7.5**), suggesting that traction generation may be required for directional migration. We

performed correlational analysis and found directional velocity correlated with bead displacement across all experimental conditions (slope=0.441, ρ=0.455, P<0.001, **Figure 7.6C**). We identified outliers in the correlation using studentized deleted residuals and observed that all outliers were cells treated with FAK inhibitor. This suggests that while active FAK is required for adhesion turnover necessary for directional migration, it is not integral for traction generation. After removal of FAK-treated cells from analysis, a stronger correlation between directional velocity and max bead displacement was observed (ρ=0.610, P<0.001, **Figure 7.6D**).

7.3.5 TGFβ treatment induces directional migration similar to MSC coculture

In order to verify that TGF-β1 was the primary factor leading to increased directional migration in coculture, we treated with growth factors known to be secreted by MSCs [29] that signal through TGFβR and RTKs to test if they induce a similar response. Treatment with TGF-β1 elicited a similar migration response to MSC coculture (**Figure 7.7A**). To further verify these findings, we also treated with recombinant PDGF-BB and VEGF-165, the ligands for the primary receptors targeted by the RTK inhibitor Sunitinib. PDGF-BB treatment induced directional migration; however, it did not increase migration to the degree TGF-β1 or coculture did. VEGF did not induce migration of MDA. These data suggest that the TGF-β pathway is primarily responsible for the migration observed in coculture. We then inhibited mechanotransduction pathways to determine if TGF-β was signaling through ROCK, FAK, and MMPs. Treatment with TGF-β1 in combination with these inhibitors elicited responses similar to coculture (**Figure 7.7B**). Together these data suggest that coculture leads to secretion of

TGF-β1 which acts through ROCK, FAK, and MMPs to induce the directional migration of MDA (**Figure 7.7C**).

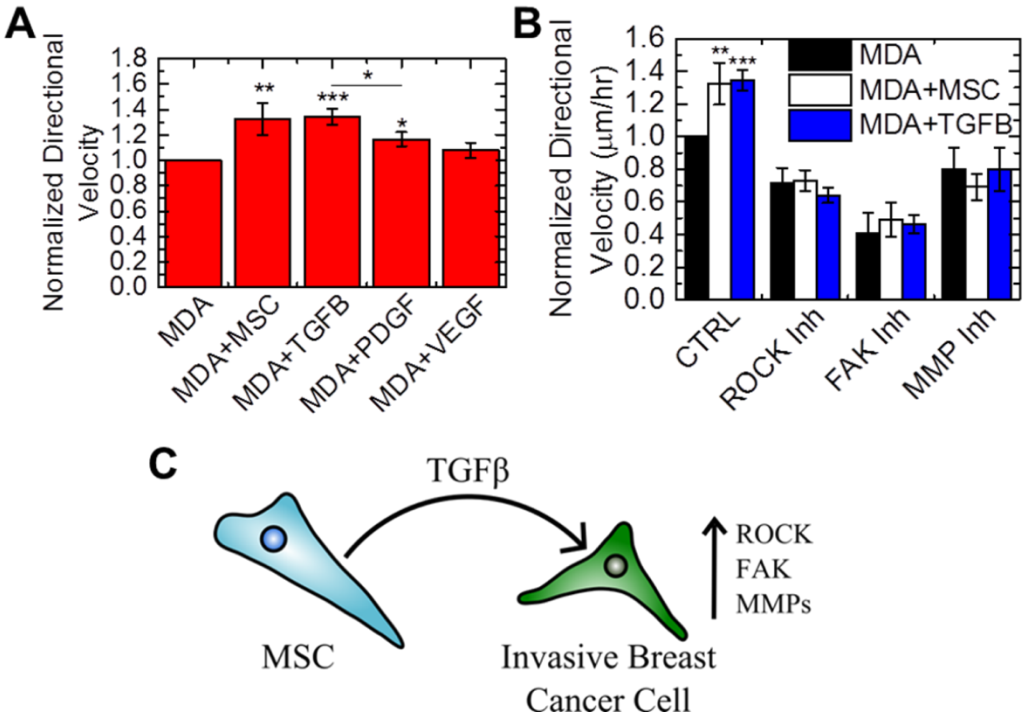

Figure 7.7 TGFβ treatment induces directional migration similar to coculture. (A) Directional velocity of MDA cocultured with MSCs or treated with 10 ng/mL TGF-β1, 10 ng/mL PDGF-BB, or 100 ng/mL VEGF-165. (B) Directional velocity of MDA cocultured with MSCs or treated with 10 ng/mL TGF-β1 with inhibitors. (C) Schematic of proposed mechanism of MSC-induced directional migration of breast cancer cells, where TGF-β is secreted in coculture which leads to activation of ROCK, FAK, and MMPs. * $P<0.05$, ** $P<0.01$, *** $P<0.001$.

7.4 Discussion

TGF-β signaling is critical for directional migration (**Figure 7.5B**); however, inhibition of TGFβR had negligible effects on random motility (**Figure 7.3**). Directional invasion through ECM is thought to be a critical step for breast cancer metastasis [185], suggesting MSCs may contribute to metastasis by increasing directional migration.

Blockade of ROCK and FAK abolished increased random motility in coculture, suggesting these pathways are critical for both directional and random migration. Both PDGFR and MMP inhibition decreased random motility, but there was still a significant increase in velocity in coculture. Mean velocity had a weaker correlation with traction generation (ρ=0.330, P=0.09) than directional velocity (**Figure 7.3**), indicating TGFβR is primarily involved in traction-dependent directional but not random motility.

Active FAK is required for MSC-induced directional migration (**Figure 7.5A**) and increased traction generation (**Figure 7.6A**). Previous studies have demonstrated that depletion of FAK hinders migration and force generation in 3D environments [190]; however, in 2D FAK depletion and FAK inhibition elicit different force responses [191]. Phosphorylation of the Y397 site of FAK, which is targeted by PF-573228, is critical for force generation [192]. This site is phosphorylated by TGF-β [193] and has been shown to be critical for growth factor-stimulated migration [194]. Treatment with TGF-β in conjunction with FAK inhibition elicited a similar migration response to coculture (**Figure 7.7B**), suggesting that TGF-β is secreted in coculture which leads to FAK-mediated migration. FAK inhibitors have been proposed as a way to target cancer stem cells and alter chemoresistance, angiogenesis, inflammation, and profibrotic signals [195]. Our findings suggest that FAK inhibitors may also target MSC-induced directional migration.

FAK inhibitor-treated cells were outliers in the correlation between directional velocity and traction generation (**Figure 7.6C**). Bead displacements exerted by cells treated with FAK inhibitor were high (**Figure 7.6A**) compared to the low directional velocities of these cells (**Figure 7.5A**) indicating the decreased velocity observed after

FAK inhibition is not entirely due to decreased traction generation. Focal adhesion formation and turnover is mediated by FAK [195], which are critical for migration in 3D [182]. Although MDA can still generate force after treatment with a FAK inhibitor (**Figure 7.6A**), focal adhesion dynamics are blocked leading to inhibited migration (**Figure 7.5A**). FAK activation also increases the expression of MMP9 [196], which in addition to cleaving ECM to facilitate migration can proteolytically activate TGF-β [197]. Traction generated by MDA treated with FAK and MMP inhibitors were similar **(Figure 7.6A)**, suggesting that these two molecules may act in conjunction to promote the activation of TGF-β. In addition, similar migratory responses were observed with coculture and TGF-β1 treatment, indicating that secreted TGF-β may activate FAK and MMPs to facilitate migration. Blockade of TGFβR in coculture inhibited migration **(Figure 7.5B)**, further supporting the hypothesis that active TGF-β signaling is required for increased directional migration of cancer cells.

Mesenchymal cells primarily utilize adhesions and cell contractility, which is mediated by Rho and ROCK, to migrate [182]. Rho also regulates actin organization, which is critical for 3D migration [182]. ROCK inhibition acts to decrease both directional migration and traction generation in MDA **(Figure 7.5A, 7.6A)**. Previous work has shown MDA require Rho-mediated contractility to invade into Matrigel [198]. Rho has also been implicated in the alignment of ECM fibers to facilitate invasion [199]. Our findings suggest that ROCK is also critical for MSC-induced traction generation required for the directional migration of cancer cells. Increased matrix stiffness can generate a malignant phenotype, increase force generation, and activate Rho [40]. Coculture with MSCs was associated with higher traction **(Figure 7.6A)**, suggesting that

MSCs may also play a role in altering the tensional homeostasis of cancer cells, similar to ECM stiffness [40]. Previous studies have demonstrated that in 2D MSCs alter their contractile gene expression in response to tumor-secreted factors [48,139] and display a myofibroblast phenotype after sustained exposure [30]. Myofibroblast contractility activates TGFβ in the ECM [200]; thus, MSC contractility may also contribute to TGF-β activation in coculture with MDA.

Previous studies have demonstrated that PDGF activates Rac1 [201], which is required induce migration [202]. Our finding that PDGFR inhibition with Sunitinib does not alter traction generation (**Figure 7.6B**) is in agreement with previous studies that showed Rac1 inhibition has negligible effects on traction generation in 3D [190]. PDGFR inhibition did not significantly alter directional migration and traction generation in coculture, suggesting that this pathway is not required for MSC-induced migration. Inhibition of PDGFR in MDA cells cultured alone was associated with decreased directional migration and PDGF treatment did induce modest directional migration (**Figure 7.7A**), indicating this signal pathway does play a minor role in directional migration, but not to the same degree as TGF-β (**Figure 7.7A**).

Inhibition of RTKs, TGFβR, and downstream migration pathways led to differential responses (**Figure 7.5**). ROCK and FAK inhibition were associated with more homogenous distributions of directional velocity (low coefficient of variation) of MDA alone and in coculture, whereas MMP, RTK, and TGFβR inhibition led to more heterogeneous responses (high coefficient of variation, **Figure 7.5C**). Cells may differentially activate these proteins, leading to a heterogeneous response to inhibitors. FAK, MMP, and RTK inhibition equally targeted the top 10% and 50% most motile

cells, suggesting these pathways are critical for directional migration of all cells (**Figure 7.5E**). Both ROCK and TGFβR appeared to be critical for the directional migration of the most motile cells, as inhibition of these pathways preferentially targeted the fastest 10% of cells.

These studies identify TGFβR as a potential target to prevent MSC-induced breast cancer cell directional migration. MSCs differentiate into CAFs in response to soluble factors secreted by tumor cells [30]. Recent studies have shown the CAF phenotype is associated with poor patient prognosis and TGF-β secreted by these cells can increase the frequency of tumor-initiating cells. By blocking TGF-β crosstalk between CAFs and cancer cells, metastasis was blocked [35]. Our studies suggest the blockade of metastasis may have been in part to decreased directional migration of cancer cells, which is thought to be critical for escape from the primary tumor site [185]. TGF-β can also directly induce EMT, where cells transition from an epithelial phenotype to an invasive mesenchymal phenotype allowing for escape from the primary tumor site [43]. EMT induced by TGF-β has also been implicated in the activation of stromal cells to CAFs, which further promote tumor progression [31]. This indicates that TGF-β secreted in coculture may induce EMT in addition to acting to directly increase directional migration through mechanosensitive pathways, further promoting metastasis.

7.5 Conclusions

In conclusion, we demonstrated that MSCs induce the elongation and traction-dependent directional migration of invasive breast cancer cells. Targeting TGF-β signaling, ROCK, FAK and MMPs abrogates directional migration and force generation differences in coculture. These data suggest TGF-β is secreted in coculture, which leads

to the activation of ROCK, FAK, and MMPs to mediate directional migration of breast cancer cells. Together, this work provides insight into MSC interactions with invasive breast cancer cells within the tumor microenvironment and potential therapeutic targets to halt invasion and metastasis.

7.6 Materials and Methods

7.6.1 Cell Culture

Human MSCs (Donor 7071) were obtained from Texas A&M Institute for Regenerative Medicine and cultured in αMEM (Corning) with 20% FBS (Atlanta Biologicals), 1% penicillin-streptomycin (Corning), and 1% L-glutamine (Corning). MDA-MB-231 cells (ATCC) were cultured in low glucose DMEM (Corning) supplemented with 10% FBS and 1% penicillin-streptomycin. MCF7 cells (ATCC) were cultured in RPMI (Corning) supplemented with 10% FBS and 1% penicillin-streptomycin.

7.6.2 Fabrication of 3D Collagen Gels

Cells were embedded in collagen gels as described [190]. MSCs were labeled with CFSE (Biolegend) in HBSS. Cells were mixed with 10X reconstitution buffer (200 μM sodium bicarbonate and 200 μM HEPES in water) and 3 μm polystyrene particles (Polysciences) and added to rat tail collagen I to obtain a 2 mg/mL collagen gel. For coculture experiments, MSCs and MDA-MB-231 cells were mixed at a 1:1 ratio. Gels were polymerized on ice for 45 minutes followed by incubation at 37˚C for 2 hours before adding RPMI (Corning) with 10% FBS and 1% penicillin-streptomycin.

7.6.3 Cell Migration Experiments

Cells were serum starved for at least 6 hours before imaging. ROCK (1 μM H-1152, Enzo), FAK (20 μM PF-573228, Sigma), MMP (20 μM GM-6001, EMD Millipore), RTK (1 μM Sunitinib, Sigma), and TGFβR (1 μM SB-505124, Sigma) inhibitors were added 2 hours before imaging. For growth factor experiments, 10 ng/mL TGF-β1 (Biolegend), 10 ng/mL PDGF-BB (Biolegend), and 100 ng/mL VEGF-165 (Biolegend) and inhibitors were added to cells 2 hours prior to imaging. Imaging was performed on a Nikon Eclipse Ti inverted epifluorescent microscope with a 10x objective. Cells were maintained at 37˚C with 5% CO_2 using an In Vivo Scientific environmental cell chamber and a Bioscience Tools CO_2 controller and imaged every 5 minutes for 16 hours using a Photometrics CoolSNAP camera. For cell shape analysis, cells were manually traced in ImageJ software (NIH). The x-y coordinates of cells were determined using Metamorph software and used to evaluate motility parameters in a custom-written MATLAB algorithm. Cells that divided during the experiment were excluded from analysis. Cell velocities were calculated over 30 minute intervals and averaged to determine mean velocity. Directional velocity was calculated as the total distance traveled divided by time. Directional velocity coefficient of variation (standard deviation divided by the mean) and percentile analyses were calculated based on at least 150 individual cells.

7.6.4 Bead Displacement Quantification

Bead positions were identified as described with minor modifications and trajectories linked using a Hungarian linker algorithm [114,138]. In brief, bright field particle images were inverted to create a bright particle on a dark background. Next, a

bandpass filter was applied to the images before determining the particle centroid to subpixel resolution based on the intensity-weighted centroid. Only beads within a 75 μm radius of a cell were used for analysis; beads outside this radius were used to assess any drift over the course of imaging. Beads were assigned to each cell using a nearest-neighbor algorithm which was verified manually for each video. The maximum displacement was determined for each bead, and then max bead displacement was taken as the top 95^{th} percentile of displacements around each cell.

7.6.5 Statistics

Data are reported as the mean ± SEM unless otherwise noted. A student t-test was used to determine significance with $P<0.05$ being statistically significant (* $P<0.05$, ** $P<0.01$, *** $P<0.001$). For correlation analysis, Pearson's correlation coefficients were calculated in MATLAB, with $\rho=-1$ being perfectly negatively correlated and $\rho=+1$ being perfectly positively correlated. Studentized deleted residuals were used to identify outliers from the data with 95% confidence.

CHAPTER 8

CONCLUSIONS AND FUTURE DIRECTIONS

In this work, we determined the effect of biochemical and mechanical signals from the microenvironment on the regenerative and cancer-promoting properties of MSCs. We found intracellular mechanics and extracellular force generation are altered during MSC differentiation. In order to implement tissue engineered constructs clinically, it is important to have an understanding of MSC lineage commitment. Current methods for detection of differentiation are staining [1] and PCR [48,114], which involve fixing or lysing the cells resulting in cell death. In addition, these techniques typically can only be used for cells that are relatively far into the differentiation process (~3-5 weeks). Our studies indicate that increases in the elastic character of the cytoplasm at 1 week into differentiation induction may be a marker of adipogenesis. MPTM can be performed on live cells and in cells embedded in 3D constructs [75], indicating that this technique may be useful for identifying differentiated cells for tissue engineering purposes. Future studies could be performed to monitor the rheological properties of MSCs during differentiation to evaluate if differentiation capacity can be detected earlier. This could be used to monitor tissue engineered constructs. In addition, we found that MSCs exerted higher traction stresses when cultured with adipogenic factors in stiff environments that were not conducive for adipogenesis. This suggests that manipulating force generation may be a way to promote more efficient directed differentiation. Together, these results have important implications for the design and testing of tissue engineered constructs.

We also found biomaterial composition can dictate what factors direct differentiation. Typical biomaterial characterization techniques include scanning electron microscopy and bulk mechanical testing. While bulk mechanical testing was indicative of differentiation potential for 10% gelatin scaffolds, it did not predict differentiation potential for 5% gelatin scaffolds. Differentiation potential for 5% gelatin scaffolds was more dependent on the hydrated pore structure probed by MPTM. These results underscore the need for a variety of biomaterial characterization techniques. In addition, these results suggest that tailoring material architectural and mechanical properties may be a way to enhance directed differentiation. Previous studies have shown there is an optimum pore size for bone regeneration [137] and immune activation [203]; thus, there may also be an optimum pore size for MSC differentiation. MPTM could be performed simultaneously on the scaffold and the cells embedded in the scaffold to simultaneously monitor hydrated pore structure and differentiation of MSCs. The material architecture and mechanical properties could be tailored to manipulate force generation, further directing MSC lineage. Consequently, these studies may aid in the design of biomaterials for MSC-mediated tissue regeneration.

We next sought to understand the role of MSCs in tumor progression. We found cadherin 11 facilitates the adhesion of MSCs to invasive cancer cells, which may be a potential mechanism MSCs utilize to engraft in invasive tumors. Future studies probing the engraftment of bone marrow transplanted GFP-labeled MSCs into non-invasive and invasive tumors would confirm this hypothesis. These studies would confirm if MSCs are recruited to invasive fronts of tumors and could be performed in conjunction with small molecule or antibody inhibition of cadherin 11 to confirm this molecule is important *in*

vivo. Bone marrow-derived cells form premetastatic niches that facilitate metastasis [204]. Thus, future studies could be performed to determine if cadherin 11 also facilitates the recruitment of tumor cells to premetastatic niches. Cadherin 11 has been shown to be upregulated in breast cancer and identified as a therapeutic target [150]. Celecoxib, an inhibitor of the inflammatory molecule COX-2, was originally developed as an arthritis drug, but has been investigated for the treatment of cancer [205]. Recent studies have demonstrated that celecoxib also inhibits cadherin 11 and blocks proliferation of breast, prostate, and brain cancer cells [169]. Our studies indicate blocking cadherin 11 may also prevent the engraftment of stromal cells, which are known to promote cancer progression [28]. In addition, cadherin 11-mediated adhesion occurred in both breast and ovarian cancer, suggesting this mechanism of adhesion may be conserved across a number of invasive cancers. Our results indicated stromal cells were able to adhere to invasive cancer cells that express cadherin 11 and/or 2, which includes most cells that have undergone EMT. Thus, celecoxib may be repurposed or other cadherin 11 inhibiting drugs or antibodies could be developed to treat a number of different invasive cancers. Previously, cadherin 11 inhibition has been investigated for cancers expressing cadherin 11 [169], but our results indicate this treatment may be effective for a broader range of cancers since it blocks stromal cell adhesion with both cadherin 11 and 2 on invasive cancer cells.

We also elucidated how MSCs induce the invasion of metastatic breast cancer cells. MSCs increase the directional migration and force generation of metastatic breast cancer cells through TGF-β and downstream mechanosensitive pathways. RTK signaling was dispensable for MSC-induced migration. The RTK inhibitor sunitinib in combination

with the chemotherapeutic docetaxel was investigated for the treatment of advanced breast cancer; however, phase III clinical trial results showed an increase in adverse events and no improvement in survival [206]. Consequently, further trials utilizing this drug were halted. Our studies indicate that RTK inhibition did not affect breast cancer cell directional migration in coculture, which may partly explain why sunitinib failed clinically. A number of drugs targeting the TGF-β pathway are currently being investigated for pancreatic, colon, brain, and lung cancer [207]. Typically cancer drugs are screened for toxicity against tumor cells; however, TGF-β inhibitors primarily target the tumor microenvironment and are not cytotoxic to tumor cells making drug screening more difficult [207]. Recent studies in colorectal cancer patients revealed a CAF gene signature is associated with poor prognosis [35]. CAFs increased the number of tumor-initiating cells and this effect was enhanced by TGF-β signaling [35]. Inhibiting TGF-β halted tumor growth and metastasis in mice [35]. Our results closely matched these studies, with TGFβR inhibition blocking MSC-induced directional migration of cancer cells. This approach is low-cost and significantly less time consuming compared to *in vivo* studies, suggesting it may be a potential *in vitro* drug screening tool. Spinning disc confocal microscopy in conjunction with image segmentation could also be used to make data analysis more automated. The system developed here could also be easily expanded to include other types of cells, including immune cells and endothelial cells, to probe interactions between tumor cells and the microenvironment. In addition, other ECM components and crosslinking agents could be added to probe the effects of matrix composition and mechanical properties on tumor cell behavior. This is especially of interest for MSC interactions with tumor cells, as MSCs increase traction forces with

increasing matrix stiffness [208] and increased contractility is known to activate latent TGF-β in the ECM [200]. While we investigated the effect of MSCs on the invasiveness of tumor cells, MSCs also have immunomodulatory effects. TGF-β has effects on almost all immune cells [207]. TGF-β causes both macrophages and neutrophils to secrete inflammatory factors, decreases the activation of B cells, and decreases the proliferation of T cells [207]. This indicates that TGF-β secreted in coculture with MSCs may also have effects on immune cells. Thus, future studies could utilize coculture studies with tumor cells and immune cells to determine how MSCs influence inflammation and tumor progression.

This work shows how chemical and mechanical cues from microenvironment influence the differentiation of MSCs. In addition, we found that MSCs utilize cadherin 11 to engraft on invasive tumor cells. MSCs induce the directional migration of metastatic breast cancer cells through TGF-β and downstream mechanosensitive pathways. Together, this work elucidates how the microenvironment influences the regenerative and cancer-promoting properties of MSCs. This work has critical implications for the design and monitoring of tissue engineered constructs and the development of novel cancer therapeutics.

REFERENCES

[1] M.F. Pittenger, A.M. Mackay, S.C. Beck, R.K. Jaiswal, R. Douglas, J.D. Mosca, et al., Multilineage Potential of Adult Human Mesenchymal Stem Cells, Science. 284 (1999) 143–147. doi:10.1126/science.284.5411.143.

[2] J.M. Karp, G.S. Leng Teo, Mesenchymal Stem Cell Homing: The Devil Is in the Details, Cell Stem Cell. 4 (2009) 206–216. doi:10.1016/j.stem.2009.02.001.

[3] T.P. Martens, F. See, M.D. Schuster, H.P. Sondermeijer, M.M. Hefti, A. Zannettino, et al., Mesenchymal lineage precursor cells induce vascular network formation in ischemic myocardium, Nat. Clin. Pract. Cardiovasc. Med. 3 (2006) S18–22.

[4] S. Aggarwal, M.F. Pittenger, Human mesenchymal stem cells modulate allogeneic immune cell responses, Blood. 105 (2005) 1815–1822. doi:10.1182/blood-2004-04-1559.

[5] A.L. Ponte, E. Marais, N. Gallay, A. Langonné, B. Delorme, O. Hérault, et al., The In Vitro Migration Capacity of Human Bone Marrow Mesenchymal Stem Cells: Comparison of Chemokine and Growth Factor Chemotactic Activities, Stem Cells. 25 (2007) 1737–1745. doi:10.1634/stemcells.2007-0054.

[6] Y. Ozaki, M. Nishimura, K. Sekiya, F. Suehiro, M. Kanawa, H. Nikawa, et al., Comprehensive analysis of chemotactic factors for bone marrow mesenchymal stem cells, Stem Cells Dev. 16 (2007) 119–29.

[7] M.-S. Liang, M. Koobatian, P. Lei, D.D. Swartz, S.T. Andreadis, Differential and synergistic effects of mechanical stimulation and growth factor presentation on vascular wall function, Biomaterials. 34 (2013) 7281–91. doi:10.1016/j.biomaterials.2013.05.073.

[8] S. Alimperti, H. You, T. George, S.K. Agarwal, S.T. Andreadis, Cadherin-11 regulates both mesenchymal stem cell differentiation into smooth muscle cells and the development of contractile function in vivo, J. Cell Sci. 127 (2014) 2627–38. doi:10.1242/jcs.134833.

[9] G. Gabbiani, The myofibroblast in wound healing and fibrocontractive diseases, J. Pathol. 200 (2003) 500–503. doi:10.1002/path.1427.

[10] S. Maxson, E.A. Lopez, D. Yoo, A. Danilkovitch-Miagkova, M.A. LeRoux, Concise Review: Role of Mesenchymal Stem Cells in Wound Repair, Stem Cells Transl. Med. . 1 (2012) 142–149. doi:10.5966/sctm.2011-0018 .

[11] S. Ma, N. Xie, W. Li, B. Yuan, Y. Shi, Y. Wang, Immunobiology of mesenchymal stem cells., Cell Death Differ. 21 (2014) 216–25. doi:10.1038/cdd.2013.158.

[12] S. Wakitani, T. Saito, A.I. Caplan, Myogenic cells derived from rat bone marrow mesenchymal stem cells exposed to 5-azacytidine, Muscle Nerve. 18 (1995) 1417–1426. doi:10.1002/mus.880181212.

[13] X. Wei, X. Yang, Z. Han, F. Qu, L. Shao, Y. Shi, Mesenchymal stem cells: a new trend for cell therapy, Acta Pharmacol. Sin. 34 (2013) 747–54. doi:10.1038/aps.2013.50.

[14] D.E. Discher, D.J. Mooney, P.W. Zandstra, Growth factors, matrices, and forces combine and control stem cells., Science. 324 (2009) 1673–7. doi:10.1126/science.1171643.

[15] I. Kratchmarova, B. Blagoev, M. Haack-Sorensen, M. Kassem, M. Mann, Mechanism of Divergent Growth Factor Effects in Mesenchymal Stem Cell Differentiation, Sci. . 308 (2005) 1472–1477. doi:10.1126/science.1107627.

[16] J.D. Boerckel, Y.M. Kolambkar, H.Y. Stevens, A.S.P. Lin, K.M. Dupont, R.E. Guldberg, Effects of in vivo mechanical loading on large bone defect regeneration, J. Orthop. Res. 30 (2012) 1067–1075. doi:10.1002/jor.22042.

[17] A.J. Engler, S. Sen, H.L. Sweeney, D.E. Discher, Matrix elasticity directs stem cell lineage specification, Cell. 126 (2006) 677–689.

[18] K.A. Kilian, B. Bugarija, B.T. Lahn, M. Mrksich, Geometric cues for directing the differentiation of mesenchymal stem cells, Proc. Natl. Acad. Sci. 107 (2010) 4872–7. doi:10.1073/pnas.0903269107.

[19] R. McBeath, D.M. Pirone, C.M. Nelson, K. Bhadriraju, C.S. Chen, Cell shape, cytoskeletal tension, and RhoA regulate stem cell lineage commitment, Dev. Cell. 6 (2004) 483–95.

[20] N. Datta, Q. P. Pham, U. Sharma, V.I. Sikavitsas, J.A. Jansen, A.G. Mikos, In vitro generated extracellular matrix and fluid shear stress synergistically enhance 3D osteoblastic differentiation, Proc. Natl. Acad. Sci. United States Am. . 103 (2006) 2488–2493. doi:10.1073/pnas.0505661103 .

[21] H. Wang, G.M. Riha, S. Yan, M. Li, H. Chai, H. Yang, et al., Shear Stress Induces Endothelial Differentiation From a Murine Embryonic Mesenchymal Progenitor Cell Line, Arterioscler. Thromb. Vasc. Biol. . 25 (2005) 1817–1823. doi:10.1161/01.ATV.0000175840.90510.a8 .

[22] G. Kasper, N. Dankert, J. Tuischer, M. Hoeft, T. Gaber, J.D. Glaeser, et al., Mesenchymal Stem Cells Regulate Angiogenesis According to Their Mechanical Environment, Stem Cells. 25 (2007) 903–910. doi:10.1634/stemcells.2006-0432.

[23] B. Carrion, Y.P. Kong, D. Kaigler, A.J. Putnam, Bone marrow-derived mesenchymal stem cells enhance angiogenesis via their α6β1 integrin receptor, Exp. Cell Res. 319 (2013) 2964–2976. doi:http://dx.doi.org/10.1016/j.yexcr.2013.09.007.

[24] S. Kachgal, B. Carrion, I.A. Janson, A.J. Putnam, Bone marrow stromal cells stimulate an angiogenic program that requires endothelial MT1-MMP, J. Cell. Physiol. 227 (2012) 3546–3555. doi:10.1002/jcp.24056.

[25] M. Schäfer, S. Werner, Cancer as an overhealing wound: an old hypothesis revisited, Nat. Rev. Mol. Cell Biol. 9 (2008) 628–638. doi:10.1038/nrm2455.

[26] J.A. Joyce, Therapeutic targeting of the tumor microenvironment, Cancer Cell. 7 (2005) 513–20. doi:10.1016/j.ccr.2005.05.024.

[27] E.L. Spaeth, J.L. Dembinski, A.K. Sasser, K. Watson, A. Klopp, B. Hall, et al., Mesenchymal stem cell transition to tumor-associated fibroblasts contributes to fibrovascular network expansion and tumor progression, PLoS One. 4 (2009) e4992. doi:10.1371/journal.pone.0004992.

[28] A. Karnoub, A. Dash, A. Vo, A. Sullivan, M. Brooks, G. Bell, et al., Mesenchymal stem cells within tumour stroma promote breast cancer metastasis, Nature. 449 (2007) 557–563.

[29] A.H. Klopp, A. Gupta, E. Spaeth, M. Andreeff, F. Marini, Concise review: Dissecting a discrepancy in the literature: do mesenchymal stem cells support or suppress tumor growth?, Stem Cells. 29 (2011) 11–9. doi:10.1002/stem.559.

[30] P.J. Mishra, P.J. Mishra, R. Humeniuk, D.J. Medina, G. Alexe, J.P. Mesirov, et al., Carcinoma-associated fibroblast-like differentiation of human mesenchymal stem cells, Cancer Res. 68 (2008) 4331–9. doi:10.1158/0008-5472.CAN-08-0943.

[31] R. Kalluri, M. Zeisberg, Fibroblasts in cancer, Nat. Rev. Cancer. 6 (2006) 392–401. doi:10.1038/nrc1877.

[32] N. Erez, M. Truitt, P. Olson, S.T. Arron, D. Hanahan, Cancer-Associated Fibroblasts Are Activated in Incipient Neoplasia to Orchestrate Tumor-Promoting Inflammation in an NF-κB-Dependent Manner, Cancer Cell. 17 (2010) 135–47. doi:10.1016/j.ccr.2009.12.041.

[33] D.T. Butcher, T. Alliston, V.M. Weaver, A tense situation: forcing tumour progression, Nat. Rev. Cancer. 9 (2009) 108–22. doi:10.1038/nrc2544.

[34] M. Shimoda, K.T. Mellody, A. Orimo, Carcinoma-associated fibroblasts are a rate-limiting determinant for tumour progression, Semin. Cell Dev. Biol. 21 (2010) 19–25. doi:10.1016/j.semcdb.2009.10.002.

[35] A. Calon, E. Lonardo, A. Berenguer-Llergo, E. Espinet, X. Hernando-Momblona, M. Iglesias, et al., Stromal gene expression defines poor-prognosis subtypes in colorectal cancer, Nat. Genet. 47 (2015) 320–329. doi:10.1038/ng.3225.

[36] J.S. Desgrosellier, D.A. Cheresh, Integrins in cancer: biological implications and therapeutic opportunities, Nat. Rev. Cancer. 10 (2010) 9–22. doi:10.1038/nrc2748.

[37] P. Kanchanawong, G. Shtengel, A.M. Pasapera, E.B. Ramko, M.W. Davidson, H.F. Hess, et al., Nanoscale architecture of integrin-based cell adhesions., Nature. 468 (2010) 580–584. doi:10.1038/nature09621.

[38] R.J. Pelham, Y.L. Wang, High resolution detection of mechanical forces exerted by locomoting fibroblasts on the substrate, Mol. Biol. Cell. 10 (1999) 935–945. doi:10.1091/mbc.10.4.935.

[39] K.A. Beningo, K. Hamao, M. Dembo, Y.L. Wang, H. Hosoya, Traction forces of fibroblasts are regulated by the Rho-dependent kinase but not by the myosin light chain kinase, Arch. Biochem. Biophys. 456 (2006) 224–231. doi:10.1016/j.abb.2006.09.025.

[40] M.J. Paszek, N. Zahir, K.R. Johnson, J.N. Lakins, G.I. Rozenberg, A. Gefen, et al., Tensional homeostasis and the malignant phenotype, Cancer Cell. 8 (2005) 241–54. doi:10.1016/j.ccr.2005.08.010.

[41] C.M. Lo, H.B. Wang, M. Dembo, Y.L. Wang, Cell movement is guided by the rigidity of the substrate, Biophys. J. 79 (2000) 144–152.

[42] P. Friedl, S. Alexander, Cancer invasion and the microenvironment: plasticity and reciprocity, Cell. 147 (2011) 992–1009. doi:10.1016/j.cell.2011.11.016.

[43] R. Kalluri, R.A. Weinberg, The basics of epithelial-mesenchymal transition, J. Clin. Invest. 119 (2009) 1420–1428. doi:10.1172/JCI39104.1420.

[44] D.J. McGrail, R. Mezencev, Q.M.N. Kieu, J.F. McDonald, M.R. Dawson, SNAIL-induced epithelial-to-mesenchymal transition produces concerted biophysical changes from altered cytoskeletal gene expression, FASEB J. 29 (2015) 1280–1289. doi:10.1096/fj.14-257345.

[45] F. Hlubek, T. Brabletz, J. Budczies, S. Pfeiffer, A. Jung, T. Kirchner, Heterogeneous expression of Wnt/β-catenin target genes within colorectal cancer, Int. J. Cancer. 121 (2007) 1941–1948. doi:10.1002/ijc.22916.

[46] L.N. Lili, L. V Matyunina, L.D. Walker, S.L. Wells, B.B. Benigno, J.F. McDonald, Molecular profiling supports the role of epithelial-to-mesenchymal transition (EMT) in ovarian cancer metastasis, J. Ovarian Res. 6 (2013) 49. doi:10.1186/1757-2215-6-49.

[47] J.P. Thiery, Epithelial-mesenchymal transitions in tumour progression, Nat. Rev. Cancer. 2 (2002) 442–454. doi:10.1038/nrc822.

[48] D.J. McGrail, D. Ghosh, N.D. Quach, M.R. Dawson, Differential mechanical response of mesenchymal stem cells and fibroblasts to tumor-secreted soluble factors, PLoS One. 7 (2012) e33248. doi:10.1371/journal.pone.0033248.

[49] T.P. Kole, Y. Tseng, I. Jiang, J.L. Katz, D. Wirtz, Intracellular mechanics of migrating fibroblasts, Biophys. J. 16 (2005) 328–338. doi:10.1091/mbc.E04.

[50] E.M. Balzer, Z. Tong, C.D. Paul, W.-C. Hung, K.M. Stroka, A.E. Boggs, et al., Physical confinement alters tumor cell adhesion and migration phenotypes, FASEB J. 26 (2012) 4045–56. doi:10.1096/fj.12-211441.

[51] D. Homouz, M. Perham, A. Samiotakis, M.S. Cheung, P. Wittung-Stafshede, Crowded, cell-like environment induces shape changes in aspherical protein., Proc. Natl. Acad. Sci. U. S. A. 105 (2008) 11754–9. doi:10.1073/pnas.0803672105.

[52] E.L. Baker, R.T. Bonnecaze, M.H. Zaman, Extracellular matrix stiffness and architecture govern intracellular rheology in cancer, Biophys. J. 97 (2009) 1013–21. doi:10.1016/j.bpj.2009.05.054.

[53] D.E. Ingber, Mechanical control of tissue morphogenesis during embryological development, Int. J. Dev. Biol. 50 (2006) 255–66. doi:10.1387/ijdb.052044di.

[54] P.J. Keller, A.D. Schmidt, J. Wittbrodt, E.H.K. Stelzer, Reconstruction of zebrafish early embryonic development by light sheet microscopy, Science. 322 (2008) 1065–1069.

[55] T. Mammoto, D.E. Ingber, Mechanical control of tissue and organ development, Development. 137 (2010) 1407–20. doi:10.1242/dev.024166.

[56] J. Vacanti, R. Langer, J. Upton, J. Marler, Transplantation of cells in matrices for tissue regeneration, Adv. Drug Deliv. Rev. 33 (1998) 165–182.

[57] S. Suresh, Biomechanics and biophysics of cancer cells, Acta Mater. 55 (2007) 3989–4014. doi:10.1016/j.actamat.2007.04.022.

[58] A. Orr, B. Helmke, B. Blackman, M. Schwartz, Mechanisms of mechanotransduction, Dev. Cell. 10 (2006) 11–20.

[59] B. Alberts, A. Johnson, J. Lewis, M. Raff, K. Roberts, P. Walter, Molecular Biology of the Cell, 4th ed., Garland Science Taylor and Francis Group, New York, 2002.

[60] E. Atilgan, D. Wirtz, S.X. Sun, Mechanics and dynamics of actin-driven thin membrane protrusions, Biophys. J. 90 (2006) 65–76. doi:10.1529/biophysj.105.071480.

[61] E. Atilgan, D. Wirtz, S.X. Sun, Morphology of the lamellipodium and organization of actin filaments at the leading edge of crawling cells, Biophys. J. 89 (2005) 3589–602. doi:10.1529/biophysj.105.065383.

[62] J. Stricker, T. Falzone, M.L. Gardel, Mechanics of the F-actin cytoskeleton, J. Biomech. 43 (2010) 9–14. doi:10.1016/j.jbiomech.2009.09.003.

[63] M.D. Treiser, E.H. Yang, S. Gordonov, D.M. Cohen, I.P. Androulakis, J. Kohn, et al., Cytoskeleton-based forecasting of stem cell lineage fates., Proc. Natl. Acad. Sci. 107 (2010) 610–5. doi:10.1073/pnas.0909597107.

[64] T.D. Pollard, R.R. Weihing, Actin and myosin and cell movement, CRC Crit. Rev. Biochem. 2 (1974) 1–65.

[65] T.A. Waigh, Microrheology of complex fluids, Reports Prog. Phys. 68 (2005) 685–742. doi:10.1088/0034-4885/68/3/R04.

[66] R.G. Larson, The Structure and Rheology of Complex Fluids, Oxford University Press, New York, 1999.

[67] Y. Tseng, E. Fedorov, J.M. McCaffery, S.C. Almo, D. Wirtz, Micromechanics and ultrastructure of actin filament networks crosslinked by human fascin: a comparison with alpha-actinin, J. Mol. Biol. 310 (2001) 351–66. doi:10.1006/jmbi.2001.4716.

[68] P. Kollmannsberger, B. Fabry, Linear and nonlinear rheology of living cells, Annu. Rev. Mater. Res. 41 (2011) 75–97. doi:10.1146/annurev-matsci-062910-100351.

[69] D. Kirmizis, S. Logothetidis, Atomic force microscopy probing in the measurement of cell mechanics, Int. J. Nanomedicine. 5 (2010) 137–45.

[70] M. Puig-de-Morales, E. Millet, B. Fabry, D. Navajas, N. Wang, J.P. Butler, et al., Cytoskeletal mechanics in adherent human airway smooth muscle cells: probe specificity and scaling of protein-protein dynamics, Am. J. Physiol. Cell Physiol. 287 (2004) C643–54. doi:10.1152/ajpcell.00070.2004.

[71] S. Yamada, D. Wirtz, S.C. Kuo, Mechanics of living cells measured by laser tracking microrheology, Biophys. J. 78 (2000) 1736–47. doi:10.1016/S0006-3495(00)76725-7.

[72] T.G. Mason, D.A. Weitz, Optical measurements of frequency-dependent linear viscoelastic moduli of complex fluids, Phys. Rev. Lett. 74 (1995) 1250–1253.

[73] J.S.H. Lee, P. Panorchan, C.M. Hale, S.B. Khatau, T.P. Kole, Y. Tseng, et al., Ballistic intracellular nanorheology reveals ROCK-hard cytoplasmic stiffening response to fluid flow, J. Cell Sci. 119 (2006) 1760–8. doi:10.1242/jcs.02899.

[74] Y. Tseng, T.P. Kole, D. Wirtz, Micromechanical mapping of live cells by multiple-particle-tracking microrheology, Biophys. J. 83 (2002) 3162–76. doi:10.1016/S0006-3495(02)75319-8.

[75] P. Panorchan, J.S.H. Lee, T.P. Kole, Y. Tseng, D. Wirtz, Microrheology and ROCK signaling of human endothelial cells embedded in a 3D matrix, Biophys. J. 91 (2006) 3499–507. doi:10.1529/biophysj.106.084988.

[76] B.R. Daniels, B.C. Masi, D. Wirtz, Probing single-cell micromechanics in vivo: the microrheology of C. elegans developing embryos, Biophys. J. 90 (2006) 4712–9. doi:10.1529/biophysj.105.080606.

[77] C.M. Hale, S.X. Sun, D. Wirtz, Resolving the role of actoymyosin contractility in cell microrheology, PLoS One. 4 (2009) e7054. doi:10.1371/journal.pone.0007054.

[78] D.J. McGrail, K.M. McAndrews, M.R. Dawson, Biomechanical analysis predicts decreased human mesenchymal stem cell function before molecular differences, Exp. Cell Res. 319 (2013) 684–96. doi:10.1016/j.yexcr.2012.11.017.

[79] T.G. Mason, A. Dhople, D. Wirtz, Linear viscoelastic moduli of concentrated DNA solutions, Macromolecules. 9297 (1998) 3600–3603.

[80] M. Dawson, D. Wirtz, J. Hanes, Enhanced viscoelasticity of human cystic fibrotic sputum correlates with increasing microheterogeneity in particle transport, J. Biol. Chem. 278 (2003) 50393–401. doi:10.1074/jbc.M309026200.

[81] Y. Tseng, K.M. An, O. Esue, D. Wirtz, The bimodal role of filamin in controlling the architecture and mechanics of F-actin networks, J. Biol. Chem. 279 (2004) 1819–26. doi:10.1074/jbc.M306090200.

[82] Y. Tseng, B.W. Schafer, S.C. Almo, D. Wirtz, Functional synergy of actin filament cross-linking proteins, J. Biol. Chem. 277 (2002) 25609–16. doi:10.1074/jbc.M202609200.

[83] Y. Tseng, K.M. An, D. Wirtz, Microheterogeneity controls the rate of gelation of actin filament networks, J. Biol. Chem. 277 (2002) 18143–50. doi:10.1074/jbc.M110868200.

[84] Y. Tseng, D. Wirtz, Mechanics and multiple-particle tracking microheterogeneity of alpha-actinin-cross-linked actin filament networks, Biophys. J. 81 (2001) 1643–56. doi:10.1016/S0006-3495(01)75818-3.

[85] J. Xu, D. Wirtz, T.D. Pollard, Dynamic cross-linking by alpha-actinin determines the mechanical properties of actin filament networks, J. Biol. Chem. 273 (1998) 9570–6.

[86] E.L. Baker, J. Lu, D. Yu, R.T. Bonnecaze, M.H. Zaman, Cancer cell stiffness: integrated roles of three-dimensional matrix stiffness and transforming potential, Biophys. J. 99 (2010) 2048–57. doi:10.1016/j.bpj.2010.07.051.

[87] E.L. Baker, J. Srivastava, D. Yu, R.T. Bonnecaze, M.H. Zaman, Cancer cell migration: integrated roles of matrix mechanics and transforming potential, PLoS One. 6 (2011) e20355. doi:10.1371/journal.pone.0020355.

[88] E.M. Darling, M. Topel, S. Zauscher, T.P. Vail, F. Guilak, Viscoelastic properties of human mesenchymally-derived stem cells and primary osteoblasts, chondrocytes, and adipocytes, J. Biomech. 41 (2008) 454–64. doi:10.1016/j.jbiomech.2007.06.019.

[89] S.C.W. Tan, W.X. Pan, G. Ma, N. Cai, K.W. Leong, K. Liao, Viscoelastic behaviour of human mesenchymal stem cells, BMC Cell Biol. 9 (2008). doi:10.1186/1471-2121-9-40.

[90] S.E. Cross, Y.-S. Jin, J. Rao, J.K. Gimzewski, Nanomechanical analysis of cells from cancer patients, Nat. Nanotechnol. 2 (2007) 780–3. doi:10.1038/nnano.2007.388.

[91] V. Swaminathan, K. Mythreye, E.T. O'Brien, A. Berchuck, G.C. Blobe, R. Superfine, Mechanical stiffness grades metastatic potential in patient tumor cells and in cancer cell lines, Cancer Res. 71 (2011) 5075–80. doi:10.1158/0008-5472.CAN-11-0247.

[92] P.-H. Wu, C.M. Hale, W.-C. Chen, J.S.H. Lee, Y. Tseng, D. Wirtz, High-throughput ballistic injection nanorheology to measure cell mechanics, Nat. Protoc. 7 (2012) 155–70. doi:10.1038/nprot.2011.436.

[93] B.R. Daniels, C.M. Hale, S.B. Khatau, S. Kusuma, T.M. Dobrowsky, S. Gerecht, et al., Differences in the microrheology of human embryonic stem cells and human induced pluripotent stem cells, Biophys. J. 99 (2010) 3563–70. doi:10.1016/j.bpj.2010.10.007.

[94] I. Titushkin, M. Cho, Modulation of cellular mechanics during osteogenic differentiation of human mesenchymal stem cells, Biophys. J. 93 (2007) 3693–702. doi:10.1529/biophysj.107.107797.

[95] R.D. González-Cruz, V.C. Fonseca, E.M. Darling, Cellular mechanical properties reflect the differentiation potential of adipose-derived mesenchymal stem cells, Proc. Natl. Acad. Sci. 109 (2012) E1523–E1529. doi:10.1073/pnas.1120349109.

[96] S. Khetan, M. Guvendiren, W.R. Legant, D.M. Cohen, C.S. Chen, J.A. Burdick, Degradation-mediated cellular traction directs stem cell fate in covalently crosslinked three-dimensional hydrogels, Nat. Mater. 12 (2013) 458–65. doi:10.1038/nmat3586.

[97] N. Huebsch, P.R. Arany, A.S. Mao, D. Shvartsman, O.A. Ali, S.A. Bencherif, et al., Harnessing traction-mediated manipulation of the cell/matrix interface to control stem-cell fate, Nat. Mater. 9 (2010) 518–26. doi:10.1038/nmat2732.

[98] J. Fu, Y.-K. Wang, M.T. Yang, R.A. Desai, X. Yu, Z. Liu, et al., Mechanical regulation of cell function with geometrically modulated elastomeric substrates, Nat. Methods. 7 (2010) 733–6. doi:10.1038/nmeth.1487.

[99] J.P. Rodríguez, M. González, S. Ríos, V. Cambiazo, Cytoskeletal organization of human mesenchymal stem cells (MSC) changes during their osteogenic differentiation, J. Cell. Biochem. 93 (2004) 721–31. doi:10.1002/jcb.20234.

[100] M. Guvendiren, J.A. Burdick, Stiffening hydrogels to probe short- and long-term cellular responses to dynamic mechanics, Nat. Commun. 3 (2012) 792. doi:10.1038/ncomms1792.

[101] A. Pillarisetti, J.P. Desai, H. Ladjal, A. Schiffmacher, A. Ferreira, C.L. Keefer, Mechanical phenotyping of mouse embryonic stem cells: increase in stiffness with differentiation, Cell. Reprogram. 13 (2011) 371–80. doi:10.1089/cell.2011.0028.

[102] M.L. Gardel, M.T. Valentine, D.A. Weitz, Microrheology, in: K. Breuer (Ed.), Microscale Diagnostic Tech., Springer Berlin Heidelberg, 2005: pp. 1–49. doi:10.1007/3-540-26449-3_1.

[103] M. Kanzaki, J.E. Pessin, Insulin-stimulated GLUT4 translocation in adipocytes is dependent upon cortical actin remodeling, J. Biol. Chem. 276 (2001) 42436–44. doi:10.1074/jbc.M108297200.

[104] H. Yu, C.Y. Tay, W.S. Leong, S.C.W. Tan, K. Liao, L.P. Tan, Mechanical behavior of human mesenchymal stem cells during adipogenic and osteogenic differentiation, Biochem. Biophys. Res. Commun. 393 (2010) 150–155. doi:http://dx.doi.org/10.1016/j.bbrc.2010.01.107.

[105] Y. Zhang, G. Marsboom, P.T. Toth, J. Rehman, Mitochondrial Respiration Regulates Adipogenic Differentiation of Human Mesenchymal Stem Cells, PLoS One. 8 (2013) e77077.

[106] A.K. Yip, K. Iwasaki, C. Ursekar, H. Machiyama, M. Saxena, H. Chen, et al., Cellular response to substrate rigidity is governed by either stress or strain, Biophys. J. 104 (2013) 19–29. doi:10.1016/j.bpj.2012.11.3805.

[107] N. Wang, I.M. Tolić-Nørrelykke, J. Chen, S.M. Mijailovich, J.P. Butler, J.J. Fredberg, et al., Cell prestress. I. Stiffness and prestress are closely associated in adherent contractile cells, Am. J. Physiol. Cell Physiol. 282 (2002) C606–16. doi:10.1152/ajpcell.00269.2001.

[108] Y. Tseng, T.P. Kole, J.S.H. Lee, E. Fedorov, S.C. Almo, B.W. Schafer, et al., How actin crosslinking and bundling proteins cooperate to generate an enhanced cell mechanical response, Biochem. Biophys. Res. Commun. 334 (2005) 183–92. doi:10.1016/j.bbrc.2005.05.205.

[109] A. Peister, J.A. Mellad, B.L. Larson, B.M. Hall, L.F. Gibson, D.J. Prockop, Adult stem cells from bone marrow (MSCs) isolated from different strains of inbred mice vary in surface epitopes, rates of proliferation, and differentiation potential, Blood. 103 (2004) 1662–8. doi:10.1182/blood-2003-09-3070.

[110] J.R. Tse, A.J. Engler, Preparation of hydrogel substrates with tunable mechanical properties, Curr. Protoc. Cell Biol. 47 (2010) 10.16.1–10.16.16. doi:10.1002/0471143030.cb1016s47.

[111] Y.-R. V Shih, K.-F. Tseng, H.-Y. Lai, C.-H. Lin, O.K. Lee, Matrix stiffness regulation of integrin-mediated mechanotransduction during osteogenic differentiation of human mesenchymal stem cells, J. Bone Miner. Res. 26 (2011) 730–8. doi:10.1002/jbmr.278.

[112] T.D. Schmittgen, K.J. Livak, Analyzing real-time PCR data by the comparative CT method, Nat. Protoc. 3 (2008) 1101–1108. doi:10.1038/nprot.2008.73.

[113] C.A. Gregory, W.G. Gunn, A. Peister, D.J. Prockop, An Alizarin red-based assay of mineralization by adherent cells in culture: comparison with cetylpyridinium chloride extraction, Anal. Biochem. 329 (2004) 77–84. doi:http://dx.doi.org/10.1016/j.ab.2004.02.002.

[114] K.M. McAndrews, M.J. Kim, T.Y. Lam, D.J. McGrail, M.R. Dawson, Architectural and Mechanical Cues Direct Mesenchymal Stem Cell Interactions with Crosslinked Gelatin Scaffolds, Tissue Eng. Part A. 20 (2014) 3252–3260. doi:10.1089/ten.tea.2013.0753.

[115] D. Wirtz, Particle-tracking microrheology of living cells: principles and applications, Annu. Rev. Biophys. 38 (2009) 301–26. doi:10.1146/annurev.biophys.050708.133724.

[116] D.J. McGrail, Q.M.N. Kieu, M.R. Dawson, The malignancy of metastatic ovarian cancer cells is increased on soft matrices through a mechanosensitive Rho-ROCK pathway, J. Cell Sci. 127 (2014) 2621–6. doi:10.1242/jcs.144378.

[117] I. Banerjee, D. Mishra, T.K. Maiti, PLGA Microspheres Incorporated Gelatin Scaffold: Microspheres Modulate Scaffold Properties, Int. J. Biomater. 2009 (2009). doi:10.1155/2009/143659.

[118] J.-Y. Lai, Y.-T. Li, C.-H. Cho, T.-C. Yu, Nanoscale modification of porous gelatin scaffolds with chondroitin sulfate for corneal stromal tissue engineering, Int. J. Nanomedicine. 7 (2012) 1101–14. doi:10.2147/IJN.S28753.

[119] Y. Huang, S. Onyeri, M. Siewe, A. Moshfeghian, S. V Madihally, In vitro characterization of chitosan-gelatin scaffolds for tissue engineering, Biomaterials. 26 (2005) 7616–27. doi:10.1016/j.biomaterials.2005.05.036.

[120] L.H.H. Olde Damink, P.J. Dijkstra, M.J.A. Luyn, P.B. Wachem, P. Nieuwenhuis, J. Feijen, Glutaraldehyde as a crosslinking agent for collagen-based biomaterials, J. Mater. Sci. Mater. Med. 6 (1995) 460–472. doi:10.1007/BF00123371.

[121] S. Avrameas, T. Ternynck, The cross-linking of proteins with glutaraldehyde and its use for the preaparation of immunoadsorbernts, Immunochemistry. 6 (1969) 53–66. doi:http://dx.doi.org/10.1016/0019-2791(69)90178-5.

[122] M.E. Bernardo, N. Zaffaroni, F. Novara, A.M. Cometa, M.A. Avanzini, A. Moretta, et al., Human Bone Marrow–Derived Mesenchymal Stem Cells Do Not Undergo Transformation after Long-term In vitro Culture and Do Not Exhibit Telomere Maintenance Mechanisms, Cancer Res. 67 (2007) 9142–9149. doi:10.1158/0008-5472.CAN-06-4690.

[123] P. Kharaziha, P.M. Hellström, B. Noorinayer, F. Farzaneh, K. Aghajani, F. Jafari, et al., Improvement of liver function in liver cirrhosis patients after autologous mesenchymal stem cell injection: a phase I–II clinical trial, Eur. J. Gastroenterol. Hepatol. 21 (2009).

[124] V. Falanga, S. Iwamoto, M. Chartier, T. Yufit, J. Butmarc, N. Kouttab, et al., Autologous bone marrow-derived cultured mesenchymal stem cells delivered in a fibrin spray accelerate healing in murine and human cutaneous wounds, Tissue Eng. 13 (2007) 1299–312. doi:10.1089/ten.2006.0278.

[125] E.M. Horwitz, P.L. Gordon, W.K.K. Koo, J.C. Marx, M.D. Neel, R.Y. McNall, et al., Isolated allogeneic bone marrow-derived mesenchymal cells engraft and

stimulate growth in children with osteogenesis imperfecta: Implications for cell therapy of bone, Proc. Natl. Acad. Sci. 99 (2002) 8932–8937. doi:10.1073/pnas.132252399.

[126] R.H. Lee, A.A. Pulin, M.J. Seo, D.J. Kota, J. Ylostalo, B.L. Larson, et al., Intravenous hMSCs Improve Myocardial Infarction in Mice because Cells Embolized in Lung Are Activated to Secrete the Anti-inflammatory Protein TSG-6, Cell Stem Cell. 5 (2009) 54–63. doi:http://dx.doi.org/10.1016/j.stem.2009.05.003.

[127] Y. Sun, C.S. Chen, J. Fu, Forcing stem cells to behave: a biophysical perspective of the cellular microenvironment, Annu. Rev. Biophys. 41 (2012) 519–42. doi:10.1146/annurev-biophys-042910-155306.

[128] E.A. Silva, E.-S. Kim, H.J. Kong, D.J. Mooney, Material-based deployment enhances efficacy of endothelial progenitor cells, Proc. Natl. Acad. Sci. 105 (2008) 14347–14352. doi:10.1073/pnas.0803873105.

[129] K.A. Mosiewicz, L. Kolb, A.J. van der Vlies, M.M. Martino, P.S. Lienemann, J.A. Hubbell, et al., In situ cell manipulation through enzymatic hydrogel photopatterning, Nat. Mater. 12 (2013) 1072–8. doi:10.1038/nmat3766.

[130] A. Bigi, G. Cojazzi, S. Panzavolta, K. Rubini, N. Roveri, Mechanical and thermal properties of gelatin films at different degrees of glutaraldehyde crosslinking, Biomaterials. 22 (2001) 763–8.

[131] M. Valentine, P. Kaplan, D. Thota, J. Crocker, T. Gisler, R. Prud'homme, et al., Investigating the microenvironments of inhomogeneous soft materials with multiple particle tracking, Phys. Rev. E. 64 (2001) 061506. doi:10.1103/PhysRevE.64.061506.

[132] T. Abete, E. Del Gado, L. de Arcangelis, Gelation kinetics of crosslinked gelatin, Polym. Compos. 34 (2013) 259–264. doi:10.1002/pc.22399.

[133] A.O. Brightman, B.P. Rajwa, J.E. Sturgis, M.E. McCallister, J.P. Robinson, S.L. Voytik-Harbin, Time-lapse confocal reflection microscopy of collagen fibrillogenesis and extracellular matrix assembly in vitro, Biopolymers. 54 (2000) 222–34. doi:10.1002/1097-0282(200009)54:3<222::AID-BIP80>3.0.CO;2-K.

[134] J.S. Park, J.S. Chu, A.D. Tsou, R. Diop, Z. Tang, A. Wang, et al., The effect of matrix stiffness on the differentiation of mesenchymal stem cells in response to TGF-β, Biomaterials. 32 (2011) 3921–3930. doi:http://dx.doi.org/10.1016/j.biomaterials.2011.02.019.

[135] Y.S. Choi, L.G. Vincent, A.R. Lee, K.C. Kretchmer, S. Chirasatitsin, M.K. Dobke, et al., The alignment and fusion assembly of adipose-derived stem cells on

mechanically patterned matrices, Biomaterials. 33 (2012) 6943–51. doi:10.1016/j.biomaterials.2012.06.057.

[136] Y.S. Pek, A.C.A. Wan, J.Y. Ying, The effect of matrix stiffness on mesenchymal stem cell differentiation in a 3D thixotropic gel, Biomaterials. 31 (2010) 385–391. doi:http://dx.doi.org/10.1016/j.biomaterials.2009.09.057.

[137] P. Kasten, I. Beyen, P. Niemeyer, R. Luginbühl, M. Bohner, W. Richter, Porosity and pore size of beta-tricalcium phosphate scaffold can influence protein production and osteogenic differentiation of human mesenchymal stem cells: an in vitro and in vivo study, Acta Biomater. 4 (2008) 1904–15. doi:10.1016/j.actbio.2008.05.017.

[138] J.C. Crocker, D.G. Grier, Methods of Digital Video Microscopy for Colloidal Studies, J. Colloid Interface Sci. 310 (1996) 298–310.

[139] D. Ghosh, L. Lilli, D.J. McGrail, L. V. Matyunina, J.F. McDonald, M.R. Dawson, Integral Role of Platelet Derived Growth Factor in Mediating Transforming Growth Factor-β1 Dependent Mesenchymal Stem Cell Stiffening, Stem Cells Dev. (2013).

[140] A. Untergasser, I. Cutcutache, T. Koressaar, J. Ye, B.C. Faircloth, M. Remm, et al., Primer3—new capabilities and interfaces, Nucleic Acids Res. 40 (2012) e115–e115. doi:10.1093/nar/gks596.

[141] D. Hanahan, R.A. Weinberg, Hallmarks of cancer: the next generation, Cell. 144 (2011) 646–74. doi:10.1016/j.cell.2011.02.013.

[142] E.R. Rayburn, S.J. Ezell, R. Zhang, Anti-Inflammatory Agents for Cancer Therapy, Mol. Cell. Pharmacol. 1 (2009) 29–43. doi:10.4255/mcpharmacol.09.05.Anti-Inflammatory.

[143] P. Carmeliet, Angiogenesis in life, disease and medicine, Nature. 438 (2005) 932–6. doi:10.1038/nature04478.

[144] S. Kidd, E. Spaeth, K. Watson, J. Burks, H. Lu, A. Klopp, et al., Origins of the tumor microenvironment: quantitative assessment of adipose-derived and bone marrow-derived stroma, PLoS One. 7 (2012) e30563. doi:10.1371/journal.pone.0030563.

[145] N. Ferrara, R.S. Kerbel, Angiogenesis as a therapeutic target, Nature. 438 (2005) 967–974.

[146] A. Orimo, P.B. Gupta, D.C. Sgroi, F. Arenzana-Seisdedos, T. Delaunay, R. Naeem, et al., Stromal Fibroblasts Present in Invasive Human Breast Carcinomas

Promote Tumor Growth and Angiogenesis through Elevated SDF-1/ CXCL12 Secretion, Cell. 121 (2005) 335–348. doi:10.1016/j.cell.2005.02.034.

[147] Y. Jung, J.K. Kim, Y. Shiozawa, J. Wang, A. Mishra, J. Joseph, et al., Recruitment of mesenchymal stem cells into prostate tumours promotes metastasis, Nat. Commun. 4 (2013) 1795. doi:10.1038/ncomms2766.

[148] P. Micke, A. Ostman, Tumour-stroma interaction: cancer-associated fibroblasts as novel targets in anti-cancer therapy?, Lung Cancer. 45 (2004) S163–75. doi:10.1016/j.lungcan.2004.07.977.

[149] U. Cavallaro, G. Christofori, Cell adhesion and signalling by cadherins and Ig-CAMs in cancer, Nat. Rev. Cancer. 4 (2004) 118–32. doi:10.1038/nrc1276.

[150] M. Pishvaian, C. Feltes, Cadherin-11 is expressed in invasive breast cancer cell lines, Cancer Res. 59 (1999) 947–952.

[151] M. Bussemakers, Complex cadherin expression in human prostate cancer cells, Int. J. Cancer. 85 (2000) 446–450.

[152] M. Yu, A. Bardia, B.S. Wittner, S.L. Stott, M.E. Smas, D.T. Ting, et al., Circulating Breast Tumor Cells Exhibit Dynamic Changes in Epithelial and Mesenchymal Composition, Science. 339 (2013) 580–584. doi:10.1126/science.1228522.

[153] G. Sardana, K. Jung, C. Stephan, E.P. Diamandis, Proteomic Analysis of Conditioned Media from the PC3, LNCaP, and 22Rv1 Prostate Cancer Cell Lines : Discovery and Validation of Candidate Prostate Cancer Biomarkers, J. Proteome Res. 7 (2008) 3329–3338.

[154] V. Kulasingam, E.P. Diamandis, Proteomics analysis of conditioned media from three breast cancer cell lines: a mine for biomarkers and therapeutic targets, Mol. Cell. Proteomics. 6 (2007) 1997–2011. doi:10.1074/mcp.M600465-MCP200.

[155] F. Kong, A.J. García, A.P. Mould, M.J. Humphries, C. Zhu, Demonstration of catch bonds between an integrin and its ligand, J. Cell Biol. 185 (2009) 1275–84. doi:10.1083/jcb.200810002.

[156] M. Morini, M. Mottolese, N. Ferrari, F. Ghiorzo, S. Buglioni, R. Mortarini, et al., The α3β1 integrin is associated with mammary carcinoma cell metastasis, invasion, and gelatinase B (MMP-9) activity, Int. J. Cancer. 87 (2000) 336–342.

[157] D.J. McGrail, N.N. Khambhati, M.X. Qi, K.S. Patel, N. Ravikumar, C.P. Brandenburg, et al., Alterations in Ovarian Cancer Cell Adhesion Drive Taxol Resistance by Increasing Microtubule Dynamics in a FAK-dependent Manner, Sci. Rep. 5 (2015) 9529. doi:10.1038/srep09529.

[158] N.A. Bhowmick, E.G. Neilson, H.L. Moses, Stromal fibroblasts in cancer initiation and progression, Nature. 432 (2004) 332–337.

[159] A.C. Shieh, H.A. Rozansky, B. Hinz, M.A. Swartz, Tumor cell invasion is promoted by interstitial flow-induced matrix priming by stromal fibroblasts, Cancer Res. 71 (2011) 790–800. doi:10.1158/0008-5472.CAN-10-1513.

[160] C. Gaggioli, S. Hooper, C. Hidalgo-Carcedo, R. Grosse, J.F. Marshall, K. Harrington, et al., Fibroblast-led collective invasion of carcinoma cells with differing roles for RhoGTPases in leading and following cells, Nat. Cell Biol. 9 (2007) 1392–400. doi:10.1038/ncb1658.

[161] P. Panorchan, M.S. Thompson, K.J. Davis, Y. Tseng, K. Konstantopoulos, D. Wirtz, Single-molecule analysis of cadherin-mediated cell-cell adhesion, J. Cell Sci. 119 (2006) 66–74. doi:10.1242/jcs.02719.

[162] Y.-S. Chu, O. Eder, W.A. Thomas, I. Simcha, F. Pincet, A. Ben-Ze'ev, et al., Prototypical Type I E-cadherin and Type II Cadherin-7 Mediate Very Distinct Adhesiveness through Their Extracellular Domains, J. Biol. Chem. 281 (2006) 2901–2910. doi:10.1074/jbc.M506185200.

[163] H. Wang, C. Yu, X. Gao, T. Welte, A.M. Muscarella, L. Tian, et al., The Osteogenic Niche Promotes Early-Stage Bone Colonization of Disseminated Breast Cancer Cells, Cancer Cell. 27 (2015) 193–210. doi:10.1016/j.ccell.2014.11.017.

[164] P. Pittet, K. Lee, A.J. Kulik, J.-J. Meister, B. Hinz, Fibrogenic fibroblasts increase intercellular adhesion strength by reinforcing individual OB-cadherin bonds, J. Cell Sci. 121 (2008) 877–86. doi:10.1242/jcs.024877.

[165] C.S. Chen, M. Mrksich, S. Huang, G.M. Whitesides, D.E. Ingber, Geometric Control of Cell Life and Death, Science. 276 (1997) 1425–1428.

[166] B. Hinz, P. Pittet, C. Chaponnier, J. Meister, Myofibroblast Development Is Characterized by Specific Cell-Cell Adherens Junctions, Mol. Biol. Cell. 15 (2004) 4310–4320. doi:10.1091/mbc.E04.

[167] B.K. Straub, J. Boda, C. Kuhn, M. Schnoelzer, U. Korf, T. Kempf, et al., A novel cell-cell junction system: the cortex adhaerens mosaic of lens fiber cells, J. Cell Sci. 116 (2003) 4985–95. doi:10.1242/jcs.00815.

[168] A. Singh, J. Settleman, EMT, cancer stem cells and drug resistance: an emerging axis of evil in the war on cancer, Oncogene. 29 (2010) 4741–4751.

[169] S. Assefnia, S. Dakshanamurthy, J.M. Guidry Auvil, C. Hampel, P.Z. Anastasiadis, B. Kallakury, et al., Cadherin-11 in poor prognosis malignancies and

rheumatoid arthritis: common target, common therapies, Oncotarget. 5 (2013) 1458–1474.

[170] Z. Yin, A. Sadok, H. Sailem, A. McCarthy, X. Xia, F. Li, et al., A screen for morphological complexity identifies regulators of switch-like transitions between discrete cell shapes, Nat. Cell Biol. 15 (2013) 860–871.

[171] A. Albini, M.B. Sporn, The tumour microenvironment as a target for chemoprevention, Nat. Rev. Cancer. 7 (2007) 131–139. doi:10.1038/nrc2066.

[172] F.R. Balkwill, M. Capasso, T. Hagemann, The tumor microenvironment at a glance, J. Cell Sci. 125 (2012) 5591–6. doi:10.1242/jcs.116392.

[173] B.G. Cuiffo, A. Campagne, G.W. Bell, A. Lembo, F. Orso, E.C. Lien, et al., MSC-Regulated MicroRNAs Converge on the Transcription Factor FOXP2 and Promote Breast Cancer Metastasis, Cell Stem Cell. 15 (2014) 762–774. doi:10.1016/j.stem.2014.10.001.

[174] T. Oskarsson, Extracellular matrix components in breast cancer progression and metastasis, The Breast. 22 Suppl 2 (2013) S66–72. doi:10.1016/j.breast.2013.07.012.

[175] P.P. Provenzano, D.R. Inman, K.W. Eliceiri, P.J. Keely, Matrix density-induced mechanoregulation of breast cell phenotype, signaling and gene expression through a FAK-ERK linkage, Oncogene. 28 (2009) 4326–4343. doi:10.1038/onc.2009.299.

[176] K.R. Levental, H. Yu, L. Kass, J.N. Lakins, M. Egeblad, J.T. Erler, et al., Matrix crosslinking forces tumor progression by enhancing integrin signaling, Cell. 139 (2009) 891–906. doi:10.1016/j.cell.2009.10.027.

[177] F. Calvo, N. Ege, A. Grande-Garcia, S. Hooper, R.P. Jenkins, S.I. Chaudhry, et al., Mechanotransduction and YAP-dependent matrix remodelling is required for the generation and maintenance of cancer-associated fibroblasts, Nat. Cell Biol. 15 (2013) 637–646. doi:10.1038/ncb2756.

[178] K. Wolf, I. Mazo, H. Leung, K. Engelke, U.H. Von Andrian, E.I. Deryugina, et al., Compensation mechanism in tumor cell migration: Mesenchymal-amoeboid transition after blocking of pericellular proteolysis, J. Cell Biol. 160 (2003) 267–277. doi:10.1083/jcb.200209006.

[179] K. Wolf, Y.I. Wu, Y. Liu, J. Geiger, E. Tam, C. Overall, et al., Multi-step pericellular proteolysis controls the transition from individual to collective cancer cell invasion, Nat. Cell Biol. 9 (2007) 893–904. doi:10.1038/ncb1616.

[180] E. Sahai, C.J. Marshall, Differing modes of tumour cell invasion have distinct requirements for Rho/ROCK signalling and extracellular proteolysis, Nat. Cell Biol. 5 (2003) 711–719. doi:10.1038/ncb1019.

[181] M.H. Zaman, L.M. Trapani, A.L. Sieminski, D. Mackellar, H. Gong, R.D. Kamm, et al., Migration of tumor cells in 3D matrices is governed by matrix stiffness along with cell-matrix adhesion and proteolysis, Proc. Natl. Acad. Sci. 103 (2006) 10889–10894.

[182] P. Friedl, K. Wolf, Tumour-cell invasion and migration: diversity and escape mechanisms, Nat. Rev. Cancer. 3 (2003) 362–74. doi:10.1038/nrc1075.

[183] D.T. Covas, R.A. Panepucci, A.M. Fontes, W.A. Silva, M.D. Orellana, M.C.C. Freitas, et al., Multipotent mesenchymal stromal cells obtained from diverse human tissues share functional properties and gene-expression profile with CD146+ perivascular cells and fibroblasts, Exp. Hematol. 36 (2008) 642–54. doi:10.1016/j.exphem.2007.12.015.

[184] M.A. Haniffa, X.-N. Wang, U. Holtick, M. Rae, J.D. Isaacs, A.M. Dickinson, et al., Adult Human Fibroblasts Are Potent Immunoregulatory Cells and Functionally Equivalent to Mesenchymal Stem Cells, J. Immunol. 179 (2007) 1595–1604. doi:10.4049/jimmunol.179.3.1595.

[185] D. Wirtz, K. Konstantopoulos, P.C. Searson, The physics of cancer: the role of physical interactions and mechanical forces in metastasis, Nat. Rev. Cancer. 11 (2011) 512–22. doi:10.1038/nrc3080.

[186] I. Carvalho, F. Milanezi, A. Martins, R.M. Reis, F. Schmitt, Overexpression of platelet-derived growth factor receptor alpha in breast cancer is associated with tumour progression, Breast Cancer Res. 7 (2005) R788–95. doi:10.1186/bcr1304.

[187] H. Bando, H. a Weich, M. Brokelmann, S. Horiguchi, N. Funata, T. Ogawa, et al., Association between intratumoral free and total VEGF, soluble VEGFR-1, VEGFR-2 and prognosis in breast cancer, Br. J. Cancer. 92 (2005) 553–61. doi:10.1038/sj.bjc.6602374.

[188] T. Imamura, A. Hikita, Y. Inoue, The roles of TGF-β signaling in carcinogenesis and breast cancer metastasis, Breast Cancer. 19 (2012) 118–24. doi:10.1007/s12282-011-0321-2.

[189] K. Polyak, Heterogeneity in breast cancer, J. Clin. Invest. 121 (2011) 3786–3788. doi:10.1172/JCI60534.

[190] S.I. Fraley, Y. Feng, R. Krishnamurthy, D.-H. Kim, A. Celedon, G.D. Longmore, et al., A distinctive role for focal adhesion proteins in three-dimensional cell motility, Nat. Cell Biol. 12 (2010) 598–604. doi:10.1038/ncb2062.

[191] A. Rape, W. Guo, Y. Wang, Microtubule depolymerization induces traction force increase through two distinct pathways, J. Cell Sci. 124 (2011) 4233–4240. doi:10.1242/jcs.090563.

[192] D.M. Pirone, W.F. Liu, S.A. Ruiz, L. Gao, S. Raghavan, C.A. Lemmon, et al., An inhibitory role for FAK in regulating proliferation: A link between limited adhesion and RhoA-ROCK signaling, J. Cell Biol. 174 (2006) 277–288. doi:10.1083/jcb.200510062.

[193] H. Wang, V. Radjendirane, K.K. Wary, S. Chakrabarty, Transforming growth factor beta regulates cell-cell adhesion through extracellular matrix remodeling and activation of focal adhesion kinase in human colon carcinoma Moser cells, Oncogene. 23 (2004) 5558–5561. doi:10.1038/sj.onc.1207701.

[194] D.J. Sieg, C.R. Hauck, D. Ilic, C.K. Klingbeil, E. Schaefer, H. Caroline, et al., FAK integrates growth-factor and integrin signals to promote cell migration, Nat. Cell Biol. 2 (2000) 249 – 256.

[195] F.J. Sulzmaier, C. Jean, D.D. Schlaepfer, FAK in cancer: mechanistic findings and clinical applications, Nat. Rev. Cancer. 14 (2014) 598–610. doi:10.1038/nrc3792.

[196] S.K. Mitra, S.-T. Lim, A. Chi, D. Schlaepfer, Intrinsic focal adhesion kinase activity controls orthotopic breast carcinoma metastasis via the regulation of urokinase plasminogen activator expression in a syngeneic tumor model, Oncogene. 25 (2006) 4429–4440. doi:10.1038/sj.onc.

[197] Q. Yu, I. Stamenkovic, Cell surface-localized matrix metalloproteinase-9 proteolytically activates TGF-β and promotes tumor invasion and angiogenesis, Genes Dev. 14 (2000) 163–176. doi:10.1101/gad.14.2.163.

[198] R. Poincloux, O. Collin, F. Lizárraga, M. Romao, M. Debray, M. Piel, et al., Contractility of the cell rear drives invasion of breast tumor cells in 3D Matrigel., Proc. Natl. Acad. Sci. 108 (2011) 1943–1948. doi:10.1073/pnas.1010396108.

[199] P.P. Provenzano, D.R. Inman, K.W. Eliceiri, S.M. Trier, P.J. Keely, Contact guidance mediated three-dimensional cell migration is regulated by Rho/ROCK-dependent matrix reorganization, Biophys. J. 95 (2008) 5374–5384. doi:10.1529/biophysj.108.133116.

[200] P.J. Wipff, D.B. Rifkin, J.J. Meister, B. Hinz, Myofibroblast contraction activates latent TGF-1 from the extracellular matrix, J. Cell Biol. 179 (2007) 1311–1323. doi:10.1083/jcb.200704042.

[201] P.T. Hawkins, A. Eguinoa, R.G. Qiu, D. Stokoe, F.T. Cooke, R. Walters, et al., PDGF stimulates an increase in GTP-Rac via activation of phosphoinositide 3-kinase, Curr. Biol. 5 (1995) 393–403. doi:10.1016/S0960-9822(95)00080-7.

[202] A.M. Doanes, K. Irani, P.J. Goldschmidt-Clermont, T. Finkel, A requirement for Rac1 in the PDGF-stimulated migration of fibroblasts and vascular smooth cells, Biochem. Mol. Biol. Int. 45 (1998) 279–287. doi:10.1080/15216549800202652.

[203] P.C.S. Bota, A.M.B. Collie, P. Puolakkainen, R.B. Vernon, E.H. Sage, B.D. Ratner, et al., Biomaterial topography alters healing in vivo and monocyte/macrophage activation in vitro, J. Biomed. Mater. Res. Part A. 95A (2010) 649–657. doi:10.1002/jbm.a.32893.

[204] J.T. Erler, K.L. Bennewith, T.R. Cox, G. Lang, D. Bird, A. Koong, et al., Hypoxia-Induced Lysyl Oxidase Is a Critical Mediator of Bone Marrow Cell Recruitment to Form the Premetastatic Niche, Cancer Cell. 15 (2009) 35–44. doi:http://dx.doi.org/10.1016/j.ccr.2008.11.012.

[205] A.J. Dannenberg, K. Subbaramaiah, Targeting cyclooxygenase-2 in human neoplasia: rationale and promise, Cancer Cell. 4 (2003) 431–436.

[206] J. Bergh, I.M. Bondarenko, M.R. Lichinitser, A. Liljegren, R. Greil, N.L. Voytko, et al., First-Line Treatment of Advanced Breast Cancer With Sunitinib in Combination With Docetaxel Versus Docetaxel Alone: Results of a Prospective, Randomized Phase III Study, J. Clin. Oncol. . 30 (2012) 921–929. doi:10.1200/JCO.2011.35.7376 .

[207] R.J. Akhurst, A. Hata, Targeting the TGFβ signalling pathway in disease, Nat. Rev. Drug Discov. 11 (2012) 790–811. doi:10.1038/nrd3810.

[208] E.M. Chandler, B.R. Seo, J.P. Califano, R.C. Andresen Eguiluz, J.S. Lee, C.J. Yoon, et al., Implanted adipose progenitor cells as physicochemical regulators of breast cancer, Proc. Natl. Acad. Sci. (2012). doi:10.1073/pnas.1121160109/-/DCSupplemental.www.pnas.org/cgi/doi/10.1073/pnas.1121160109.